



Entergy Operations, Inc.
1340 Echelon Parkway
Jackson, Mississippi 39213-8298
Tel 601-368-5758

William K. Hughey
Director, Licensing – New Plant
(601) 368-5327
wkhughey@entergy.com

CNRO-2008-00020

June 30, 2008

U. S. Nuclear Regulatory Commission
Attn.: Document Control Desk
Washington, DC 20555-0001

SUBJECT: Supplemental Information Regarding Methodology Used to Develop
Horizontal and Vertical Site-Specific Hazard Consistent Uniform Hazard
Response Spectra

Grand Gulf Nuclear Station, Unit 3
Docket No. 52-024

- REFERENCES:
1. Entergy Operations, Inc. letter to USNRC – Application for Combined License for Grand Gulf Unit 3 (CNRO-2008-00008), dated February 27, 2008
 2. USNRC letter to Entergy Operations, Inc. – Grand Gulf Nuclear Station Unit 3 Combined License Application Review Schedule (CNRI 2008-00006), dated May 16, 2008

Dear Sir or Madam:

In Reference 1, Entergy Operations, Inc. (Entergy) submitted an application for a Combined License (COL) for Grand Gulf Nuclear Station (GGNS), Unit 3.

On March 19, 2008, Entergy met with the NRC Staff to discuss technical aspects of the COL application in support of the NRC's acceptance review of the application. During this meeting, it was noted that random vibration theory (RVT) and Approach 3 (NUREG/CR-6728¹, -6769²) were used to develop horizontal and vertical hazard consistent site-specific uniform hazard response spectra at the GGNS Unit 3. The selection and use of RVT and Approach 3 methodology are described in FSAR Section 2.5.2.4. As discussed in FSAR Section 2.5.2.4.2, the fully probabilistic Approach 3 was selected for use at GGNS because it satisfies

¹ "Technical Basis for Revision of Regulatory Guidance on Design Ground Motions: Hazard- and Risk-Consistent Ground Motion Spectra Guidelines," NUREG/CR-6728, U.S. Nuclear Regulatory Commission, Washington, DC, 2001

² "Technical Basis for Revision of Regulatory Guidance on Design Ground Motions: Development of Hazard- and Risk-Consistent Seismic Spectra for Two Sites," NUREG/CR-6769, U.S. Nuclear Regulatory Commission, Washington, DC, 2002

D079
NRD

the requirement for a performance-based method called for in Regulatory Guide 1.208. In discussions subsequent to the March 19 meeting, Entergy committed to provide supplemental information on the use of RVT and Approach 3 for the Unit 3 site to support NRC Staff review. This commitment was documented by the NRC in Reference 2.

In compliance with this commitment, this letter provides the supplemental information in the enclosed report. This report provides a detailed presentation of analysis methodology, specifically addressing calculation approaches for development of amplification estimates using RVT and development of horizontal and vertical hazard consistent uniform hazard response spectra using Approach 3 and incorporation of site-specific aleatory and epistemic variabilities in dynamic material properties. The enclosed report supplements the analysis results presented in the COL application, Part 2, FSAR Section 2.5.2, for the GGNS Unit 3.

Should you have any questions, please contact me or Tom Williamson (601-368-5786).

This letter contains no new commitments

I declare under penalty of perjury that the foregoing is true and correct.

Executed on June 30, 2008.

Sincerely,



WKH/gaz

Enclosure: 1. Development of Horizontal and Vertical Site-Specific Hazard Consistent Uniform Hazard Response Spectra at the Grand Gulf Nuclear Station Unit 3

cc: Mr. T. A. Burke (ECH)
Mr. S. P. Frantz (Morgan, Lewis & Bockius)
Mr. B. R. Johnson (GE-Hitachi)
Ms. M. Kray (NuStart)
Mr. P. D. Hinnenkamp (ECH)

NRC Project Manager – GGNS COLA
NRC Director – Division of Construction Projects (Region II)
NRC Regional Administrator - Region IV
NRC Resident Inspectors' Office: GGNS

ENCLOSURE 1

To

CNRO200800020

**GRAND GULF NUCLEAR STATION UNIT 3
COMBINED CONSTRUCTION PERMIT AND OPERATING LICENSE COL PROJECT
DEVELOPMENT OF HORIZONTAL AND VERTICAL SITE-SPECIFIC HAZARD
CONSISTENT UNIFORM HAZARD RESPONSE SPECTRA AT
THE GRAND GULF NUCLEAR STATION UNIT 3**

June 30, 2008

Page intentionally left blank

ACRONYMS AND SYMBOLS

The definitions of acronyms and symbols used in this technical report are listed below.

1D - One Dimensional
AEF - Annual Exceedance Frequency
AEP - Annual Exceedance Probability
CCDF - complementary cumulative distribution function
CENA - Central and Eastern North America
COV - coefficient of variability
D - distance in kilometers or miles
ESP - Early Site Permit
EPRI - Electric Power Research Institute
FAS - Fourier Amplitude Spectra
FIRS - Foundation Input Response Spectra
fps - feet per second
FSAR - Final Safety Analysis Report
g - acceleration unit
GMRS - Ground Motion Response Spectra
Hz - Hertz
km - kilometers
M - Moment Magnitude
P - compressional wave
PSD - Power Spectral Density
PSHA - Probabilistic Seismic Hazard Analysis
RMS - Root Mean Square
RVT - Random Vibration Theory
SDF - Single Degree of Freedom
SV - vertically polarized shear wave
UHRS - Uniform Hazard Response Spectra
V/H - Vertical-to-Horizontal Ratio
V_p - compressional wave velocity
V_s - shear wave velocity
WNA - Western North America
km/sec - kilometers per second
> - Greater than
< - Less than
≤ - Equal to or less than
≥ - Greater than or equal to
% - Percent

Table of Contents

Cover Sheet	1
Revision Status	2
Acronyms and Symbols	3
Table of Contents	4
List of Tables	5
List of Figures	6
OVERVIEW	11
1.0 INTRODUCTION	11
2.0 IMPLEMENTATION OF RANDOM VIBRATION THEORY (RVT) FOR SITE RESPONSE ANALYSES	12
2.1 RVT Durations	13
2.2 RVT-Based Equivalent-Linear Site-Response	14
3.0 APPROACHES TO DEVELOP SITE-SPECIFIC HAZARD	23
3.1 Description of Approaches	23
3.2 Approach 3 – Full Integration Method	26
3.3 Approach 3 – Approximate Method	27
3.4 Implementation of Approach 3	29
4.0 APPLICATION TO VERTICAL HAZARD	36
4.1 Development of V/H Ratios	37
4.2 Implementation of V/H Ratios In Developing Vertical Hazard	42
5.0 CONCLUSIONS	43
6.0 REFERENCES	45
7.0 TABLES AND FIGURES	49

List of Tables

Cover Page	50
Table 1 Definitions of Locations for Motions in Site-Response Analyses	51
Table 2 Hard Rock Expected Horizontal Peak Acceleration Levels, Point Source Distances, and Durations, Parameters and Hard Rock Crustal Model	52
Table 3 Sample Size Required For Percent Error In The Standard Deviation for A Normal Distribution	52
Table 4 Amplification Factor M and V/H Ratios M and D Ranges.....	53
Table 5 Model Weights.....	54

List of Figures

Cover Page	56
Figure 1 Comparison of median RVT and SDF (computed from acceleration time histories) 5% damped response spectra. RVT computed using Equation 24 in Boore (1983). Medians computed over 30 realizations.....	57
Figure 2 Amplification factors, median and ± 1 sigma estimates, computed for a 25 ft thick (randomized ± 10 ft) layer of 1,000 ft/sec shear-wave velocity over hard rock crustal model (Table 2) at a suite of loading levels. Magnitude is 5.0	58
Figure 3a Base-case shear-wave velocity profiles developed for the Grand Gulf Nuclear Station Unit 3 reactor to depths of 500 ft. (Adapted from FSAR Figure Section 2.5.2-212 (EOI, 2008))	59
Figure 3b Base-case shear-wave velocity profiles developed for the Grand Gulf Nuclear Station Unit 3 reactor to depth of 4000 ft. (Adapted from FSAR Figure Section 2.5.2-213 (EOI, 2008))	60
Figure 4a Example of median and ± 1 sigma estimates of amplification factors computed for the Grand Gulf Reactor embedded profile 1 (Figures 3a and 3b) using site-specific G/G_{max} and hysteretic damping curves (EOI, 2008). Single-corner point-source magnitude is 6.25.....	61
Figure 4b Example of median and ± 1 sigma estimates of amplification factors computed for the Grand Gulf Reactor embedded profile 1 (Figures 3a and 3b) using site-specific G/G_{max} and hysteretic damping curves (EOI, 2008). Single-corner point-source magnitude is 7.69.....	63
Figure 5a Illustration of the effects of magnitude on median amplification factors computed for the Grand Gulf reactor embedded profile 1 (Figures 3a and 3b) using site-specific G/G_{max} and hysteretic damping curves (EOI, 2008). Single-corner point-source magnitudes are 6.25 and 7.69.	65
Figure 5b Illustration of the effects of magnitude on median amplification factors computed for the Grand Gulf reactor embedded profile 1 (Figures 3a and 3b) using site-specific G/G_{max} and hysteretic damping curves (EOI, 2008). Single-corner point-source magnitudes are 5.0, 6.0, and 7.0.....	67
Figure 6a Response spectral shapes (median estimates) computed at the suite of distances to obtain the target peak acceleration values. Single-corner point source magnitude is 6.25.	69
Figure 6b Response spectral shapes (median estimates) computed at the suite of distances to obtain the target peak acceleration values. Single-corner point source magnitude is 7.69.	70
Figure 7 Test case illustrating the effect of magnitude on median amplification factors computed for a deep stiff soil site in the CENA. Distances were adjusted to obtain the target hard rock (input) median peak acceleration values. Single-corner point-source magnitudes are 5.0, 6.0, and 7.0. Plotted verses structural frequency.	71

Figure 8a Illustration of the effects of single-corner versus double-corner source spectra on median amplification factors computed for the Grand Gulf reactor embedded profile 1 (Figures 3a and 3b) using site-specific G/G_{max} and hysteretic damping curves (EOI, 2008). Hard rock reference expected peak acceleration ranges from 0.01g to 1.50g. Single-corner and double-corner point-source magnitudes are 6.25.73

Figure 8b. Illustration of the effects of single-corner versus double-corner source spectra on median amplification factors computed for the Grand Gulf reactor embedded profile 1 (Figures 3a and 3b) using site-specific G/G_{max} and hysteretic damping curves (EOI, 2008). Single-corner and double-corner point-source magnitudes are 7.69.....75

Figure 9 Test cases illustrating the effect of single-verses double-corner source spectra on median amplification factors computed for a deep stiff soil site in the CENA. Distances were adjusted to obtain the target hard rock (input) median peak acceleration values. Plotted verses structural frequency. Single-corner and double-corner point-source magnitudes are 7.0.....77

Figure 10 Illustration of the effect of magnitude on median amplification factors and sigma value (σ_{in}) computed for the Grand Gulf reactor embedded profile 1 (Figures 3a and 3b) using site-specific G/G_{max} and hysteretic damping curves (EOI, 2008). Plotted verses reference site ground motion (5% damped spectral acceleration (S_a)) at three structural frequencies.....79

Figure 11a Illustration of the effect of single-verses double-corner source spectra on median amplification factors and sigma value (σ_{in}) computed for the Grand Gulf reactor embedded profile 1 (Figures 3a and 3b) using site-specific G/G_{max} and hysteretic damping curves (EOI, 2008). Single-corner and double-corner point-source magnitude is 6.25.80

Figure 11b Illustration of the effect of single-verses double-corner source spectra on median amplification factors and sigma value (σ_{in}) computed for the Grand Gulf reactor embedded profile 1 (Figures 3a and 3b) using site-specific G/G_{max} and hysteretic damping curves (EOI, 2008). Single-corner and double-corner point-source magnitude is 7.69.81

Figure 12 Interpolation test case illustrating the rapid convergence to integration stability. Note the small change in hazard for a large increase in the number of interpolation points.82

Figure 13a. Median and sigma estimates computed for numbers of realizations from 15 to 240 using five different random seeds for the Grand Gulf reactor embedded profile 1 (Figures 3a and 3b) using site-specific G/G_{max} and hysteretic damping curves (EOI, 2008).....83

Figure 13b Median and sigma estimates computed for numbers of realizations from 15 to 240 using five different random seeds for a deep stiff soil site in the CENA84

Figure 14 Grand Gulf Nuclear Site Unit 3 hard rock horizontal hazard curves (EOI, 2008).....85

Figure 15 Test case illustrating Approach 3 using a simple bilinear reference site hazard curve (dotted line, slope = 3, 6). Median amplification factor is 2.0, $\sigma_{in} = 0.2$.	86
Figure 16 Test case illustrating Approach 3 using a simple bilinear reference site hazard curve (dotted line, slope = 3, 6). Median amplification factor is 2.0, $\sigma_{in} = 0.4$.	87
Figure 17 Test case illustrating Approach 3 using a realistic (WNA) reference site hazard curve (solid line). Median amplification factor is 2.0, $\sigma_{in} = 0.1, 0.2, 0.3, 0.4$.	88
Figure 18 Test case illustrating Approach 3 using a realistic (WNA) reference site hazard curve (solid line). Median amplification factor is 2.0, $\sigma_{in} = 0.3$.	89
Figure 19a Deaggregation for the Grand Gulf Nuclear Station Unit 3: low-frequency, 1 Hz to 2.5 Hz (FSAR Figure 2.5.2-210, EOI, 2008)	90
Figure 19b Deaggregation for the Grand Gulf Nuclear Station Unit 3: high-frequency, 5 Hz to 10 Hz (FSAR Figure 2.5.2-211, EOI, 2008)	91
Figure 20a Comparison of UHRS computed for the Grand Gulf Nuclear Station Unit 3 profiles 1 to 4 (Figures 3a and 3b). Each profile UHRS reflects a weighted mean over the two sets of G/G _{max} and hysteretic damping curves (Table 5). AEF 10^{-4} .	92
Figure 20b Comparison of UHRS computed for the Grand Gulf Nuclear Station Unit 3 profiles 1 to 4 (Figures 3a and 3b). Each profile UHRS reflects a weighted mean over the two sets of G/G _{max} and hysteretic damping curves (Table 5). AEF 10^{-5} .	93
Figure 21a Comparison of UHRS computed for the Grand Gulf Nuclear Station Unit 3 uncorrected and corrected G/G _{max} and hysteretic damping curves (Table 5). Each profile UHRS reflects a weighted mean over the four profiles in Figures 3a and 3b (Table 5). AEF 10^{-4} .	94
Figure 21b Comparison of UHRS computed for the Grand Gulf Nuclear Station Unit 3 uncorrected and corrected G/G _{max} and hysteretic damping curves (Table 5). Each profile UHRS reflects a weighted mean over the four profiles in Figures 3a and 3b (Table 5). AEF 10^{-5} .	95
Figure 22 Approach 2A scaled reference earthquake spectra computed for 1 Hz to 2.5 Hz (M 7.64, <i>D</i> 466 km) and 5 Hz to 10 Hz (M 6.33, <i>D</i> 82 km) using a weighted average of the EPRI (2004) attenuation relations. AEF 10^{-4} .	96
Figure 23 Approach 2A, example of low- and high-frequency mean amplification factors computed for profile 1 (Figures 3a and 3b) using uncorrected G/G _{max} and hysteretic damping curves. AEF 10^{-4} .	97
Figure 24 Approach 2A deterministic spectra compared to UHRS computed using Approach 3. Approach 2A results shown for each combination of profile (1 to 4, Figures 3a and 3b) and sets of G/G _{max} and hysteretic damping curves (labeled as RE.1 – RE.8, P1 to P4 correspond to RE.1 to RE.4 and P5 to P8 correspond to RE.5 to RE.8, respectively; refer to Section 3.4.2.3). AEF 10^{-4} .	98

Figure 25 Approach 2A scaled reference earthquake spectra computed for 1 Hz to 2.5 Hz (M 7.64, <i>D</i> 466 km) and 5 Hz to 10 Hz (M 6.33, <i>D</i> 82 km) using a weighted average of the EPRI (2004) attenuation relations. AEF 10^{-5}	99
Figure 26 Approach 2A, example of low- and high-frequency mean amplification factors computed for profile 1 (Figures 3a and 3b) using uncorrected G/G_{max} and hysteretic damping curves. AEF 10^{-5}	100
Figure 27 Approach 2A deterministic spectra compared to UHRS computed using Approach 3. Approach 2A results shown for each combination of profile (1 to 4, Figures 3a and 3b) and sets of G/G_{max} and hysteretic damping curves (labeled as RE.1 – RE.8, P1 to P4 correspond to RE.1 to RE.4 and P5 to P8 correspond to RE.5 to RE.8, respectively; refer to Section 3.4.2.3). AEF 10^{-5}	101
Figure 28a Example of median V/H ratios computed for the Grand Gulf Reactor Unit 3 using site-specific G/G_{max} and hysteretic damping curves (EOI, 2008) with a single-corner source model and M 6.25: profile 1.....	102
Figure 28b Example of median V/H ratios computed for the Grand Gulf Reactor Unit 3 using site-specific G/G_{max} and hysteretic damping curves (EOI, 2008) with a single-corner source model and M 6.25: profile 3.....	103
Figure 29 Example of median V/H ratios computed for the Grand Gulf Reactor Unit 3 using site-specific G/G_{max} and hysteretic damping curves (EOI, 2008) with a single-corner source model and M 7.69: profile 1. Reference site expected horizontal peak acceleration values and corresponding distances from Table 2.....	104
Figure 30a WNA empirical V/H ratios computed for M 6.25 at a suite of distances for soft rock site conditions: Abrahamson and Silva (1997). Peak acceleration values for horizontal component rock site conditions.....	105
Figure 30b WNA empirical V/H ratios computed for M 6.25 at a suite of distances for soft rock site conditions: Campbell and Bozorgnia (2003). Peak acceleration values for horizontal component rock site conditions.....	106
Figure 31a WNA empirical V/H ratios computed for M 6.25 at a suite of distances for deep firm soil site conditions: Abrahamson and Silva (1997). Peak acceleration values for horizontal component rock site conditions.....	107
Figure 31b WNA empirical V/H ratios computed for M 6.25 at a suite of distances for deep firm soil site conditions: Campbell and Bozorgnia (2003). Peak acceleration values for horizontal component rock site conditions.....	108
Figure 32a WNA empirical V/H ratios computed for M 7.69 at a suite of distances for soft rock site conditions: Abrahamson and Silva (1997). Peak acceleration values for horizontal component rock site conditions.....	109
Figure 32b WNA empirical V/H ratios computed for M 7.69 at a suite of distances for soft rock site conditions: Abrahamson and Silva (1997). Peak acceleration values for horizontal component rock site conditions.....	110
Figure 33a WNA empirical V/H ratios computed for M 7.69 at a suite of distances for deep firm soil site conditions: Abrahamson and Silva (1997). Peak acceleration values for horizontal component rock site conditions.....	111

Figure 33b WNA empirical V/H ratios computed for **M** 7.69 at a suite of distances for deep firm soil site conditions: Abrahamson and Silva (1997). Peak acceleration values for horizontal component rock site conditions.....112

Figure 34 Horizontal and vertical component UHRS at annual exceedance probabilities (AEP) 10^{-4} , 10^{-5} , 10^{-6} , yr^{-1} : Grand Gulf Nuclear Station Unit 3 (EOI, 2008).....113

Figure 35 V/H Ratio Based on Ratios of UHRS for Reactor Embedment at AEF 10^{-3} to 10^{-6}yr^{-1} (EOI, 2008).....114

OVERVIEW

As part of the acceptance review of the Grand Gulf Nuclear Station Unit 3 Combined License Application (COLA), the NRC identified the need for supplemental information regarding the specific application of Approach 3 in the Unit 3 COLA. In order to support the NRC Staff review, it was determined that supplemental information was required regarding the description of the Approach 3 methodology in final safety analysis report (FSAR) Section 2.5.2, and how the methodology was used with random vibration theory (RVT) to develop the final site ground motions. Therefore, this report presents and describes the detailed methodology used to develop horizontal and vertical hazard consistent site-specific uniform hazard response spectra (UHRS) at the Grand Gulf Nuclear Station Unit 3 site. The information presented in this technical report provides a detailed presentation of the analysis methodology, specifically addressing calculation approaches using RVT, development of location-specific UHRS using Approach 3 (described in NUREG/CR-6728, -6769), and incorporation of site-specific aleatory and epistemic variabilities in dynamic material properties. This document supplements the analysis results presented in FSAR Section 2.5.2 of the Grand Gulf Unit 3 FSAR.

The site-specific UHRS were computed at the reactor foundation level as free-field motions. As described in FSAR (Section 2.5.4; EOI, 2008) the site is located in the lower Mississippi Embayment and rests on over 10,000 ft of alluvium and sedimentary materials above pre-Cambrian hard rock basement material, for which the reference site probabilistic seismic hazard analysis (PSHA) was performed. To address this configuration, location-specific UHRS were developed for the Unit 3 reactor foundation, the location of the Unit 3 GMRS (FSAR Section 2.5.2.5; EOI, 2008). The UHRS analysis goal is to achieve site-specific response spectra which reflect the desired exceedance frequencies, or stated another way, preserve the reference site hazard level and result in full site-specific horizontal and vertical hazard curves. The analyses described in this report apply to the development of horizontal and vertical UHRS for Grand Gulf Nuclear Station Unit 3.

1.0 INTRODUCTION

In developing site-specific design response spectra, the standard approach involves, as a first step, a PSHA reflecting an outcropping reference site condition. The reference site condition typically is rock and for central and eastern North America (CENA) this reflects a theoretical shear-wave velocity over the top 1 km of the crust of 2.83 km/sec with a shallow crustal damping kappa value of 0.006 sec (EPRI, 1993). The shear-wave velocity is based on the empirical Mid-continent compressional-wave velocity model of Pakiser and Mooney (1989), taken by EPRI (1993) to represent the CENA, and an assumed Poisson ratio of 0.25. Since the 2.83 km/sec is a defined value, its range (over velocity and depth) could be developed, resulting in a realistic range in hard rock site conditions for which hard rock attenuation relations and resulting hazard directly apply.

The kappa value, which controls high frequency motions, is empirical and based on examining motions recorded at hard rock sites (Silva and Darragh, 1995). Subsequent to the reference site condition PSHA, adjustments are made to the resulting reference site UHRS to compensate for any significant differences in dynamic material properties that may exist between the local site (Table 1) and the reference site. In applying the adjustments,

* Site condition reflected in the attenuation relations used in the PSHA

the goal or objective is to achieve site-specific response spectra which reflect the desired exceedance frequencies, that is, preserve the reference site annual exceedance frequency (AEF) (hazard consistent). Typically the site-specific UHRS are computed as free-field motions at the ground surface, although other elevations or locations within a profile may be specified (Table 1).

In general, the overall approach involves two independent analyses. The first or initial computation is the development of relative amplification factors (5% damped response spectra) between the site of interest and the reference site ($S_a^{site}(f) / S_a^{reference}(f)$) that typically accommodates nonlinear site response. Currently the state-of-practice approach involves vertically propagating shear-waves and approximations using equivalent-linear analysis using either a time history method to compute maximum cyclic shear-strains (e.g., SHAKE) or a more computationally efficient frequency domain RVT method.

Subsequent to the development of the amplification factors, site-specific motions are computed by scaling the reference site motions with the transfer functions. In the past, purely deterministic methods have been used but these generally result in site-specific motions that reflect higher probability than desired. More recently, semi-deterministic methods have been developed to conservatively achieve desired hazard levels, still using a fundamentally deterministic method (NUREG/CR-6728). Along with these semi-deterministic methods, fully probabilistic methods were also developed that accurately preserve the reference site hazard level and result in full site-specific hazard curves. The fully probabilistic approaches represent a viable and preferred mechanism to properly incorporate parametric aleatory and epistemic variabilities and achieve desired hazard levels and performance goals.

This report presents an illustration of the two components used in the development of hazard consistent site-specific UHRS: RVT equivalent-linear site-response and fully probabilistic site-specific hazard analyses.

2.0 IMPLEMENTATION OF RANDOM VIBRATION THEORY (RVT) FOR SITE RESPONSE ANALYSES

RVT reflects a classical engineering method for estimating population mean peak time domain values based on a single root mean square (RMS) estimate of the response of a system, provided the system excitation reflects stationary random noise. The advantage of using the RVT formulation is that a large number of time domain analyses is not required to obtain stable estimates of mean response. The entire response analysis can be done in the frequency domain through the use of Parseval's relation (Boore, 1983). This relation is a direct correspondence between the Fourier amplitude spectra (FAS) or power spectral density (PSD), and the time domain root-mean-square response for any system parameter (acceleration, particle velocity, shear-strain, factor of safety against liquefaction, etc.). Specifically RVT provides a robust estimate of the time domain peak-to-RMS ratio (Boore, 1983). Multiplication of this ratio with the RMS computed with the Fourier amplitude spectra via Parseval's relation results in a mean estimate of the peak time domain value.

The combination of RVT and Parseval's relation then permits a single linear system analysis in the frequency (power spectral) domain resulting in an estimate of time domain response

that reflects a mean response over the entire population of time histories whose Fourier amplitude spectra match that of the system demand or load function. In other words, for a linear system, one which admits a frequency domain analysis and spectral superposition is appropriate (no transfer of energy between frequencies), RVT results in a peak time domain response for the entire population of phase spectra which can be associated with the PSD of the load function. In principle the load function must reflect random noise whose statistics do not vary with time (remain stationary). In applications to strong ground motions, e.g., acceleration or velocity time histories, clearly this does not appear to be the case as typical records show changes in amplitude and perhaps frequency content with time. However the randomness constraint is, fortunately, a weak constraint and extensive testing (e.g., Boore, 1983; Boore and Joyner, 1984; EPRI 1993; Silva et al., 1997; Boore, 2003) has shown the application to strong ground motion in terms of response spectra, peak acceleration, peak particle velocity, and peak shear-strains to be quite robust.

In general, for applications to site response and strong motion, RVT is used in two distinct places: 1) in estimating response spectra (oscillator time domain peak values) and peak particle velocities given a ground motion FAS and duration, and 2) estimating peak shear-strain time domain values given a shear-strain FAS and a duration.

2.1 RVT Durations

For both applications, estimating spectral accelerations and peak particle velocities as well as peak shear-strains, durations are taken as the inverse of the source corner frequency (Boore, 1983) with a distance-dependent term to accommodate the increase in duration due to wave scattering (Herrmann, 1985). For the Grand Gulf Nuclear Station Unit 3, Table 2 lists the point-source model parameters and durations used in developing site-specific amplification factors (Section 2.2.2.1.1) and V/H ratios (Section 4.1.1).

2.1.1 Peak-to-RMS Ratio

Several relations exist between the time domain RMS, estimated by integrating the PSD over frequency, and the corresponding peak time domain values (Boore, 1983; 2003). These relations reflect varying degrees of approximation in the peak-to-RMS ratio, increasing in complexity and accuracy as the number of extrema over the duration decreases. Boore (1983) illustrates a range in RVT ground motion parameter estimates computed using different approximations. The maximum range is about 10% for the extreme case of only 2 extrema ($M = 3.0$; Boore, 1983) over the source duration. Based on extensive comparisons of response spectra computed from time histories (referred to as single degree of freedom (SDF) spectra) with RVT estimates, an intermediate approximation is typically implemented. The intermediate approximation is an asymptotic expression for the peak-to-RMS ratio (Equation 24; Boore, 1983) and was used in the Grand Gulf Nuclear Station Unit 3 analyses.

To integrate the PSD, numerical integration is performed rather than analytical integration, as the PSD includes site response in addition to the FAS of the simple point-source model. Because the PSD is reasonably smooth, a simple and rapid Simpson's three-point scheme is implemented but with a very dense sampling to fully accommodate the presence of peaks and troughs. Typically 25,000 points are used from 0.007 Hz (about 150 sec) to 150 Hz. The wide integration range is to ensure inclusion of potential high- and low-frequency amplification. Additionally, the RMS is sensitive to the integration over low-frequency so it is

prudent to extend its range to at-least an order of magnitude below the lowest frequency of interest, 0.1 Hz for nuclear applications (e.g., Grand Gulf Nuclear Station Unit 3). For application to other types of structures (e.g., long-span bridges, liquid natural gas facilities, etc.) requiring estimates of motions to lower frequency, the integration range in Fourier Amplitude Spectra (FAS) is extended from 0.0001 Hz to 150 Hz.

2.1.2 Computation of RVT Response-Spectra

A number of procedures (equations) exist for computing response spectra (peak time domain oscillator amplitude). These equations accommodate the increasing non-stationarity of oscillatory time histories as oscillator frequency decreases. Non-stationarity becomes critical as oscillator frequency becomes lower than the source corner frequency. Under these conditions, the oscillator duration exceeds the source duration, severely violating the weak assumption of stationarity. For these cases, various correction procedures have been developed for RVT that reflect a range in computed response spectra of about 10%. Boore (2003) gives an excellent illustration of two very different correction procedures showing their similarity for both small and large magnitude earthquake sources. For applications to transfer functions, horizontal amplification factors and vertical-to-horizontal (V/H) ratios, differences in response spectra due to different corrections at low-frequency are cancelled through taking ratios, as long as the corrections are applied consistently.

In typical Western North America (WNA) and CENA, source durations (inverse corner frequency) scale with moment magnitude (**M**) such that for **M** 5, 6, and 7; durations are approximately 1, 3, and 9 seconds respectively. As a result, corrections only become important for oscillator periods below approximately 1, 3, or 9 seconds, depending on the magnitude used in generating the transfer functions.

Figure 1 shows an example comparison using 30 time histories from a finite fault simulation reflecting randomly selected model parameters (e.g., slip model, nucleation point, shear-wave velocity profiles etc.). Figure 1 compares median response spectra computed from time histories with RVT response spectra computed from the corresponding PSDs. In general, over the entire frequency range, the RVT spectrum agrees quite well with the SDF, reflecting a slightly smoother version. At low frequency, the RVT spectrum is slightly above the SDF spectrum.

An illustration that the correction effects are not an issue, as their impacts are cancelled in the ratios, is seen in the amplification factors at low-frequency (≤ 1 Hz) computed for a very shallow profile, to place the resonance at high-frequency (Figure 2). A range in loading levels (0.01g to 1.50g) was used to fully test the ratios over a wide range in nonlinearity. The amplification factors remain unity down to 0.1 Hz, nearly a factor of 10 lower than the source corner frequency for an **M** 5 source.

2.2 RVT-Based Equivalent-Linear Site-Response

The RVT site-response computational formulation that has been most widely employed to evaluate 1D site response assumes vertically-propagating plane shear-waves (S-waves). Departures of soil response from a linear constitutive relation are treated in an approximate manner through the use of the equivalent-linear formulation. The equivalent-linear formulation, in its present form, was introduced by Idriss and Seed (1968). A stepwise iterative analysis approach was formalized into a 1D, vertically propagating S-wave code

called SHAKE (Schnabel *et al.*, 1972). Subsequently, this code has become the most widely used and validated analysis package for 1D site response calculations.

Careful validation exercises between equivalent-linear and fully nonlinear formulations using recorded motions (peak horizontal acceleration) from 0.05g to 0.5g and a range in profile stiffness (soft, e.g., LoTung, Taiwan to firm, e.g., Gilroy 2, California; EPRI, 1993) showed little difference in results for response spectral ordinates (EPRI, 1993). Both formulations compared favorably to recorded motions suggesting both the adequacies of the vertically-propagating S-wave model and the approximate equivalent-linear formulation. While the assumptions of vertically propagating S-waves and equivalent-linear soil response represent approximations to actual conditions, their combination has achieved demonstrated success in modeling observations of site effects and represent a stable, mature, and reliable means of estimating the effects of site conditions on strong ground motions (Schnabel *et al.*, 1972; EPRI, 1988, 1993; Schneider *et al.*, 1993; Silva *et al.*, 1997).

It is clear the vertically propagating shear-wave approach cannot successfully model amplitudes to arbitrarily long periods at deep soil sites at large source distances, as this formulation does not consider horizontally propagating surface waves. It is not clear, however, under what circumstances (profile depth, source size and distance, and structural frequency) the 1D vertically propagating shear-wave model would under predict low-frequency motions. Validation exercises consisting of modeling recorded motions using the 1D approximation at deep soil sites in tectonically active regions suggest the simple model performs well in terms of spectral amplitudes to periods of at least several seconds (EPRI, 1993; Silva *et al.*, 1997; Hartzell *et al.*, 1999), periods long enough to accommodate nuclear facilities.

A clear advantage of the equivalent-linear vertically propagating shear-wave model is its simplicity, resulting ease of implementation, and transparency. Due to its computational efficiency, the modeling approach is easily able to accommodate site-specific aleatory and epistemic variabilities in dynamic material properties in design ground motions. This is accomplished by varying input parameters and computing the resulting motions. Unfortunately, to develop stable estimates of computed motions for each suite of parameters, multiple time histories (e.g., 5 to 15), each matched to the control motion response or Fourier amplitude spectra, must be analyzed. This is the case as peaks and troughs in response spectra as well as peak shear-strains are sensitive to the phase spectra of the control motion. For the traditional equivalent-linear formulation (e.g., SHAKE), since peak time domain shear-strains are used to iterate or soften the system (approximate nonlinear response), each time history results in somewhat different response, with the same dynamic material properties. The stacking (averaging) of responses necessary to achieve stability over multiple input time histories (all matched to the same control motion spectrum) renders the time domain (SHAKE) approach difficult to properly develop fully probabilistic design spectra.

As a practical alternative for the computation of site-response, the RVT based equivalent-linear approach (RASCALS) was developed (EPRI, 1988, 1993) and thoroughly validated (EPRI, 1993; Silva *et al.*, 1997). In this approach, which propagates an outcrop (control motion) power spectral density through a 1D soil column, RVT is used to predict peak time domain values of shear strain based upon the shear-strain power spectrum. The control

motion power spectrum is propagated through the 1D rock/soil profile using the plane-wave propagators of Silva (1976). Using RVT to provide an estimate of peak time domain shear-strains results in estimates that reflect, in a single run, the mean over the entire population of control motion phase spectra, conditional on a single control motion power or FAS. The computational efficiency of the RVT approach then easily allows the large number of site response analyses required to develop fully probabilistic hazard consistent design spectra as it precludes the use of the multiple time histories. For each suite of dynamic material properties, only a single site-response analysis is necessary, resulting in a mean system response over the population of phase spectra associated with the control motion PSD. Additionally, for amplification factors computed with any time domain site-response analysis procedure, the frequency-to-frequency and record-to-record variability in the computed soil response due to the time history propagation introduces additional variability. This additional variability reflects a double counting as frequency-to-frequency and record-to-record variability has already been accommodated in the aleatory variability in the attenuation relations used in developing the reference PSHA. Employment of an RVT approach, because the control motion reflects a smooth spectrum, properly neglects the frequency-to-frequency and record-to-record variability in response spectra computed from real or realistic time histories and avoids double counting of frequency-to-frequency and record-to-record variability in the computed site response.

In the RVT implementation for peak shear-strains, the simple asymptotic expression of Equation 24 in Boore (1983) is used (Section 2.2). Based on extensive validations, this simple approach adequately reflected peak shear-strains through the soil column resulting in close comparisons between SHAKE, nonlinear codes, and recorded motions (EPRI, 1993). Careful validation exercises in modeling motions recorded from 19 earthquakes at over 500 sites quantified the accuracy of the RVT equivalent-linear approach along with the use of a point-source model to characterize control motions (EPRI, 1993; Silva et al., 1997).

2.2.1 Amplification Factors

To generate amplification factors (site-specific soil S_a /reference S_a) which properly accommodate site-specific aleatory variability, a randomization process of dynamic material properties is typically implemented (EPRI, 1993) about a base-case profile. In this process, layer thickness and shear-wave velocity are randomized based on a correlation model resulting from an analysis of variance on over 500 measured shear-wave velocity profiles (EPRI, 1997). In this model, velocities are represented by a distribution at a given depth coupled to a correlation with depth, to prevent unrealistic random velocity excursions above and below a given layer. The layer thickness model is also based on measured profiles and replicates the overall observed decrease in velocity fluctuations as depth increases. This realistic trend is accommodated through increasing layer thicknesses with increasing depth. The correlation and layering model prevents unconservative profile realizations with uncorrelated velocity fluctuations over depth resulting in increased effective overall damping due to wave scattering at impedance boundaries (scattering κ). This condition is exacerbated at high loading levels due to nonlinearity, concentrating shear strains in low velocity layers. As a check on this possibility it is important to compare the median response spectrum over multiple realizations with that from a single analysis with base-case properties, at low (linear) loading levels. If the median spectrum falls below that computed using the base-case dynamic material properties at high frequency by more than about 5%, a significant amount of scattering κ has been added in the velocity randomization,

resulting in an overall larger kappa value than desired and unconservative high-frequency motions at low loading levels. This should then be compensated by appropriately lowering the kappa value in the control motions; another advantage of using a point-source model to generate control motions as it is not an unambiguous endeavor to adjust control motions developed from attenuation relations or spectral shapes (NUREG/CR-6728) for lower (or larger) kappa values.

In addition to velocity and layer thickness variations, depth to basement material (2.83 km/sec at Grand Gulf Nuclear Station Unit 3) is also typically randomized to cover the anticipated range over the site. For large impedance contrasts at the base of the soil, this variability smoothes the fundamental column resonance which may not be stable over multiple earthquakes (Silva et al., 1986) suggesting some degree of smoothing may be appropriate.

It is also essential to consider aleatory variability in nonlinear dynamic material properties both laterally across the site as well as vertically (where the same base-case properties are employed over a depth range). This variability in modulus reduction and damping curves is accommodated by assuming a log-normal distribution at a strain value where the curves are changing rapidly, 0.03%, randomly sampling a distribution and applying this perturbation to the base-case curves. The perturbation is tapered approaching the ends of the curves to preserve the shape of the base-case curves. Empirical sigma values, based on laboratory test of materials of the same general type (e.g., gravely sands) such that the G/G_{max} and hysteretic damping curves would be applied over depth ranges which boring logs or laboratory index property tests indicate appropriate, are 0.15 (σ_{ln}) and 0.30 (σ_{ln}) for modulus reduction and hysteretic damping respectively.

The G/G_{max} and hysteretic damping curves are randomized independently. Intuitively one may expect a random excursion to a more linear modulus reduction curve would be accommodated with a higher probability of a damping curves reflecting less damping. However, such intuition may be more properly associated with mean curves rather than random excursions about mean properties. Additionally, extensive tests with negatively correlated curves showed very little difference in the variability of computed motions. This result confirms the observation that hysteretic damping has a much less significant impact on computed motions than does modulus reduction. A given percentage change in G/G_{max} results in a much larger impact on computed motions than a similar percentage change in hysteretic damping. Shear-wave velocity affects both amplification as well as energy loss through the dependence of the energy loss term on wave velocity while hysteretic damping affects only energy loss. The overwhelming sensitivity of equivalent-linear site response is in the modulus reduction curves (Silva, 1992).

2.2.2 Control Motions

Control motions¹ (PSD) may be generated by use of the single-corner (and double-corner for the CENA) point-source model reflecting the magnitude contribution to the hazard. With this approach motions are generated for reference site-conditions as well as local site-conditions by propagation from the source to the site (EPRI, 1993). Implicit in this approach

¹ Control Motion: Motion used as input to site response analyses. This can be reflected in time histories matched or scaled to a response spectrum or, in the case of RVT, a PSD.

is the validity of the point-source ground motion model in terms of spectral shape. Validations of the point-source model (EPRI, 1993; Silva et al., 1997; Boore, 2003) have shown the model produces realistic response spectra for a wide range in M , distance, and site-conditions. These validation exercises have demonstrated the appropriateness of the model to serve as control motions for site-response analyses and resulted in the use of the model in developing hard rock response spectral shapes and V/H ratios for the CENA (NUREG/CR-6728). A limitation of the model is its demonstrated over prediction of low-frequency response spectra at large M ($M \geq 7.0$) and at close distances (≤ 20 km) in the WNA (Silva et al., 1997). This observation led Atkinson and Silva (1997) to introduce a double-corner source model for large M WNA earthquakes. For the CENA, the appropriateness of the single- or double-corner source models remains an unresolved issue with most CENA attenuation relations based on the point-source model with the implied assumption the single-corner source model is appropriate for large magnitude earthquakes in CENA (EPRI, 2004). Uncertainty in single-verses double-corner models results in the recommendation of computation of amplification factors using both models and combining the resulting hazard curves with the same relative weights as used in developing the reference (e.g., hard rock) PSHA.

For applications to the WNA, rock control motions may be generated using empirical attenuation relations, after adjusting the surface outcrop motions to base-of-soil conditions (NUREG/CR-6728). Alternatively, the point-source single-corner frequency model may be used with M limited to about M 7.0 for deep soil sites to avoid overdriving the soil column at low-frequency (< 1 Hz). Alternatively or in conjunction, the WNA double-corner source model (Atkinson and Silva, 1997) may be used as control motions. Use of the point-source models reflects computational efficiency as it avoids the intermediate step of spectral matching to the empirical spectra, which are not well constrained for all M at distances exceeding about 100 km.

2.2.2.1 Effects of Spectral Shape

In the development of amplification factors, the shape of the control motion spectrum plays an important role due to nonlinearity in the site-response. In general, spectral shape is controlled by three factors: magnitude (through the source corner frequency), single-verses double-corner source spectra, and distance (through depletion of high-frequency energy as distance increases) (Silva and Green, 1989; Silva et al., 1997). In principle all three dependencies in control motion spectral shape should be accommodated in developing amplification factors. Accommodating these potential dependencies on control motion spectral shape would result in development of hundreds of mean amplification factors at a fine discrete grid of values for M , e.g., every 0.1 unit in M , and in distance, e.g., every 1 to 2 km in distance over the ranges of contributions to the reference hazard. For the CENA, separate suites of amplification factors computed for both single- and double-corner source models would be required as well. However, the actual dependencies have been examined through sensitivity analyses, resulting in general guidelines in magnitude and distance dependencies that produce significant ($\geq 10\%$) differences in mean amplification factors.

For deterministic approaches in developing site-specific UHRS (Section 3, Approaches 1 and 2), typically only two magnitudes and associated distance are used reflecting the high-frequency (5 Hz to 10 Hz) and low-frequency (1 Hz to 2.5 Hz) contributions to the reference hazard (NUREG/CR-6728). However, for the fully probabilistic approach to developing site-

specific UHRS (Section 3, Approach 3), a wide range in levels of reference site spectra is required as the entire reference (e.g., hard rock) hazard curve has contributions to each point (exceedance frequency) on the site-specific (e.g., soil) hazard curve. Typically the range in levels of reference site spectra is accommodated through a suite of expected reference site peak acceleration values, conditional on **M**, generated by varying source distances (Table 2). This approach then is intended to naturally accommodate any dependence on distance in the amplification factors due to the effects of distance on control motion spectral shape.

2.2.2.1.1 Effects Of Spectral Shape On Grand Gulf Amplification Factors

To illustrate effects of control motion loading level, amplification factors were computed for the Grand Gulf Nuclear Station Unit 3 reactor embedded profile 1 (Figures 3a and 3b) using **M** 6.25 and **M** 7.69 single-corner-frequency source models. The suite of four base-case shear-wave velocity profiles reflect epistemic variability, uncertainty in mean velocities, near the maximum depth of measurements as well as beyond. The site, located in the lower Mississippi Embayment, rests on over 10,000 ft of alluvium and sedimentary materials above pre-Cambrian basement (hard rock reference site material). Figure 3b illustrates the multiple extrapolations to basement material which were based on a generic Embayment profile. The depth to basement (1 km, Figure 3b) was taken to include amplification to the lowest frequency for which reference site hazard was defined, 0.5 Hz. The development of the base-case profiles is presented in FSAR Section 2.5.4.7.1 (EOI, 2008) with the reactor embedded profiles reflecting conditions at a depth of about 65 ft (FSAR Section 2.5.4.7.3; EOI, 2008). Figures 3a and 3b represent the profiles for which the ground motion response spectrum (GMRS) was computed (FSAR Section 2.5.2.5; EOI, 2008). For the reactor embedded profile presented herein, the upper 65 ft. were not considered in this analysis.

Nonlinear dynamic material properties were based on laboratory dynamic testing and resulted in two sets of site-specific modulus reduction and hysteretic damping curves (FSAR Section 2.5.4.2.2.3; EOI, 2008). The first set of curves were based directly on the laboratory dynamic testing while the second set reflects a minor adjustment for the effects of confining pressure (FSAR Section 2.5.4.2.2.3; EOI, 2008). Both sets of G/G_{max} and hysteretic damping curves result in varied ground motions (FSAR Section 2.5.2.4.2.1.6; EOI, 2008).

Figures 4a and 4b show median and ± 1 sigma estimates of the amplification factors. The magnitude range is intended to capture the contributing sources to the hazard over the structural frequency range of 0.5 Hz to 100 Hz and AEF 10^{-3} to 10^{-6} , the dominant contributors to mean hazard at AEF 10^{-4} and 10^{-5} (Section 3.4.2.3.1). Reference site (hard rock, Table 2) expected peak accelerations range from 0.01g to 1.50g (at 11 discrete values). Corresponding distances range from about 200 km to 0 km (4 km depth) for **M** 6.25 and about 400 km to 6 km for **M** 7.69 (Table 2). Reference site motions (5% damped response spectra) are developed at the surface of the hard rock profile with a point-source spectrum at depth (Table 2) while corresponding site-specific soil motions are developed by placing the local profile (Figures 3a and 3b) on top of the hard rock crustal model. Point-source model parameters are listed in Table 2. As Figure 4 clearly shows, at frequencies exceeding about 2 Hz, amplification decreases as loading levels increase due to nonlinearity. Also apparent, at high frequency, is a moderate increase in sigma with

* Median estimates

increasing loading levels (e.g., compare 0.10g with 1.00g in ranges between the 16th and 84th percentiles). This is due to the inclusion of aleatory variability through the randomization of modulus reduction and hysteretic damping curves. As loading levels increase, nonlinearity becomes more important, appropriately reflecting a larger total aleatory variability.

Also apparent in Figures 4a and 4b are the large deamplification at very high loading levels reaching a minimum for the median at about 30 Hz between 0.3 and 0.2. The minimum value shown in Figure 4 of about 0.2 to 0.3 may be a result of the equivalent-linear approximation, using a single value of shear-wave velocity and damping at all frequencies. Based on empirical attenuation relations (e.g., Abrahamson and Shedlock, 1997), the minimum for observations available through 1997 is about 0.5. As a result, a minimum amplification of 0.5 is implemented.

An important feature in Figures 4a and 4b are the large difference in high frequency (≥ 10 Hz) amplification factors at low loading levels (0.01g to 0.10g) between **M** 6.25 (Figure 4a) and **M** 7.69 (Figure 4b). This difference is due to the effect of distance on CENA hard rock spectral shapes and is illustrated more clearly in the following discussion on the effect of magnitude on amplification factors.

To illustrate the effect of magnitude on amplification factors, Figure 5a compares median amplification factors computed for **M** 6.25 and **M** 7.69 while Figure 5b shows factors computed for **M** 5, 6, and 7, all for the same Grand Gulf Nuclear Station Unit 3 reactor embedded profile 1 (Figures 3a and 3b). As with Figures 4a and 4b, control motions were generated with the single-corner-frequency point-source model. At low levels of motion, 0.01g to 0.10g, there is a strong **M** dependency at high-frequency (≥ 20 Hz). This is principally due to distance effects, depleting the larger **M** high-frequency control motion. This observation is due to the increased width of the oscillator transfer function as oscillator frequency increases. At the large distances for **M** 6 and **M** 7 (beyond 200 km and 300 km respectively), the Fourier amplitude spectrum is severely depleted at high-frequency. As a result, the high-frequency oscillators are driven by low-frequency amplitudes such that the amplification factors reflect lower frequency values. This is precisely the same phenomenon which causes response spectral acceleration to saturate to peak acceleration at high frequency. While these **M** dependencies due to distance are quite large at high-frequency, they become insignificant at frequencies of interest (≤ 30 Hz) for loading levels of concern (above 10%g).

To show the effects of distance on the control motions (hard rock site condition reference) spectral shapes implied in developing the amplification factors, Figures 6a and 6b compare median shapes computed at the surface of the hard rock profile (Table 2) for **M** 6.25 (Figure 6a) and **M** 7.69 (Figure 6b). For **M** 6.25, the effects of a 200 km distance on spectral shape is dramatic shifting the peak spectral acceleration from over 30 Hz to the 3 Hz to 5 Hz range. With the point-source parameters listed in Table 2, the 5 Hz Fourier amplitude is reduced by a factor of two due to inelastic attenuation with higher frequencies suffering an even larger reduction. This reduction has the same effect as kappa, shifting the spectral peak to lower frequency as kappa increases (Silva and Darragh, 1995). For **M** 6.25 (Figure 6a) and **M** 7.69 (Figure 6b), it appears the typical CENA hard rock spectral shape returns at distances

within about 100 km, expected peak accelerations of exceeding about 5%g and 20%g for **M** 6.25 and **M** 7.69 respectively.

This observation of distance dependency at low levels of motion also points out a possible limitation of the CENA spectral shapes in NUREG/CR-6728. For consistency with the empirical WNA shapes, the CENA shapes were defined only to a distance of 200 km. Use of these shapes for larger distances will likely result in too much high-frequency energy and unconservative amplification factors at low levels of motions and at high-frequency.

As the sensitivity of magnitude on amplification factors is important in accommodating the magnitude deaggregation in site response, a further illustration is presented in Figure 7, for a till-like site which consists of about 1,000 ft of 1,500 ft/sec very dense silty sands. Figure 7 shows trends quite similar to those of the Grand Gulf profile (Figures 3a and 3b) with a slightly stronger magnitude dependency beyond about 5 Hz at the higher loading levels (e.g., $\geq 0.40g$). These two profiles, Grand Gulf Unit 3 profile 1 and the till-like profile, are representative of the typically stiff soils underlying foundations at nuclear power stations and illustrate the general trends in magnitude dependencies on amplification factors.

Of significance for the development of UHRS for nuclear facilities is the range in median amplification over the 1 Hz to 20 Hz range for **M** 5, 6, and 7 shown in Figures 5b and 7. In general, for loading levels up to about 0.75g which covers the range of interest for AEF of 10^{-4} and 10^{-5} over most of the CENA, the range in amplification is about 10% to 20% for a unit change in magnitude. Based on sensitivity analyses such as these as well as the observation of Bazzurro and Cornell (2004) of an even weaker magnitude dependency, from analyses with recorded motions, a conservative guideline for accommodation of magnitude dependencies in the reference hazard deaggregation is about one half magnitude unit. That is, one should maintain the model magnitudes as a function of structural as well as exceedance frequency from the reference deaggregation to a precision of about one half magnitude unit. This approximation recognizes both the magnitude dependency of amplification factors as well as the range in magnitudes contributing to the reference hazard at a given structural and exceedance frequency. Use of the mode is clearly more appropriate than the mean, even though there is rarely a single peak over magnitude. Also, in the context of Approach 3 as it involves integration of the entire hard rock (reference) hazard curve with the amplification factors (Section 3), magnitude contributions for AEF ranging from about 10^{-3} to 10^{-6} , the dominant contributors to AEF 10^{-4} and 10^{-5} , should be considered in development and application of amplification factors. These results point out the inappropriateness of simply scaling control motions up and down to reflect either different magnitude sources or different distances, conditional on magnitude.

To illustrate the potential effects of source processes on amplification factors in the CENA in terms of single- versus double-corner source spectra, Figures 8a and 8b show a comparison of median amplification factors computed for the same suite of expected horizontal hard rock (reference) peak acceleration values and using the Grand Gulf Unit 3 reactor embedded profile 1 (Figures 3a and 3b). Figure 8a shows the comparison for **M** 6.25 while Figure 8b has the comparison for **M** 7.69. As with the magnitude dependencies shown in the low loading levels in Figures 5b and 7, the differences between the amplification factors computed for **M** 6.25 and **M** 7.69 at 0.01g are likely due to the differences in distance (some 200 km and 400+ km for **M** 6.25 and **M** 7.69 respectively, Table 2). Similar trends are seen

in the differences between amplification factors computed with single- and double-corner source models for **M** 6.25 and **M** 7.69. A slightly greater difference exists at **M** 7.69 as the differences in source spectra between the two models (single- versus double-corner frequency) increases with increasing magnitude (Atkinson, 1993). To provide more generality in assessing the impacts of CENA source processes on computed amplification factors, Figure 9 shows comparison using **M** 7.0 and the same generic CENA deep stiff soil used in Figure 7 illustrating magnitude dependencies. In general the trends in the differences are quite similar to those shown in Figure 8b with **M** 7.69 and the site-specific Grand Gulf Unit 3 profile (Figures 3a and 3b). Of significance are the differences in median amplification factors at higher loading levels ($> 0.20g$) in the 1 Hz to 30 Hz frequency range. In this frequency range, considering both profiles, the differences steadily increase from about 5% to 10% around 0.2g to 0.3g to over 20% at 0.75g, with the amplification factors computed with the two-corner model exceeding those computed with the single-corner source model. For the generic profile, the converse is true below the fundamental column resonance near 0.2 Hz. These trends are a result of lower intermediate frequency source spectra for the double-corner source model compared to the single-corner model (NUREG/CR-6728). This results in lower loading levels, more linear response, for the double-corner model, leading to larger intermediate frequency amplification and less of a shift the fundamental column resonance to lower frequency. It is important to point out this effect would be greater for larger magnitudes as well as less for smaller magnitudes, becoming insignificant for magnitude less than about 5.25. This can be appreciated by comparing response spectral shapes illustrated in NUREG/CR-6728 as the spectral sag of the double-corner source model largely disappears at **M** 5.0.

To provide a further illustration of the impacts of magnitude and source processes on median amplification factors as well as their associated aleatory variabilities computed for the Grand Gulf Unit 3 profile 1 (Figures 3a and 3b), Figures 10, 11a and 11b show results plotted versus reference (hard rock) response spectra for selected frequencies (100 Hz, 10 Hz, and 1.0 Hz). These plots display the factors and standard deviations in the manner of which they are implemented in the fully probabilistic approach to developing site specific UHRS (Section 3.0). Figure 10 shows the effects of control motion magnitude (**M** 5, 6, 7, 7.69) on median amplification factors and their aleatory variabilities conditional on the reference spectral acceleration. The range in loading level (0.01g to 1.50g) is seen in the frame for 100 Hz (peak acceleration by definition). The corresponding ranges in 10 Hz and 1 Hz hard rock response spectra are displayed in the corresponding frames. Figure 10 illustrates the smooth nature of the factors and their aleatory variabilities as well as the clear magnitude and loading level dependencies. The overall smoothness of the amplification factors and standard deviations is important as linear (log) interpolation is used to develop estimates between the discrete loading levels (e.g., Table 2).

As previously mentioned, the positive slope of the sigma values reflects the important impact of the aleatory variability in the randomization of the G/G_{max} and hysteretic damping curves. As loading level increases, nonlinear dynamic material properties exert more of an influence (become more important) on computed motions. As expected, peak acceleration has the lowest variability. Empirically, peak acceleration is the most stable and therefore most accurately known strong ground motion parameter (Abrahamson and Shedlock, 1997). The decrease in variability with increasing magnitude and increasing loading level is also expected. Larger magnitude sources are statistically stable (stationary) for longer durations

and, as loading level increases, nonlinearity tends to buffer or reduce fluctuations or variability in response. At low levels of loading, doubling control motions may double soil peak acceleration while at high loading levels, due to nonlinearity, doubling control motions increases soil motions by a smaller degree.

Completing the illustration, Figures 11a and 11b show a similar comparison between single- and double-corner source models for **M** 6.25 (Figure 11a) and **M** 7.69 (Figure 11b). As with Figure 10, similar trends are shown for the double-corner source model, smooth variation of median amplification and aleatory variability with variations in loading levels.

Alternatively, in lieu of the point-source model, the spectral shapes of NUREG/CR-6728 may be used as hard (CENA, single- and double-corner) rock or soft (WNA) rock (adjusted for base-of-soil conditions, NUREG/CR-6728) control motions. For use in the RVT equivalent-linear analyses, an RVT spectral match is performed generating a FAS whose RVT response spectrum matches the target or appropriate spectral shape (NUREG/CR-6728). In use of the NUREG/CR-6728 spectral shapes for CENA control motions, as previously discussed, care should be taken at low loading levels (large distances) in assessing amplification factors as the shapes may not adequately accommodate the shift in peak spectral acceleration at large distances. As another alternative for control motions, the attenuation relations used in developing the reference PSHA may be used, provided the reference site condition is rock and for soft outcropping rock, the resulting rock spectra are adjusted for base-of-soil conditions (NUREG/CR-6728). With this approach, separate amplification factors should be developed using spectra computed for each attenuation relation as control motions to accommodate potential epistemic variability in site-response due to the differences in spectral shape among the attenuation relations. The resulting amplification factors should then be combined with the same relative weights as used in developing the reference PSHA. Additionally, for the CENA, amplification factors computed for the single- and double-corner source models should be combined with the same relative weights as used in developing the reference PSHA.

3.0 APPROACHES TO DEVELOP SITE-SPECIFIC HAZARD

In developing site-specific UHRS or hazard there are two goals which must be met to achieve desired risk levels:

- 1) Preserve the hazard level (AEF) of the reference site PSHA across structural frequency (hazard consistent),
- 2) Incorporate site-specific aleatory (randomness) and epistemic (uncertainty) variabilities of dynamic material properties in the hazard.

3.1 Description of Approaches

In general there are four fairly distinct approaches intended to accomplish the stated goals. The approaches range from the simplest and least accurate (Approach 1), which scales the reference site UHRS on the basis of a site-response analysis using a broad-band control motion to the most complex and most accurate, a PSHA computed using attenuation relations, median estimates and standard deviations, developed for the specific-site (Approach 4).

Approach 1: This approach is fundamentally deterministic and involves, for a rock reference site, use of the outcrop UHRS to drive the site-specific column(s). By definition it assumes a rock outcrop hazard (UHRS) has similar characteristics as rock beneath soil, not generally a valid assumption for soft rock (NUREG/CR-6728), and has no mechanism to conserve the outcrop AEF. For cases where the hazard is dominated by earthquakes with significantly different M at low (e.g., ≤ 1 Hz to 2.5 Hz) and high (e.g., ≥ 5 Hz to 10 Hz) structural frequencies, the outcrop UHRS may be quite broad, unlike any single earthquake, resulting in unconservative high-frequency motions (too nonlinear in site response). Even if only a single earthquake is the major contributor at all structural frequencies, variabilities incorporated in the hazard analysis may result in a broad spectrum, again unlike any single earthquake. For these reasons, this approach is discouraged and Approach 2, an alternative semi-deterministic method may be used.

Approach 2: This approach is also fundamentally deterministic and is intended to avoid the broad-band control motion of Approach 1. For a rock reference site, Approach 2 uses low- and high-frequency (and intermediate if necessary) deterministic spectra computed from the attenuation relations used in the PSHA, or suitable spectral shapes (NUREG/CR-6728), reflecting expected rock conditions beneath the local soils, scaled to the UHRS at the appropriate frequencies (e.g., RG 1.165). These scaled motions, computed for the modal deaggregation M and D are then used as control motions to develop multiple (typically 2 to 3) mean transfer functions based on randomized soil columns. If the control motions are developed from the attenuation relations used in the reference PSHA, the generic site condition they reflect must be appropriate for the rock beneath the local soils. Additionally, separate control motions should be developed for each attenuation relation to include the effects of spectral shape uncertainty (epistemic) on soil response. The resulting mean transfer functions would then be combined using the same relative weights as in the reference PSHA. The mean transfer functions are then enveloped with the resulting transfer function applied to the outcrop (rock or soil) UHRS. This method was termed Approach 2A in NUREG/CR-6728. The use of mean (rather than median) transfer functions followed by enveloping is an empirical procedure to conservatively maintain the outcrop exceedance probability (NUREG/CR-6728, 6769), as this fundamentally deterministic approach does not include the contributions to soil spectra from the entire range in rock or reference site hazard (Bazzurro and Cornell, 2004). The motivation for this "empirical" procedure is discussed in Section 3.3 (Approach 3 – Approximate Method).

For cases where there may be a wide magnitude range contributing to the hazard at low- or high-frequency and/or the site has highly nonlinear dynamic material properties, low, medium, and high M control motion spectra may be developed at each frequency of interest (e.g., 1.0 Hz to 2.5 Hz, 5.0 Hz to 10.0 Hz, and others as needed; NUREG/CR-6728). A weighted mean transfer function (e.g., weight of 0.2, 0.6, 0.2 reflecting 5%, mean, 95% M contributions) is then developed at each structural frequency of interest. Following Approach 2A, the weighted mean transfer functions for each frequency of interest are then enveloped with the resultant applied to the outcrop UHRS. This more detailed analysis procedure was termed Approach 2B.

Approach 3: This approach is a fully probabilistic analysis procedure which moves the site response, in an approximate way, into the hazard integral. The approach is described by Bazzurro and Cornell (2004) and NUREG/CR-6769. In this approach, the hazard at the soil

surface is computed by integrating the site-specific hazard curve at the bedrock level with the probability distribution of the amplification factors (Lee *et al.*, 1998; 1999). The site-specific amplification, relative to CENA rock (in the case of the Grand Gulf Nuclear Station Unit 3), is characterized by a suite of frequency-dependent amplification factors that can account for nonlinearity in soil response. Approach 3 involves approximations to the hazard integration using suites of transfer functions, which result in complete hazard curves at the ground surface, or any other location, for specific ground motion parameters (e.g., spectral accelerations) and a range of frequencies.

The basis for Approach 3 is a modification of the standard PSHA integration:

$$P[A_S > z] = \iiint P\left[AF > \frac{z}{a} \mid m, r, a\right] f_{M,R|A}(m, r; a) f_A(a) dm dr da \quad (1)$$

where A_S is the random ground motion amplitude on soil at a certain natural frequency, z is a specific level of A_S , m is earthquake magnitude, r is distance, a is an amplitude level of the random reference site (e.g., hard rock) ground motion, A , at the same frequency as A_S , $f_A(a)$ is derived from the rock hazard curve for this frequency (namely it is the absolute value of its derivative), and $f_{M,R|A}$ is the deaggregated hazard (i.e., the joint distribution of M and R , given that the rock amplitude is level a). AF is an amplification factor defined as:

$$AF = A_S/a \quad (2)$$

where AF is a random variable with a distribution that can be a function of m , r , and a . To accommodate epistemic uncertainties in site dynamic material properties, multiple suites of AF may be used and the resulting hazard curves combined with weights to properly reflect mean hazard and fractiles.

Soil response, in terms of site amplification ($S_a(\text{site})/S_a(\text{reference})$), is controlled primarily by the level of rock motion and m , so Equation 1 can be approximated by:

$$P[A_S > z] = \iint P\left[AF > \frac{z}{a} \mid (m, a)\right] f_{M|A}(m; a) f_A(a) dm da \quad (3)$$

where r is dropped because it has an insignificant effect in most applications. To implement Equation 3, only the conditional magnitude distribution for relevant amplitudes of a is needed. $f_{M|A}(m; a)$ can be represented (with successively less accuracy) by a continuous function, with three discrete values or with a single point, (e.g., $m^1(a)$, the model magnitude given a). With the latter, Equation 3 can be simplified to:

$$P[A > z] = \int P\left[AF > \frac{z}{a} \mid a, m^1(a)\right] f_A(a) da \quad (4)$$

where, $f_{M|A}(m; a)$ has been replaced with m^1 derived from deaggregation. With this equation, one can integrate over the rock acceleration, a , to calculate $P[A_S > z]$ for a range of soil amplitudes, z .

It is important to note there are two ways to implement Approach 3. The full integration method described below or simply modifying the attenuation relation ground motion value during the hazard analysis with a suite of transfer functions (Cramer, 2003). Both implementation result in very similar site-specific hazard (Cramer, 2003) and both will tend to double count site aleatory variability, once in the suite of transfer function realizations and again in the aleatory variability about each median attenuation relation. The full integration method tends to lessen any potential impacts of the large total site aleatory variability (Bazzurro and Cornell, 2004). Approximate corrections, for the site component of aleatory variability, may be made by implementing the approximate technique (Equation 7, Section 3.3) with $C = 0$, $AF = 1$, and a negative exponential, where a_{rp} = the soil amplitude and σ the

component of variability that is removed. For the typical aleatory variability of the amplification factors ($\sigma_{ln} \approx 0.1-0.3$ e.g., Figures 5 and 6) and typical hazard curve slopes in the CENA ($\kappa \approx 2-3$, Figure 13, the reduction in motion is about 5% to 10%.

Approach 4: Approach 4 entails the development and use of site-specific attenuation relationships, median estimates and aleatory variabilities, developed specifically for the site of interest which incorporate the site response characteristics of the site. The PSHA is performed using these site-specific relationships for the specified AEF. This approach is considered the most accurate as it is intended to accommodate the appropriate amounts of a aleatory variability into site and region specific attenuation relations. Epistemic variability is appropriately captured through the use of multiple attenuation relations. Approach 3 is considered as a fully probabilistic approximation to Approach 4.

3.2 Approach 3 – Full Integration Method

The site-specific hazard curve can be calculated using the discretized form of Equation 3 from Bazzurro and Cornell (2004).

$$G_z(z) = \sum_{all\ x_j} P\left[Y \geq \frac{z}{x} \middle| x_j\right] p_x(x_j) = \sum_{all\ x_j} G_{Y|X}\left(\frac{z}{x} \middle| x_j\right) p_x(x_j) \quad (5)$$

where $G_z(z)$ is the sought hazard curve for $S_a^s(f)$, that is, the annual probability of exceeding level z .

$$G_{Y|X}\left(\frac{z}{x} \middle| x\right) = \hat{\Phi} \left(\frac{\ln\left[\frac{z}{x}\right] - \ln\left[\hat{m}_{Y|X}(x)\right]}{\sigma_{\ln Y|X}} \right) \quad (6)$$

where $G_{Y|X}$ is the complementary cumulative distribution function of (CCDF) $Y = AF(f)$, conditional on a rock amplitude x . This is simply the CCDF of the site amplification factors as a function of control motion (e.g., rock or reference site) loading level.

$\hat{\Phi} = 1 - \Phi$ - the widely tabulated complementary standard Gaussian cumulative distribution function.

$\hat{m}_{Y|X}$ - the conditional median of Y (the amplification factor).

$\sigma_{\ln Y|X}$ - the conditional standard deviation of the natural logarithm of Y (aleatory variability of the amplification factor).

$p_X(x_j)$ - the probability that the rock or reference site control motion level is equal to (or better, in the neighborhood of) x_j .

Equation 5 is the essence of Approach 3 and simply states that the soil hazard curve is computed as the product of the soil amplification (specifically its CCDF), conditional on a reference (rock) amplitude x , times the probability of obtaining that reference amplitude, summed over all reference amplitudes.

The soil amplifications, median and σ_{\ln} estimates are all that is required and are generated by driving the soil column at a suite of reference site motions (Section 2.2). At each reference motion, multiple realizations of randomized dynamic material properties are developed followed by site response analyses to generate a suite, typically 30 to 100 (Section 3.4.1), of amplification factors. From that suite, a median and σ_{\ln} is computed, generally assuming a log-normal distribution.

The probability of obtaining a reference motion is simply the derivative of the reference (e.g., rock) hazard curve obtained from the PSHA. This is done numerically and is a stable process as the hazard curves are quite smooth. Equation 5 can quite easily be put into an EXCEL spread sheet. Approach 3 is indeed, one simple equation.

3.3 Approach 3 – Approximate Method

An alternative solution to Equation 4 can also be calculated using Equation (7) from Bazzurro and Cornell (2004). This is a closed form approximation of the integration of the amplification factor over a range of rock amplitudes.

$$z_{rp} = a_{rp} \overline{AF}_{rp} \exp\left(\frac{\sigma_{\delta}^2}{2} \frac{\kappa}{1-C}\right) \quad (7)$$

where z_{rp} is soil amplitude z associated with return period r_p ; a_{rp} is the reference spectral acceleration a associated with return period r_p ; \overline{AF}_{rp} is the geometric mean (mean log) amplification factor for the reference (e.g., rock) motions with return period r_p ; κ is the log-log slope of the reference hazard curve that is calculated at each point from the reference hazard curve and typically ranges from about 2 to 3 for CENA and possibly as large as 6 for WNA. C is the log-log slope (absolute value) of the amplification factor with respect to the reference motion that is calculated at each point from the amplification factors, AF and is a measure of the degree of soil nonlinearity. If $C = 0$, the response is linear and highly nonlinear for C approaching 1, where the approximation breaks down (Bazzurro and Cornell, 2004). As previously mentioned, C typically ranges from about 0.1 to about 0.8 (Bazzurro and Cornell, 2004). The log standard deviation of the AF, σ_{δ} , is typically around 0.3 (σ_{\ln}) or less (Figures 10, 11a, and 11b). In other words, at a given AEF or point on the

reference site hazard curve, the corresponding soil amplitude is given as the median soil amplification times the rock or reference site amplitude plus an exponential factor.

The exponential factor is necessary to maintain the reference AEF and accommodates both the aleatory variability as well as the degree of nonlinearity of the site amplification. The slope of the reference hazard curve is a weighting factor that includes the contributions to the soil amplitude for all reference hazard levels. Equation 7 clearly demonstrates the additional factors needed over median amplification to preserve the hazard level (AEF) of the reference motion. This equation shows that in order to preserve the reference site (e.g., rock) hazard level, multiplying the reference motion by the median soil amplification requires an additional exponential term. This additional term includes the aleatory variability of the soil or amplification factor, the slope of the reference site hazard curve, as well as the slope of the amplification factors (e.g., with varying reference motion). This exponential factor accommodates the potential contributions to a given soil motion by the entire range in reference site motions due to soil nonlinearity. That is, a given soil motion may have the same value at low levels of reference loading (relatively linear response) and at high loading levels (relatively nonlinear response). To preserve the reference site exceedance frequency, all the contributions to a given soil motions over the entire range in reference loading levels must be included in the soil hazard. These contributions are not explicitly considered in the deterministic Approach 2 method. Additionally, the effects of aleatory variability in the soil amplification due to lateral variability in velocities and depth to basement as well as randomness in G/G_{\max} and hysteretic damping curves are included in the exponential term. For a linear site, C is zero so it is easy to see the exponential term then accommodates the effects of profile variability in the soil hazard. The reference hazard curve slope (κ in Equation 7) is present to accommodate the impacts of the soil variability and nonlinear amplification over the entire reference site motion or hazard curve. In the case $C = 0$ and for a reference hazard slope near 1, the median amplification times the exponential term simply reflects the mean, for a lognormal distribution. This was the motivation for using mean, rather than median amplification factors in Approach 2. However, for more realistic reference site hazard curve slopes, use of the mean amplification alone will result in motions that are too low for the assumed AEF. The difference or underestimate increases as soil nonlinearity, characterized through C , becomes larger for a given aleatory variability in the amplification factors. This was the motivation for the "empirical" correction in Approach 2 of enveloping the low- and high-frequency transfer functions. The high-frequency transfer function will typically have lower high-frequency amplification than the low-frequency amplification factor as it reflects higher loading levels, resulting in a higher degree of nonlinearity, and a greater value of C . Use of mean amplification alone may then depart significantly from Equation 7 resulting in higher probability motions than would be consistent with the reference hazard level, depending on the value of C and the slope of the reference hazard curve. Using an envelope of the low-frequency amplification, which typically does not reflect nearly as high loading levels at high-frequency, and the high-frequency amplification was an ad-hoc manner of conservatively achieving the desired AEF using deterministic analyses.

It is important to point out that a similar issue, though less significant, can occur at low-frequency. In this case the high-frequency amplification has larger low-frequency amplification than the low-frequency amplification. The envelope at low-frequency is then

controlled by the high-frequency amplification, compensating for the neglect of the complete exponential in the low-frequency mean amplification (NUREG/CR-6728).

3.4 Implementation of Approach 3

Approach 3 is implemented using the full integration method which consists simply of coding Equation 5. The soil (or rock) amplification distributions relative to the reference site condition are developed by driving the site-specific column at a suite of distances generated on a grid of expected reference site peak accelerations (Table 2), to accommodate nonlinear soil response. At each distance, or reference site expected peak acceleration, random suites of dynamic material properties are generated resulting in a distribution of structural frequency dependent amplification factors ($S_a(\text{site})/S_a(\text{reference})$). For a given structural frequency, say 1 Hz, this process results in median and sigma estimates, for each loading level, from which a complementary cumulative distribution function (CCDF) is produced using standard asymptotic expressions, accurate typically to the fourth decimal place. For each loading level, reference S_a at 1 Hz, the amplification CCDF is then available to integrate over the entire 1 Hz hazard curve. This is precisely the motivation for the wide range in reference peak accelerations, 0.01g to 1.50g (Table 2), to cover the entire reference hazard curve for each structural frequency. For reference site motion outside the range, the closest values are used. To minimize any error in interpolation (log) for reference site motions between grid points (Table 2), a dense sampling of typically 11 values of expected reference site peak accelerations are used. The array of peak accelerations is sampled more densely over the range in values contributing most to the hazard, typically 0.2g to 0.5g. Since the amplification factors are smooth (e.g., Figures 11a and 11b; Bazzurro and Cornell, 2004; Silva et al., 1999), interpolation is not a significant issue and the 11 point grid listed in Table 2 is adequate to capture site nonlinearity.

To compute the probability of reference motions ($P(x)$ in Equation 5), the reference motion hazard curve is numerically differentiated using central differences. Although hazard curves are smooth so differencing is a stable process, the curves are interpolated to 100 points to maximize the integration accuracy of Equation 5. The use of 100 points was established by increasing the number of points until stability (no change in derived soil hazard) was achieved. This typically occurred at about 50 points so 100 points has been adopted as a conservative value for integration. Figure 12 illustrates the rapid convergence with the number of integration points showing little change in hazard between 50 and 100 points.

It is important to point out, because multiple levels of reference motions contribute to the soil or site-specific hazard, a wider range in reference hazard than soil hazard is necessary to achieve accuracy in the soil hazard. Extensive tests have shown that a conservative range over which to integrate the reference hazard is a factor of 10 in AEF beyond that desired for the soil or site-specific AEF. In other words, if site-specific hazard is desired to 10^{-6} AEF, reference hazard is required to an AEF of 10^{-7} . Additionally, the same consideration applies at high exceedance frequencies. In this case, if site-specific hazard is desired at 10^{-2} AEF, reference hazard is conservatively required to an AEF of 10^{-1} .

Approach 3 is also appropriate for computing site-specific vertical hazard from horizontal site-specific hazard curves, producing vertical UHRS at the same AEF as the horizontal UHRS. Resulting horizontal and vertical GMRS and foundation input response spectra (FIRS) then both achieve the same target performance goals. As with the horizontal site-

specific hazard, regarding the range in the reference site hazard, accuracy in the vertical hazard requires a wide integration range over the site-specific horizontal hazard. As a result to achieve an AEF of 10^{-6} for the vertical site-specific hazard requires the reference site hazard to an AEF of 10^{-8} .

3.4.1 Optimum Number of Realizations

Ideally the objective of the randomization process is to develop statistically stable estimates of median values and standard deviations with as few analyses as possible. Bazzuro and Cornell (2004) suggest as few as 10 realizations are sufficient for application of Approach 3. As Table 3 indicates, simple statistics indicates stability is a slowly varying function of sample size, particularly for standard deviations. For a tolerance of the statistical sample being within 20% of the population standard deviation at the 90% confidence level, the number of samples is 30 and naturally less for median estimates. Because sigma (\ln) is less than 1, typically around 0.1 to 0.4, and it enters as σ_{\ln}^2 (e.g., Equation 7), its impacts are generally not large. As Table 3 indicates, improving the accuracy in the aleatory variability to 10% requires a four-fold increase in sample size to 130 realizations at the 90% confidence limit. These trends are reflected in Figures 13a and 13b, which shows the range in median and sigma estimates computed for various sample sizes with five different random seeds using the Grand Gulf Unit 3 profile 1 (Figure 13a) as well as the generic till-like profile (Figure 13b). In general, neither median nor sigma estimates are truly stable for fewer than about 200 realizations. Such observations led to 300 realizations to achieve less than a 10% error in sigma estimates in NUREG/CR-6728. In that research exercise, high accuracy was desired as comparisons were made between Approaches 2, 3, and 4. Achievement of similar accuracy in development of hazard consistent UHRS is simply not warranted in view of the impact on computed transfer functions. As both the simple statistics (Table 3) and Figures 13a and 13b show, doubling the number of realizations from 30 to 60 does not generally result in a significant improvement in accuracy. Increasing the number of samples beyond 100, as Figure 13 illustrates, is required to achieve highly stable results.

However, it is really the desired accuracy in the computed hazard which should inform the number of samples required. Based on Equation 7 (Section 3.3), for a given percent accuracy in amplitude, the required accuracy in the standard deviation depends on the slope of the reference hazard curve as well as the degree of nonlinearity through the slope of the amplification factors C. For the Grand Gulf Nuclear Station Unit 3 profile, from Figure 10, the slope of the amplification factors has a maximum at about 0.5 and the σ_{\ln} averages about 0.2 or less with a hard rock hazard curve slope (log, log) near 2 as shown in Figure 14, the exponential term containing σ_{\ln} in Equation 7 has a value of about 1.1. A 50% increase in σ_{\ln} results in a value of about 1.2, or a 10% change. At the 90% confidence level, fewer than 5 realizations are required (30 were run for the Grand Gulf Nuclear Station Unit 3 analyses), increasing to 13 at the 99% confidence level and of course fewer still for estimates of the mean. Conversely, for a σ_{\ln} near 0.5, a steep hazard curve slope near 4, and over a highly nonlinear loading level with C near 0.5, the exponential term is about 2.7. In this case a 10% increase in σ_{\ln} results in an exponential value of about 3.4, or about a 20% increase in amplitude, which is significant. For cases such as these, to achieve a 10% accuracy in amplitude requires better than a 5% accuracy in σ_{\ln} . From Table 3 the number of samples increases from 5 to 550 at the 90% confidence level to over 1,000 at the 99% confidence level. Clearly, for application of fully probabilistic approaches to developing site-

specific hazard, the number of realizations should be case specific and possibly magnitude dependent, determined with preliminary analyses. For the deterministic approach, since the mean is given by the median times an exponential of σ_{in}^2 divided by 2, to achieve a 10% accuracy in the mean requires only about a 30% accuracy in σ_{in} , or about 15 realizations at the 90% confidence limit, 35 samples at the 99% confidence limit.

3.4.2 Example Illustrations

A straight-forward way to illustrate the fully probabilistic Approach 3 is through comparisons with the Approximate method (Equation 7) as well as a fully deterministic method using a median amplification. As previously discussed, the approximation renders the full integration quite transparent and it is easy to illustrate the impacts of median amplification, slope of the reference site hazard curve, and amplification variability (σ_{in}) with simple cases.

3.4.2.1 Illustration Using a Horizontal or Vertical Mock Reference Hazard Curve

To clearly demonstrate Approach 3, the results of the simplest case of a linear (i.e. $C = 0$ in Equation 7) reference hazard curve and a linear median amplification or V/H ratio of 2.0 is considered in Figure 15. The aleatory variability of the amplification is taken as 0.2 (σ_{in}) and the slope of the reference hazard curve is 3 (log-log) initially then increased to an extreme value of 6. Figure 15 compares three derived hazard curves obtained using: Approach 3 full integration (Equation 5), Approach 3 Approximate (Equation 7), and simply median amplification or V/H ratio (2.0) times the reference hazard. For horizontal components, this latter (deterministic) curve effectively reflects Approach 2, which would use the mean amplification. However for this example, the mean is only 2% larger than the median. In general it is clear that for a slope near 3, there is little difference between the deterministic and fully probabilistic results. The accurate Approach 3, full integration method, results in the largest motions for a given AEF with the results using the approximate fully probabilistic method very slightly lower. For the steeper slope, it is easy to see from Equation 7 the expected impacts of Approach 3. The exponential term in Equation 7 becomes larger for the steeper (by a factor of 2) slope, resulting in the difference between the median deterministic amplification and fully probabilistic Approach 3 becoming significant, approaching 15% to 20%.

Increasing the amplification variability to 0.4 (σ_{in}) (Figure 16), now shows a substantial difference between deterministic and fully probabilistic results, a difference near 25% for a slope of 3 and nearly 70% for an extreme case with a slope of 6. Use of the mean amplification would only increase the corresponding soil hazard curve by about 8%, leaving it a full 15% below the fully probabilistic Approach 3, illustrating the recommendation in NUREG/CR-6728 for enveloping high- and low-frequency mean amplification factors as an empirical means of conservatively maintaining the desired hazard level.

This simple example also serves to illustrate the inherent stability of the Approach 3 full integration method. In both Figures 15 and 16, near the discontinuity in slope of the reference site hazard curve (going from a slope of 3 to a slope of 6), the derivative of the reference hazard curve is undefined (very large) at that point, causing the observed bulge in the hazard curve computed using the approximate Approach 3 method. The full integration method simply integrates through the singularity, resulting in a gradual change in slope of the resulting soil hazard curve. Because real hazard curves can not have such

discontinuities, this extreme case illustrates the appropriateness of the numerical differentiation (e.g., density of points in the hazard reference site hazard curve) as well as the numerical integration scheme employed.

Also apparent in Figures 15 and 16 is the breakdown of the Approach 3 full integration method near the limits of the reference site (input) hazard curve. At low AEF (10^{-10}), the reference hazard curve extends to 10^{-11} AEF so the Approach 3 full integration hazard is correct to an AEF of 10^{-10} , as is evident in Figures 15 and 16. However, at high exceedance frequency, the reference site hazard curve extends to an AEF of 10^{-1} . Near this AEF the Approach 3 full integration hazard shows a decreasing slope and convergence to the reference site hazard. The full integration method simply reflects decreasing contributions to the integral (sum, Equation 5) as the limit of the reference site hazard curve is approached.

3.4.2.2 Illustration Using a Horizontal or Vertical Realistic Reference Hazard Curve

While the previous simplified example cases gave a clear illustration of using the full integration and approximate Approach 3 through examining the differences between deterministic and fully probabilistic approaches to developing UHRS, further insights can be provided by a more realistic case. For this example, a real WNA reference site hazard curve for peak acceleration was used and serves to illustrate the impact of increasing slope of the reference site hazard curve on developing fully probabilistic site-specific motions. As can be seen in Figure 17, the reference site hazard curve has a slope which increases significantly with decreasing AEF. As with the previous example, median amplification or V/H ratio is set at 2.0 and is taken as linear (again $C = 0$ in Equation 7). Figure 17 illustrates the effect of increasing slope of the reference site hazard curve as the AEF decreases for a range in amplification aleatory variability ($\sigma_{in} = 0.1$ to 0.4). From Figure 17 it is easy to appreciate the impacts of the exponential term in Equation 7, the increase in motion for a fully probabilistic analysis compared to a deterministic approach, as both the slope and σ_{in} increase. For a typical σ_{in} in the range of 0.2 to 0.3, accommodating aleatory variability in velocities, depth to basement, and modulus reduction and hysteretic damping curves across a site, the difference between the median deterministic soil hazard curve and the fully probabilistic hazard curve is about 25% near the AEF of 10^{-4} . Recall that this example, as well as the last one, assume linear response in order to provide a more transparent illustration. Consequently the exponential term in Equation 7 is a minimum, resulting in a minimum difference between deterministic and fully probabilistic methods.

Figure 18 illustrates the comparison between deterministic and fully probabilistic analysis results including the approximate Approach 3 method. A typical σ_{in} value of 0.3 is considered and the results illustrated in Figure 18 shows good agreement between the full integration and approximate methods to an AEF of about 2×10^{-5} . Below this exceedance frequency the approximate method breaks down in this example as the exponential term is becoming too large (Bazzurro and Cornell, 2004).

This example also provides a check on the implementation of the full integration method in terms of differencing the reference site hazard curve (density of points) as well as the numerical integration procedure (Simpson's Rule). The full integration method agrees quite well with the approximate result over AEFs where it is expected to do so. At high probability,

the reference site hazard curve slope is quite small so the deterministic and fully probabilistic approaches should agree (see Equation 7).

3.4.2.3 Illustration for the Grand Gulf Nuclear Station Unit 3 Horizontal UHRS

In this illustration a direct comparison is made between deterministic Approach 2A (Section 3.1) and the probabilistic Approach 3 using the full integration method (Section 3.2). Site conditions reflect the four reactor embedded profiles (Figures 3a and 3b) as well as the two sets of site-specific modulus reduction and damping curves, uncorrected and corrected for potential effects of sample disturbance (FSAR Section 2.5.4.2.2.3; EOI, 2008). This site-specific epistemic variability reflects eight distinct base-cases which are labeled P1 to P4 for profiles 1 to 4 combined with uncorrected curves and P5 to P8 for profiles 1 to 4 combined with corrected curves. In the comparison, Approach 3 will employ amplification factors computed separately for cases P1 to P8 as well as single- and double-corner source models and low- and high-frequency dominant or reference earthquakes based on the hazard deaggregation (Section 3.4.2.3.1). Approach 2A will also develop mean amplification factors for the 1 Hz to 2.5 Hz (low-frequency) as well as 5 Hz to 10 Hz (high-frequency) reference earthquakes and for each profile, P1 to P8.

The reference earthquake spectra used for computing amplification factors for Approach 2A were developed from the suite of attenuation relations and corresponding weights used in computing the reference site hazard. While not strictly desirable, as amplification factors should be developed with scaled spectra from each attenuation relation, in the context of deterministic Approach 2A, treatment of epistemic variability is not unambiguous.

3.4.2.3.1 Hazard Deaggregation For The Grand Gulf Nuclear Station Unit 3

Figures 19a and 19b shows source contributions in magnitude and distance based on mean hazard at 1 Hz to 2.5 Hz and 5 Hz to 10 Hz computed for the Grand Gulf Nuclear Station Unit 3. In general there are contributions from three controlling sources: small background sources with M around 5 and distances within about 15 km, moderate magnitude sources (e.g., Saline River; FSAR Section 2.5.2.1, EOI, 2008) with $M \leq 6.5$ within about 50 km, and New Madrid with M 7 to 8 and distances beyond 300 km. For low-frequencies, M 7 to 8 dominates at AEF 10^{-4} to 10^{-6} . At high-frequencies, the small background and moderate magnitude sources become more dominant as AEF decreases from 10^{-4} to 10^{-6} . The median deaggregation, which generally reflects more accurately actual source contributions (R.G. 1.165) resulted in modes of M 6.25 and M 7.69 for high- (5 Hz to 10 Hz) and low (1 Hz to 2.5 Hz) frequency respectively at AEF 10^{-5} , the midpoint of the range of primary interest (AEF 10^{-4} to 10^{-6}). These magnitudes were adopted as adequately reflecting the range in earthquakes dominating the hazard at the site.

3.4.2.3.2 Comparison Of Approaches 2A and 3

To provide a complete basis for the comparison between Approaches 2A and 3 as well as to clearly illustrate the ambiguity in accommodating site epistemic variability in a fundamentally deterministic analysis with an objective to achieving a target exceedance level or probability, results for profiles 1 to 4 and both sets of modulus reduction and hysteretic damping curves are presented.

For Approach 3, in order to generally accommodate the magnitude contributions to the hazard at high- and low-structural frequencies, the amplification factors computed for M 6.25

and **M** 7.69 were assigned as follows in Table 4: **M** 6.25 for 5.0 Hz and above and **M** 7.69 for 2.5 Hz and below. In accommodating site epistemic variability for application of Approach 3, profiles 1 to 4 (Figures 3a and 3b), uncorrected and corrected modulus reduction and hysteretic damping curves, as well as single- versus double-corner source models were all given equal weight as listed in Table 5 (EOI, 2008). Figures 20a and 20b show the suite of UHRS, Figure 20a and 20b at AEF 10^{-4} and 10^{-5} respectively, computed for the four base-case profiles as well as the mean estimate (over exceedance frequency) along with the reference site (hard rock) UHRS. Each profile UHRS reflects a mean over hazard curves computed with each set of G/G_{max} and hysteretic damping curves (uncorrected and corrected, Table 5). Little difference is seen among the profiles with the stiffest profile at depth (profile 3, Figures 3a and 3b) reflecting, as expected, the lowest low-frequency motion. Of particular note, above about 20 Hz the profiles deamplify (amplification less than 1) the hard rock motions as the amplification factors shown in Figure 4a depict, at the appropriate loading level (about 0.10g). Considerable nonlinearity is exhibited by these relatively stiff soils, about 1,000 ft/sec over the top \approx 40 ft (Figures 3a and 3b) and increases with increasing loading levels (AEF 10^{-4} and 10^{-5} , Figures 20a and 20b respectively). This nonlinearity is likely due to the steep velocity gradient below the shallow layer, increasing the high-frequency wave amplitudes input to the top layer. This is likely the case as the fundamental column resonance near 0.2 Hz (Figure 4a) remains quite stable up to 1.50g loading levels for both **M** 6.25 and **M** 7.69 (Figure 4a and 4b respectively). The deeper portion of the profile (below \approx 100 ft) is generally too stiff to exhibit highly or even moderately nonlinear dynamic behavior. The peak in the UHRS at 5 Hz is likely due to the shallow layer with a low-strain shear-wave velocity of about 1,000 ft/sec (Figures 3a and 3b). Completing the comparison, Figures 21a and 21b show UHRS (AEF 10^{-4} and 10^{-5} , Figures 21a and 21b respectively) computed for each set of modulus reduction and hysteretic damping curves. In this case, each UHRS reflects a weighted mean over the four profiles (Figures 3a and 3b). Compared to the profiles (Figure 20) even less difference is seen between the curves. This is likely due to a combination of the overall low loading levels (\approx 0.1g to 0.2g), the stiffness of the profiles below the top layer, and the difference between the uncorrected and corrected curves being both small and occurring at the larger cyclic shear strains (FSAR Section 2.5.4.2.2.3; EOI, 2008). The large site amplification over hard rock approaches a factor of 3 at low frequency with a moderate increase in peak acceleration as well a decrease at 25 Hz compared to hard rock motions (Figures 4a and 4b). It is important to note that discrete frequencies where the hard rock hazard curve is specified or extrapolated (0.1 Hz) are at 0.1, 0.2, 1.0, 2.5, 5.0, 10.0, 25.0, and 100.0 Hz. A soil spectral shape has not been used to interpolate as this process is somewhat ambiguous due to the change in contributing **M** and **D** as well as the effects of aleatory and epistemic variability on UHRS spectral shapes. Additionally, any smoothing that change motions at the seven discrete frequencies, e.g., filling in the point at 2.5 Hz to smooth the shape, alters the exceedance frequencies. If the smoothing is not done in precisely the same manner for the UHRS at AEF 10^{-4} and 10^{-5} , the slope can be in considerable error impacting the performance based design spectra in both the UHRS at AEF 10^{-4} as well as the scale factors (Regulatory Guide 1.208).

For Approach 2A, Figure 22 shows the reference earthquake spectra (1 Hz to 2.5 Hz; **M** 7.64, **D** 466 km and 5 Hz to 10 Hz; **M** 6.33, **D** 82 km) based on model deaggregations at AEF 10^{-5} . These reference earthquake spectra were taken from the original early site permit (ESP) safety analysis report (SSAR Figure 2.5-67; SERI, 2006) and reflect the control

motions used to drive the soil columns (NUREG/CR-6728) after being scaled to the 1 Hz to 2.5 Hz and 5 Hz to 10 Hz spectral ordinates of the reference site UHRS (Figure 22). The slight differences in model magnitudes between the ESP safety analysis report (SSAR Figure 2.5-67; SERI, 2006) and current hazard environments (FSAR Section 2.5.2.2.1) will have a very minor impact on the Approach 2 amplification factors (e.g., Figure 5b). Additionally, use of the scaled median AEF 10^{-5} model reference earthquake spectra as control motions at AEF 10^{-4} will also have little impact on amplification factors as the hazard deaggregations have only minor differences between AEF 10^{-4} and 10^{-5} (Figures 19a and 19b). From Figure 23, the higher loading levels of 5 Hz to 10 Hz scaled reference spectra compared to the 1 Hz to 2.5 Hz scaled spectra (Figure 22) result in a more nonlinear response and lower mean amplification factors for frequencies above about 0.3 Hz. Below 0.3 Hz, near the fundamental column resonance, the more nonlinear response results in slightly larger amplification. These trends are expected, with the amplification at high-frequency, typically at frequencies above the fundamental column resonance, being lower for the high-frequency scaled reference spectra compared to amplification computed with the low-frequency scaled spectra (NUREG/CR-6728). As previously discussed (Section 3.1), to conservatively maintain the reference rock hazard level (AEF), the envelope of the high- and low-frequency mean amplification factors are applied to the reference site (hard rock) UHRS at AEF of 10^{-4} and 10^{-5} . The enveloping process was intended to conservatively accommodate the neglect of integrating the full suite of amplification factors with the entire reference site hazard curve (Approach 3, Section 3). Recall this effect is succinctly illustrated in the exponential term of the approximate Approach 3 method (Equation 7, Section 3.3). The exponential term is proportional to the slope of the reference site hazard curves as well as the slope and σ_{in} of the amplification factors. For this site, as previously discussed in Section 3.4.1, the slope of the reference site hazard curves is near 2 (Figure 14), the slope of the amplification factors with loading level is about 0.5 (e.g., Figure 10), and the σ_{in} averages about 0.2. With these values, the increase in the mean amplification (Figure 23) is less than 10% (1.06). At high-frequency, above 10 Hz, where the 1 Hz to 2.5 Hz mean amplification exceeds the 5 Hz to 10 Hz mean amplification by more than about 10%, Approach 2A will result in a conservative estimate of the AEF 10^{-4} UHRS. This conservative trend is illustrated in Figure 24 which compares Approach 2A deterministic spectra computed for each combination of profile and set of G/G_{max} and hysteretic damping curves (P1 to P8 Section 3.4.2.3). In general Approach 2A reflects the appropriate AEF for frequencies up to about 5 Hz, above which the level of conservatism increases dramatically. At 25 Hz Approach 2A, using envelope mean amplification factors, is nearly a factor of two conservative. This degree of conservatism exceeds that revealed in the NUREG/CR-6728 analyses, which ranged from about 5% to about 40% at AEF 10^{-4} , for the particular hazard environments, profiles, and nonlinear dynamic material properties considered. The degree of conservatism introduced in enveloping mean transfer functions with Approach 2A depends strongly on the hazard environment (slope of the reference site hazard curve) and degree of soil nonlinearity (σ_{in} and slope of the amplification factors). For the cases considered in NUREG/CR-6728, at AEF 10^{-4} Approach 2A was conservative at high-frequency by about 10% to 20% while at AEF 10^{-5} Approach 2A ranged from a conservatism of nearly 50% to being slightly unconservative, depending on hazard environment and profile. For the Grand Gulf site, due to the combination of hazard environment and profile, Approach 2A results in extremely conservative high-frequency (≥ 10 Hz) motions at AEF 10^{-4} .

Considering AEF 10^{-5} , Figures 25, 26, and 27 show corresponding plots of scaled spectra, amplification factors, and approach comparison. At AEF 10^{-5} Figure 25 shows the reference site UHRS with a peak acceleration near 0.2g as compared to 0.1g at AEF 10^{-4} . Comparing Figures 26 and 23, the high loading levels at AEF 10^{-5} result in a greater degree of nonlinear response for both the high- and low-frequency control motions. The comparison of Approach 2A with Approach 3 is shown in Figure 27 and reveals nearly as high a degree of conservatism with Approach 2A at high-frequency as was the case at AEF 10^{-4} (Figure 24). In this case however, near 2 Hz, Approach 2A is somewhat unconservative by about 10% to 20%. This could be easily accommodated with a smooth envelope across structural frequency. At very low frequency, below 0.5 Hz, the lowest frequency for which reference site UHRS were available, both the reference site and Approach 3 UHRS were extrapolated assuming constant spectral velocity (Section 4.2.1).

In general, the comparison of Approach 2A with Approach 3 showed that Approach 2A was very conservative (up to 100%) at high-frequency (≥ 5 Hz to 10 Hz) for AEF 10^{-4} and generally consistent with the Approach 3 UHRS at low-frequency. At AEF 10^{-5} , Approach 2A was nearly as conservative compared to Approach 3 at high-frequency but showed a small degree of unconservatism at low-frequency (near 2 Hz). For frequencies below 0.5 Hz, the lowest frequency for which reference site hazard was available, a constant spectral slope of -1 (constant spectral velocity) has been applied to the reference site UHRS and Approach 3 UHRS (Section 4.2.1).

4.0 APPLICATION TO VERTICAL HAZARD

Typically the vertical UHRS is developed by a deterministic application of V/H ratios applied to the horizontal UHRS. Since V/H ratios vary with both magnitude and distance for sites with nonlinear response and with distance for linear sites (e.g., hard rock) (Silva, 1997; NUREG/CR-6728), it is essential to capture these dependencies, identified through model deaggregations, in developing the vertical UHRS. For the deterministic approach, paralleling Approach 2 for the horizontals (Section 3.0), conservative estimates of appropriate V/H ratios must be used to ensure achievement of the same hazard levels and target performance goals as the horizontal UHRS. Additionally, V/H ratios reflect epistemic variability as is evidenced by WNA empirical soft rock and deep firm soil V/H ratios (Abrahamson and Shedlock, 1997), further pointing out the necessity of conservatism in a deterministic approach to developing vertical UHRS. As previously discussed in the context of Approach 2 and illustrated in Section 3.4.2.3 for the horizontal UHRS, incorporation of epistemic variability in a deterministic framework is not unambiguous as one can not simply average over suites of motions or transfer functions which reflect epistemic variability. This process will not generally achieve desired hazard levels and reliance on conservatism in V/H ratios remains the most reliable option. These considerations, along with a desire for easy implementation as a function of expected horizontal peak acceleration, led to the purposeful incorporation of conservatism in development of the CENA hard rock V/H ratios (NUREG/CR-6728).

To accurately achieve desired hazard levels as well as performance goals, the only reasonable alternative is a fully probabilistic approach, directly paralleling that for the horizontal hazard. Implementation of the full integration Approach 3 (Section 3.2) for vertical hazard simply substitutes V/H ratios for horizontal amplification factors. In this case, the distribution of V/H ratios are integrated with the horizontal site-specific hazard curves

(presumably developed using Approach 3). As with the horizontal case, Approach 3 then admits the proper and unambiguous incorporation of both aleatory and epistemic variabilities in V/H ratios, achieving desired hazard levels. Again, in parallel with development of the horizontal hazard, model deaggregations are used but, as previously stated, in addition to magnitude, source distance is required as V/H ratios depend on distance as well as magnitude for soil or soft rock site conditions.

4.1 Development of V/H Ratios

In the following sections the development of site-specific ratios and the motivation for inclusion of empirical V/H ratios is presented.

4.1.1 Site-Specific V/H Ratios

To develop site-specific vertical motions, incident inclined P-SV waves are modeled from the source to the site using the plane-wave propagators of Silva et al. (1976) assuming a shear-wave point-source spectrum (Boore; 1983, 2003). The point-source model is used to accommodate the effects of source distance and source depth on V/H ratios. For consistency, both the horizontal and vertical motions are modeled using the same source and path parameters (Table 2). The horizontal motions are modeled as vertically propagating shear-waves. For the vertical motions, the angles of incidence are computed by two-point ray tracing through the crust and site-specific profile. To model site response, the near-surface V_P and V_S profiles are placed on top of the crustal structure, the incident P-SV wavefield is propagated to the surface assuming a linear analysis, and the vertical motions are computed.

For the Grand Gulf Nuclear Station Unit 3, compressional-wave profiles were developed corresponding to the shear-wave profiles shown in Figures 3a and 3b (FSAR Section 2.5.4.7.1; EOI, 2008). For the reactor embedded profile, over the top 100 ft or so, the gradient in the compressional-wave profile is much steeper than that for the shear-wave profile, both reflecting somewhat higher velocities than typical Holocene alluvium. The difference in gradients between shear- and compressional-wave profiles is typically the case for soils (Silva, 1997) and indicates both the relevance of empirical WNA relations for estimates of V/H ratios and the expectation of large high frequency vertical motions for close-in sources (Campbell, 1997; Silva 1997; Bozorgnia and Campbell, 2004). Both the overall stiffness of the profile at depth, 2,000 ft/sec at a depth of about 100 ft increasing to about 2,500 to 3,000 ft/sec at a depth of about 400 ft for profiles 2 to 4 (Figures 3a and 3b), indicate conditions that do not reflect the vast majority of soils that dominate the WNA vertical and horizontal empirical attenuation relations (Abrahamson and Shedlock, 1997; Silva, 1997). As a result, development and inclusion of site-specific V/H ratios is warranted.

For typical crustal structures without strong near-surface V_P gradients and at close distances, the predominant motion on the vertical component is principally due to the SV wavefield. In a soil column (particularly deep profiles), however, because there is usually a large V_P gradient (larger for P-waves than for S-waves as Poisson ratios generally decrease with increasing depth), the vertical component is usually controlled by the compressional wavefield at high frequency (Silva, 1997; Amirbekian and Bolt, 1998; Beresnev et al., 2002).

In the implementation of the equivalent-linear approach to estimate V/H response spectral ratios, the horizontal component analyses are performed for vertically propagating shear-

waves. To compute the vertical motions, a linear analysis is performed for incident inclined P-SV waves using low-strain V_P and V_S derived from the base-case profiles. The P-wave damping is assumed to be equal to the low strain S-wave damping (Johnson and Silva, 1981). The horizontal component and vertical component analyses are assumed to be independent.

The approximations of linear analysis for the vertical component and uncoupled vertical and horizontal components have been validated in two ways. Fully nonlinear modeling using a 3-D soil model shows that the assumption of largely independent horizontal and vertical motions for loading levels up to about 0.5g (soil surface, horizontal component) for moderately stiff profiles is appropriate (EPRI, 1993). Additionally, validation exercises with recorded motions have been conducted at over 50 sites that recorded the 1989 **M** 6.9 Loma Prieta and 1992 **M** 6.7 Northridge earthquakes (EPRI, 1993). These validations show the overall bias and variability is acceptably low for engineering applications but is higher than that for horizontal motions. The vertical model does not perform as well as the model for horizontal motions (EPRI, 1993; Silva, 1997). An indirect validation was also performed by comparing V/H ratios from WNA empirical attenuation relations with model predictions over a wide range in loading conditions (Silva, 1997). The results show a favorable comparison with the model exceeding the empirical V/H ratios at high frequency, particularly at high loading levels. In the V/H comparisons with empirical relations, the model also shows a small under prediction at low frequency (≤ 1 Hz) and at large distance (≥ 20 km).

To model the site-specific V/H ratios, the same **M**, stress drops, and suite of distances are used as in developing horizontal transfer functions (Table 2). For the vertical analyses, a total kappa value of 0.02 sec, half that of the horizontal, was used. This factor of 50% is based on observations of kappa at strong motion sites (Anderson and Hough, 1984), validation exercises (EPRI, 1993), as well as the observation that the peak in the vertical spectral acceleration (5% damped) for WNA rock and soil sites is generally near 10 to 12 Hz compared to the horizontal motion peak that occurs at about 5 Hz, conditional on **M** 6.5 at a distance of about 10 to 30 km (Abrahamson and Silva 1997; Campbell 1997; Campbell and Bozorgnia 2003). This difference of about 2 in peak frequency is directly attributable to differences in kappa of about 2. Similar trends are seen in CENA hard rock spectra with the vertical component peaking at higher frequencies than the horizontal component.

As with the horizontal analyses, multiple base cases were run to accommodate epistemic variability: site-specific velocity profiles 1 to 4 for each structure location as well as **M** 6.25 and **M** 7.69 and both single- and double-corner source models. Multiple G/G_{max} and hysteretic damping curves were not run for the verticals as the analysis is linear, using the lowest small strain damping between uncorrected and corrected curves (FSAR Section 2.5.4.2.2.3; EOI, 2008). However V/H ratios do reflect multiple base-case modulus reduction and hysteretic damping curves in the denominator, or horizontal motions. Additionally, in the profile randomization for the verticals, low strain damping as well as velocities were randomized to accommodate aleatory variability (Section 4.1.3).

An example of the site-specific V/H ratios, Figures 28a and 28b show median estimates computed with the stochastic model for **M** 6.25 single corner-frequency model. Figure 28a shows V/H ratios computed for profile 1 (Figures 3a and 3b) while Figure 28b shows ratios computed for profile 3, which showed the largest difference in horizontal UHRS between the

profiles (Figures 20a and 20b). Analyses for both profiles used uncorrected G/G_{\max} and hysteretic damping curves (FSAR Section 2.5.4.2.2.3; EOI, 2008). Distances range from 190 km (0.01g, horizontal motion) to 0 km (0.75g, horizontal motion), which adequately accommodates the hazard deaggregations (Figures 19a and 19b). The ratios range from about 0.3 to 0.4 at low-frequency (≤ 2 Hz) to about 3 near the peak at 30 Hz. As the verticals are run linearly, the increase in the ratio as loading level increases (source distance decreases) is due to reduced motions in the horizontal but also due to a decrease in incidence angle for the P-SV wavefield, dominated by compression-waves at high frequency. Between the ratios computed for profiles 1 and 3 (Figures 28a and 28b respectively), little difference is seen, suggesting minor impacts of site epistemic variability on vertical as well as horizontal UHRS. To complete the comparison, Figure 29 shows V/H ratios computed for profile 1 (Figures 3a and 3b) and uncorrected modulus reduction and hysteretic damping curves using M 7.69. When the differences in distances are considered, in general, the shapes are quite similar to the corresponding V/H ratios computed with M 6.25. The largest ratio for M 6.25 is naturally at 0 km distance, as a result it exceeds the ratio computed for M 7.69 which, for 0.75g, is at 16 km. Since M 7.69 is used only at distances exceeding 100 km (Table 2), showing V/H ratios at closer distances has little added value.

As previously discussed, the model predictions of V/H ratios may be slightly unconservative at low-frequency and conservative at high frequency. While it is important to include site-specific effects on the vertical hazard, potential model deficiencies are compensated with inclusion of empirical V/H ratios computed from WNA generic rock and soil site attenuation relations. Based on empirical relations (Abrahamson and Shedlock, 1997; Bozorgnia and Campbell, 2004) a lower bound of 0.4 is placed on all V/H ratios based on examination of the full suite of M , D , and site conditions for which empirical relations are currently available.

4.1.2 Empirical V/H Ratios

Empirical western North America V/H ratios for soft rock and deep firm soil are included in the development of vertical motions in addition to site-specific point-source simulations. The use of WNA empirical V/H ratios implicitly assumes similarity in shear- and compression-wave profiles and nonlinear dynamic material properties between site condition in WNA and the Grand Gulf Nuclear Station Unit 3 column (Silva et al., 1997). Whereas this may not be the case for the average WNA rock and Holocene alluvium soil profile (Silva, 1997), the range in site conditions sampled by the WNA empirical generic rock and deep firm soil relations likely accommodates site-specific conditions. Due to the stiffness of the site reactor embedded profile (Figures 3a and 3b), significantly greater than that for typical WNA deep firm soils (Silva, 1997), both deep soil and soft rock V/H ratios are used. To accommodate this epistemic variability, hazard is computed for each case and weights applied to the resulting hazard curves. To accommodate the stiff soils for the reactor embedded profile, the soft rock V/H ratios were given a weight of 0.2 (20%, Table 5). The relative weights between WNA soft rock and deep firm soil were based on judgment regarding overall stiffness between WNA soft rock and soil sites and the four embedment profiles (Figures 3a and 3b). Additionally, because the model for vertical motions is not as thoroughly validated as the model for horizontal motions (EPRI, 1993), inclusion of empirical models is warranted. The additional epistemic variability introduced by inclusion of both analytical and empirical models also appropriately reflects the difficulty and lack of consensus regarding the modeling of site-specific vertical motions (EPRI, 1993). In the

implementation of Approach 3 to develop vertical hazard curves, the epistemic variability is properly accommodated in the vertical mean UHRS, reflecting a weighted average over multiple vertical hazard curves computed for Unit 3 using multiple models. The vertical FIRS (and UHRS) then maintain the desired risk and hazard levels, consistent with the horizontal UHRS.

For the empirical V/H ratios, both Abrahamson and Silva (1997) and Campbell and Bozorgnia (2003) soft rock and deep firm soil WNA relations are used with equal weights (Table 5). These are the only two relatively recent relations for which complementary horizontal and vertical spectra exist. To illustrate the uncertainty in V/H ratios, even for empirical relations based largely on the same suite of recorded motions (Abrahamson and Shedlock, 1997), and the implied prudence of properly incorporating it in developing vertical hazard, the full suite of empirical V/H ratios used in the analyses is presented.

To begin the comparison, Figures 30a, 30b and 31a, 31b show V/H ratios for **M** 6.25 (rock and soil sites as well as both relations) while Figures 32a, 32b and 33a, 33b show results for **M** 7.69. For **M** 6.25 Figures 30a and 30b show V/H ratios for soft rock with Abrahamson and Silva (1997) (hereinafter referred to as AS) in Figure 30a and Campbell and Bozorgnia (2003) (hereinafter referred to as CB) in Figure 30b. In general the ratios are similar in shape and level, about 0.5 at low-frequency and peaking at high-frequency (10 Hz to 20 Hz). At peak acceleration (100 Hz) the ratios are at about 0.7. Over the entire frequency range (the lowest frequency defined in the relations is 0.2 Hz which has been extrapolated to 0.1 Hz) the CB ratios show a much larger distance (and loading level) dependency than is shown by AS.

In Figures 31a and 31b soil site V/H ratios are compared between AS and CB, again for **M** 6.25. The expected differences between the soft rock and deep firm soil ratios are clearly seen with the soil ratios lower than the rock ratios at low-frequency (≤ 1 Hz) and higher at high-frequency (Silva, 1997). For the soil ratios the distance scaling is more similar between AS and CB, particularly at high-frequency, however the AS and CB soil V/H ratios peak at different frequencies at high loading levels (about 20 Hz for AS and about 10 Hz for CB). In general the two relations AS and CB show generally similar V/H ratios for both rock and soil site conditions.

For the larger magnitude (**M** 7.69) V/H ratios the differences shown in Figures 32a, 32b and 33a, 33b are much greater. This is expected as there were no data for magnitudes greater than about 7.5 up through the 1997 time frame. As a result, much of the empirical relations (magnitude, distance, site dependencies) for **M** greater than about **M** 7+ was driven by extrapolation. Comparing **M** 7.69 V/H ratios for soft rock sites Figure 32a shows large differences between AS and CB in overall levels as well as distance dependencies and frequencies where the ratios peak. The soil site comparison, Figure 33a and b shows even larger differences, particularly at high-frequency where AS has a peak near 3.0 while CB has a peak just below 2.0, about 50% lower.

Compared to the site-specific V/H ratios (Figures 28a, 28b, and 29) the trends are similar between the site-specific and empirical soil ratios. The site-specific ratios show more structure and stronger distance dependencies as they reflect a particular column (with uncertainty) and source distance and depth and not averaged over many rock and soil sites

as well as earthquakes, as in the empirical V/H ratios. The analytical ratios are somewhat lower than the empirical at low-frequency and higher at high-frequency (Silva, 1997).

Distance bins differ between the empirical and analytical V/H ratios because the empirical ratios use a generic suite of distances used on several projects while the analytical V/H ratios are region specific. It is important to note the site-specific and generic V/H ratios peak at very different frequencies, about 30 Hz and about 10 to 20 Hz, respectively, with the site-specific having generally higher V/H ratios, particularly at close distances. Use of an empirical V/H ratio alone may underestimate the vertical hazard at high frequency, provided the model predictions are reasonably accurate.

4.1.3 Aleatory Variability In V/H Ratios

In addition to the epistemic variability accommodated through the use of multiple models for V/H ratios, aleatory variability due to randomness of dynamic material properties varying vertically and laterally across the site should be accommodated as well. However, in developing the vertical hazard, since site-specific aleatory variability has been incorporated in developing the horizontal site-specific hazard curves, it is advisable to constrain the sigma of the site-specific V/H ratios to values less than about 0.15 to 0.20 (σ_n). This range is to accommodate the observation of slightly larger variability about median attenuation relations in the vertical component compared to the horizontal component (Abrahamson and Silva, 1997). Limiting the σ_n of the site-specific V/H ratios avoids potential double counting site-specific aleatory variability in developing vertical hazard. It should be noted that for the computation of site-specific V/H ratios, the denominator (horizontal component) should be taken as the median (i.e. not varied) and multiple realizations of the vertical component taken to form the basis for the aleatory variability in the V/H ratios. This approach is intended to properly isolate the variability in the V/H ratios to that of the verticals, recognizing the variability in the horizontal component has already been accommodated in the randomization of shear-wave dynamic material properties. The occasion to limit the V/H ratio variability may arise due to the randomization process incorporated in the model for the vertical motions. For simplicity, the randomization of the compressional-wave velocities fixes the Poisson ratios in the profile at the values of the base-case shear- and compressional-wave velocities. The profile randomization scheme (Section 2.2.1), based on shear-wave velocities and layer thickness, produces realizations of shear-wave velocities with corresponding compressional-wave velocities using the original Poisson ratios. This process results in a suite of random shear- and compressional-wave profiles, all with the same Poisson ratios (verses depth). It may very well be the case this simplifying assumption results in too large a range in compressional-wave velocities, perhaps due to a coupling between shear-wave velocity and Poisson ratio. Obviously, because horizontal components and consequently shear-waves are of major concern and because there are many more measured shear-wave velocity profiles than both shear- and compressional-wave velocity profiles, the profile randomization scheme has concentrated on shear-waves. Additionally, a more statistically correct compressional-wave randomization scheme would have little impact as a 20% to 30% change in the aleatory variability, if small, has a very minor impact (3% to 4%) on the vertical hazard for typical ranges in the slope (κ) of the horizontal hazard curve (2 to 6) and slope of the V/H ratios with loading level (distance), as illustrated in Equation 7 and Section 3.4.1.

Returning to the empirical V/H ratios, Figures 30 to 33, as only median estimates are available through horizontal and vertical attenuation relations (Abrahamson and Silva, 1997; Campbell and Bozorgnia, 1997, 2003), in application of Approach 3 which requires aleatory variability (e.g., Equation 7) in the V/H ratios, a value of 0.15 (σ_{in}) is used.

4.2 Implementation of V/H Ratios In Developing Vertical Hazard

In assigning the V/H ratios in the Approach 3 analysis, the source **M** and **D** change significantly with structural frequency as exceedance frequency changes (Section 3.4.2.3.1, Figures 19a and 19b). To accommodate the deaggregation in (contributing sources) integrating the horizontal hazard with the distributions of V/H ratios, the **M** and **D** selection follows that listed in Table 4. The magnitudes selected are intended to capture the dominant sources: **M** 6.25 for small and moderate size sources within about 50 km of the site and **M** 7.69, the New Madrid source at distances beyond 300 km from the site. The weights listed in Table 5 are intended to approximate the relative contributions of the sources across structural frequency and exceedance probability. Because the V/H ratios vary slowly with distance, only a smooth approximation to the hazard deaggregation is necessary. To adequately capture the change in **M** and **D** with AEF, only a few distance bins were required for the empirical V/H ratios, 8 km and 57 km (Table 4). The analytical V/H ratios **M** 6.25 required two distance bins, 10 km for the single-corner source model (13 km for the double-corner source model) as well as 190 km for the single-corner source model (197 km for the double-corner source model). For **M** 7.69 only one distance bin was required as this source is at a distance of over 300 km (Section 3.4.2.3.1), 163 km for the single-corner source model (172 km for the double-corner source model).

To illustrate the vertical hazard computed using Approach 3 with the empirical and site-specific V/H ratios, Figure 34 shows horizontal and vertical UHRS computed for the Grand Gulf Nuclear Station Unit 3 profile for AEF 10^{-4} , 10^{-5} , and 10^{-6} . The magnitude and distance deaggregation (Figure 19, Section 3.4.2.3.1) is seen to be captured in the apparent V/H ratios shown in Figure 35 (vertical UHRS divided by the horizontal UHRS). As the AEF decreases and both the high- and low-frequency source contributions move closer to the site (Table 4, Figure 19), higher weight is placed on the closer empirical and site-specific V/H ratios resulting in larger apparent V/H ratios. The fully probabilistic approach then results in hazard consistent vertical UHRS that properly accommodate site-specific aleatory and epistemic variability as well as the effect of magnitude and distance on vertical motions. This is especially the case at high-frequency and low AEF at 10^{-6} .

4.2.1 UHRS Interpolation and Extrapolation

Because the reference (hard rock) hazard is computed at only seven frequencies, namely 0.5, 1.0, 2.5, 5.0, 10.0, 25.0, and 100.0 Hz (taken as peak acceleration), the site-specific hazard has been both extrapolated to 0.1 Hz and at high-frequency, the reference hazard curves were interpolated at 34 and 50 Hz, as these may be critical frequencies to define the Unit 1 UHRS shapes beyond 25 Hz. The interpolation is performed by using the deterministic shapes (NUREG/CR-6728) for the appropriate **M** to interpolate the hard rock UHRS at AEF of 10^{-4} , 10^{-5} , and 10^{-6} yr⁻¹, resulting in three points on 34 and 50 Hz hazard curves. The adjacent hazard curves at 25 and 100 Hz are then used as shapes to extrapolate to lower and higher exceedance probabilities, resulting in approximate hard rock hazard curves. Approach 3 (full integration method) is then applied to develop site-specific horizontal and vertical UHRS at the same exceedance probability as the 25 and 100 Hz

hard rock hazard. For the vertical component, because the site-specific V/H ratios peak at high-frequency (beyond 25 Hz), it may be important to maintain the appropriate hazard levels between 25 and 50 Hz.

Below 0.5 Hz, because the aleatory variability in attenuation relations increases with period (Abrahamson and Shedlock, 1997; EPRI, 2004), use of a median spectral shape (NUREG/CR-6728) to extrapolate at low-frequency may be inappropriate and result in potentially unconservative hazard or higher probability than desired. To address this uncertainty, a conservative approach is adopted by extrapolating the 0.5 Hz 10^{-4} , 10^{-5} , and 10^{-6} hard rock UHRs, assuming a constant slope in spectral velocity (+1 slope in pseudo-absolute spectral acceleration) (BSSC, 2004). The extrapolation is extended at low-frequency to the earthquake source corner frequency, where the slope is increased to a constant spectral displacement. Since the source corner frequency, or transition from approximately constant spectral velocity to spectral displacement, depends on magnitude, an average representative magnitude of **M** 7.7 is assumed to apply for frequencies below 0.5 Hz, based on the low-frequency deaggregation (Figures 19a and b). Application of the empirical relation

$$\text{Log } T = -1.25 + 0.3 \mathbf{M} \quad (8)$$

(BSSC, 2004) results in a corner period (*T*) of approximately 12 sec (0.08 Hz). As a result, constant spectral velocity was assumed from 0.5 to 0.1 Hz. Comparisons of the extrapolation from 0.5 to 0.1 Hz with spectral shapes computed from recordings of large **M** earthquakes (**M** > 7) (NUREG/CR-6728) confirmed the assumption of constant spectral velocity while suggesting the possibility of conservatism at very low frequency. While the exact probability of spectral ordinates for frequencies below 0.5 Hz remains unknown, the likelihood of conservatism in the extrapolation suggests that exceedance probabilities below 0.5 Hz are lower than those at higher frequencies (e.g., 0.5 Hz and above).

5.0 CONCLUSIONS

For the Grand Gulf Nuclear Station Unit 3, a fully probabilistic methodology (Approach 3) was used to develop the site-specific UHRs (NUREG/CR-6728, -6769). As part of this approach, site-specific amplification factors as well as V/H ratios were developed using RVT (EPRI, 1993; Silva et al., 1997; NUREG/CR-6728).

Regarding site response, the two areas where RVT is used directly in estimating response spectra and peak cyclic shear strains for equivalent-linear analyses have been presented and discussed. Other related considerations in site response such as choice of control motion, effects of control motion spectral shape, and incorporation of aleatory and epistemic variabilities in dynamic material properties have been presented and discussed in terms of potential impacts to the development of site-specific UHRs. Additionally, general guidelines for implementing RVT in terms of site response have been presented and discussed.

All four methodologies for developing site-specific ground motions (Approach 1 to 4) have been presented and discussed in order of increasing accuracy and complexity. The fully probabilistic approach used in computing the Grand Gulf Nuclear Station Unit 3 UHRs (Approach 3) was developed through the derivation of basic equations, illustrating the various simplifications as well as assumptions comparisons. Comparisons were presented between Approaches 2A and 3 which showed Approach 2A performed adequately at low-

frequency (≤ 5 Hz) and was very conservative at high-frequency for AEF 10^{-4} , compared to the Approach 3 UHRS for the Grand Gulf Nuclear Station Unit 3 hazard environment and dynamic material properties. At AEF 10^{-5} , Approach 2A remained conservative for frequencies above about 5 Hz while generally remaining adequate at low-frequency, but showed some unconservatism (10% to 20%) near 2 Hz. Possible reasons for the conservatism and unconservatism have been presented and discussed. Also presented and discussed are implementation limitations of Approach 3, as well as the other approaches, and how these limitations are addressed to preserve accuracy, or conservatism in the case of deterministic approaches, in computing site-specific hazard curves. Sensitivities of the fully probabilistic approach to various parameters have also been explored to illustrate the essential elements in the methodology, which enables the approach to achieve hazard consistency. Also presented is a discussion of the optimum number of site response realizations, in terms of confidence levels, to achieve a given accuracy in ground motion at a given hazard level for implementation of the fully probabilistic approach.

Important considerations in application of Approach 3 to develop horizontal and vertical hazard consistent UHRS have been discussed and include: 1) peak-to-RMS ratio approximations, 2) integration steps in the Fourier amplitude spectra and its extension to low-frequency, 3) corrections to RVT for the effects of non-stationary, 4) limitations in loading levels for the equivalent-linear approximation and limitations in low-frequency amplification at deep soil sites for the vertically propagating shear-wave model, 5) compensation for the effects of low-strain scattering kappa induced by profile randomization, 6) effects of control motion spectral shape on site amplification (magnitude, distance, and single- versus double-corner source models), 7) consideration of aleatory and epistemic variabilities in dynamic material properties, 8) range in AEF of the reference hazard curves as well as differentiation and integration steps, 9) number of realizations in randomization of dynamic material properties, 10) accommodation of magnitude and distance dependencies as well as alternative models in V/H ratios, 11) limitation of aleatory variability in V/H ratios (already accommodated in horizontal site-specific UHRS), and 12) effects of magnitude (low-frequency spectral shape) in extrapolating UHRS to frequencies lower than that defined by the reference (hard rock) hazard.

Finally, specific parameter values and results have been presented for applications to the Grand Gulf Nuclear Station Unit 3 horizontal and vertical UHRS.

6.0 REFERENCES

- Abrahamson, N.A and K.M. Shedlock, 1997, "Overview." *Seismological Research Letters*, 68(1), 9-23.
- Abrahamson, N.A. and W.J. Silva, 1997, "Empirical Response Spectral Attenuation Relations for Shallow Crustal Earthquakes." *Seismological Research Letters*, 68(1), 94-127.
- Amirbekian, R.V. and Bolt, B.A., 1998, "Spectral Comparison of Vertical And Horizontal Seismic Strong Ground Motions in Alluvial Basins." *Earthquake Spectra*, 14(4), 573-595.
- Anderson, J. G. and S. E. Hough, 1984, "A Model for the Shape of the Fourier Amplitude Spectrum of Acceleration at High Frequencies." *Bulletin of Seismological Society of America*, 74(5), 1969-1993.
- Atkinson, G.M and W.J. Silva, 1997, "An Empirical Study of Earthquake Source Spectra for California Earthquakes." *Bulletin of Seismological Society of America*, 87(1), 97-113.
- Atkinson, G.M., 1993, "Notes on Ground Motion Parameters for Eastern North America: Duration and H/V Ratio." *Bulletin of Seismological Society of America*, 83(2), 587-596.
- Bazzurro, P. and C.A. Cornell, 2004, "Nonlinear Soil-Site Effects in Probabilistic Seismic-Hazard Analysis." *Bulletin of Seismological Society of America*, 94(6), 2110-2123.
- Beresnev, I.A, Nightengale, A.M. Silva, W.J., 2002, "Properties of Vertical Ground Motions." *Bulletin of the Seismological Society of America*, 92(2), 3152-3164.
- Boore, D.M., 2003, "Simulation of Ground Motions Using the Stochastic Method," *Pure and Applied Geophysics*, 160; 635-676.
- Boore, D.M., 1983, "Strong-Motion Seismology." *Reviews of Geophysics*, 21, 308-1318.
- Boore, D.M. and Joyner, W.B., 1984, "A Note on the Use of Random Vibration Theory to Predict Peak Amplitudes of Transient Signals." *Bulletin of Seismological Society of America*, 74, 2035-2039.
- Bozorgnia, Y. and Campbell, K., 2004, "The Vertical-to-Horizontal Response Spectral Ratio and Tentative Procedures for Developing Simplified V/H and Vertical Design Spectra," *Journal of Earthquake Engineering*, 8(2), 175-207.
- Building Seismic Safety Council (BSSC), 2004, "National Earthquake Hazards Reduction Program (NEHRP), Recommended Provisions for Seismic Regulations for New Buildings and Other Structures (FEMA 450), Report prepared for the Federal Emergency Management Agency (FEMA).
- Campbell, K W., 1997, "Empirical Near-Source Attenuation Relationships for Horizontal and Vertical Components of Peak Ground Acceleration, Peak Ground Velocity, and Pseudo-Absolute Acceleration Response Spectra." *Bulletin of the Seismological Society of America*, 68, (1):154-176.

Campbell, K.W. and Y. Bozorgnia, 2003, "Updated Near-Source Ground Motion (Attenuation) Relations for the Horizontal and Vertical Components of Peak Ground Acceleration and Acceleration Response Spectra." *Bulletin of the Seismological Society of America*, 93, (1):314-331

Campbell, K.W. and Y. Bozorgnia, 1994, "Near-Source Attenuation of Peak Horizontal Acceleration from Worldwide Accelerograms Recorded from 1957 To 1993." in proceedings, Fifth U.S. National Conference on Earthquake Engineering. Chicago, Illinois. vol. III, p. 283-292.

Cramer, C. H., 2003, "Site-Specific Seismic Hazard Analysis that is Completely Probabilistic." *Bulletin of Seismological Society of America*, 93, 1841-1846.

Electric Power Research Institute, 2004, "CEUS Ground Motion Project Final Report." EPRI, Palo Alto, CA, Dominion Energy, Glen Allen, VA, Entergy Nuclear, Jackson, MS, and Exelon Generation Company, Kennett Square, PA:1009684, 2004.

Electric Power Research Institute, 1993; "Guidelines for Determining Design Basis Ground Motions." Palo Alto, California: Electric Power Research Institute, vol. 1-5, EPRI TR-102293.

Electric Power Research Institute, 1988, "Engineering Model of Earthquake Ground Motion for Eastern North America." Palo Alto, California: Electric Power Research Institute, EPRI NP-6074.

Entergy Operations, Inc., 2008, "Grand Gulf Nuclear Station Unit 3 Combined License Application Part 2: Final Safety Analysis Report."

Hartzell, S., S. Harmsen, A. Frankel, and S. Larsen, 1999, "Calculation of Broadband Time Histories of Ground Motion: Comparison of Methods and Validation Using Strong-Ground Motion from the 1994 Northridge Earthquake." *Bulletin of Seismological Society of America*, 89(6), 1484-1504.

Herrmann, R.B., 1985, "An Extension of Random Vibration Theory Estimates of Strong Ground Motion to Large Distance." *Bulletin of Seismological Society of America*, 75, 1447-1453.

Idriss, I. M.; Seed, H. B.. 1968, "Seismic Response of Horizontal Soil Layers." *Journal of the Soil Mechanics and Foundations Division, ASCE*, 94(SM4), 1003-1031.

Johnson, L.R., and W.J Silva, 1981, "The Effects of Unconsolidated Sediments upon the Ground Motion during Local Earthquakes." *Bulletin of Seismological Society of America*, 71, 127-142.

Lee, R., M. E. Maryak, and J. Kimball, 1999, "A Methodology to Estimate Site-Specific Seismic Hazard for Critical Facilities on Soil or Soft-Rock Sites." *Seismological Research Letters*, 70, 230.

Lee, R., W.J. Silva, and C. A. Cornell, 1998, "Alternatives in Evaluating Soil- and Rock-Site Seismic Hazard." *Seismological Research Letters*, 69, 81.

NUREG/CR-6728, "Technical Basis for Revision of Regulatory Guidance on Design Ground Motions: Hazard- and Risk-Consistent Ground Motions Spectra Guidelines." Prepared for Division of Engineering Technology, Washington, D.C., 20555-0001, 2001.

NUREG/CR-6769, "Technical Basis for Revision of Regulatory Guidance on Design Ground Motions: Development of Hazard- and Risk-Consistent Seismic Spectra for Two Sites." U.S. Nuclear Regulatory Commission, Office of Nuclear Regulatory Research, Washington, D.C., 20555-0001, 2002.

Pakiser, L.C. and W. D. Mooney, 1989, "Geophysical Framework of the Continental United States." *Geological Society of America Memoir* 172.

Schnabel, P.B., Lysmer, J., and Seed, H.B., 1972, SHAKE: A Computer Program for Earthquake Response Analysis of Horizontally Layered Sites. Earthquake Engineering Research Center (EEEC), University of California at Berkeley, EERC 72-12.

Schneider, J.F., W.J. Silva, and C.L. Stark, 1993, Ground Motion Model for the 1989 M6.9 Loma Prieta Earthquake Including Effects of Source, Path and Site. *Earthquake Spectra*, 9(2), 251-287.

Silva, W.J., 1997, Characteristics of Vertical Strong Ground Motions for Applications to Engineering Design, in Proceedings FHWA/NCEER Workshop on the National Representation of Seismic Ground Motion for New and Existing Highway Facilities, Technical Report NCEER-97-0010, National Center for Earthquake Engineering Research, Buffalo, New York.

Silva, W.J., 1992, "Factors Controlling Strong Ground Motions and their Associated Uncertainties." *Seismic and Dynamic Analysis and Design Considerations for High Level Nuclear Waste Repositories*, ASCE 132-161.

Silva, W.J., 1976, "Body Waves in a Layered Anelastic Solid." *Bulletin of Seismological Society of America*, vol. 66(5), 1539-1554.

Silva, W. J., S. Li, B. Darragh, and N. Gregor, 1999, "Surface Geology Based Strong Motion Amplification Factors for the San Francisco Bay and Los Angeles Areas." A PEARL Report to PG&E/CEC/Caltrans, Award No. SA2120-59652.

Silva, W.J., N. Abrahamson, G. Toro, C. Costantino, 1997, "Description and Validation of the Stochastic Ground Motion Model." Report Submitted to Brookhaven National Laboratory, Associated Universities, Inc. Upton, New York.

Silva, W.J. and R. Darragh, 1995, "Engineering Characterization of Earthquake Strong Ground Motion Recorded at Rock Sites." Palo Alto, California: Electric Power Research Institute, TR-102261.

Silva, W.J. and R.K. Green, 1989, "Magnitude and Distance Scaling of Response Spectral Shapes for Rock Sites with Applications to North American Tectonic Environment." *Earthquake Spectra*, 5(3):591-624.

Silva, W.J., T. Turcotte and Y. Moriwaki, 1986, "Soil Response to Earthquake Ground Motions." Palo Alto, California: Electric Power Research Institute, EPRI Research Project RP 2556-07.

System Energy Resources, Inc., 2006, Grand Gulf Site Early Site Permit Application, Part 2, Site Safety Analysis Report.

7.0 TABLES AND FIGURES

TABLES

Table 1

Definitions of Locations for Motions in Site-Response Analyses

1. Outcrop: May be specified at the surface or at any depth within a profile.
 - A. Surface Outcrop: All material above the outcrop location is removed. Motion comprised as the sum of upgoing and downgoing waves. For vertically propagating waves (shear or compressional) the free surface effect results in an amplification of exactly 2 over upgoing waves (incident wavefield).
 - B. At-Depth Outcrop: Material above the outcrop location remains in place. Motion comprised of upgoing wavefields only. However the upgoing wavefields at the outcrop location may contain wavefields which propagated above the outcrop location, reflected from impedance contrasts and the free surface, and propagated down past the outcrop location. If there are significant impedance contrasts below the outcrop location, these reflected wavefields contribute to the upgoing wavefields at the outcrop location and may increase or decrease the upgoing wavefield.
2. At Depth In-Column or Total Motions: As with the Outcrop-At-Depth, material above the location of the computed motions remains in place. Motions are comprised of upgoing and downgoing wavefields (total motion) and reflect motions experienced by a buried instrument (e.g., vertical array).
3. Free-Field: Surface or At-Depth motions unaffected to a significant degree (< 10%) by the built environment. For recording instruments, this is generally achieved at a foundation dimension away from structures. For in-structure motions, this is achieved at ground level and light structures of two stories or fewer.
4. Site: In this document the term site is used in its classical sense to reflect a single geographical point, rather than the area occupied by a nuclear station.

Table 2					
Hard Rock Expected Horizontal Peak Acceleration Levels, Point Source Distances, Durations, Parameters and Hard Rock Crustal Model					
M 6.25 1c⁽¹⁾, M 6.25 2c⁽²⁾, M 7.69 1c, M 7.69 2c					
PGA (g)	Distance (km)	Depth (km)	$T_{source}^{(sec)}$	$T_{path}^{(sec)}$	$T_{total}^{(sec)}$
1.50	0, 0, 6, 8	4, 5, 8, 8	3.60,3.34,18.89,17.51	0.15,0.19,0.44,0.52	3.75,3.52,19.34,18.03
1.25	0, 0, 8, 11	4, 6, 8, 8	3.60,3.34,18.89,17.51	0.18,0.23,0.53,0.63	3.79,3.57,19.43,18.13
1.00	0, 0, 12, 14	6, 7, 8, 8	3.60,3.34,18.89,17.51	0.24,0.30,0.65,0.76	3.84,3.63,19.55,18.27
0.75	0, 4, 16, 19	8, 8, 8, 8	3.60,3.34,18.89,17.51	0.32,0.40,0.86,0.99	3.90,3.73,19.76,18.50
0.50	7, 10, 24, 28	8, 8, 8, 8	3.60,3.34,18.89,17.51	0.48,0.59,0.12,0.14	4.09,3.92,20.11,18.91
0.40	10, 13, 29, 33	8, 8, 8, 8	3.60,3.34,18.89,17.51	0.60,0.71,0.15,0.17	4.20,4.05,20.35,19.17
0.30	15, 18, 37, 42	8, 8, 8, 8	3.60,3.34,18.89,17.51	0.78,0.91,0.18,0.21	4.38,4.25,20.74,19.59
0.20	21, 25, 50, 56	8, 8, 8, 8	3.60,3.34,18.89,17.51	0.11,0.13,0.25,0.28	4.67,4.60,21.38,20.28
0.10	37, 42, 92, 103	8, 8, 8, 8	3.60,3.34,18.89,17.51	0.18,0.21,0.46,0.51	5.43,5.42,23.46,22.62
0.05	59, 67, 163, 172	8, 8, 8, 8	3.60,3.34,18.89,17.51	0.29,0.33,0.81,0.86	6.53,6.66,27.01,26.06
0.01	190, 197, 480, 443	8, 8, 8, 8	3.60,3.34,18.89,17.51	0.95,0.98,0.24,0.22	13.05,13.14,42.85,39.61

Notes:

- (1)1c = single corner source model
- (2)2c = double corner source model (Atkinson, 1993)

Additional parameters used in the point-source model are:

$Q = 670 f^{0.33}$

$\Delta\sigma$ (1c) = 110 bars

$\kappa = 0.006$ sec, hard rock

$\rho = 2.71$ cgs

$\beta = 3.52$ km/sec

$R_c = 60$ km, crossover hypocentral distance to $R^{-0.5}$ geometrical attenuation

$T = 1/fc + 0.05 R$, RVT duration, $R =$ hypocentral distance (km)

Generic Hard Rock Crustal Model (EPRI, 1993)			
Thickness (km)	Vs (km/sec)	Vp (km/sec)	ρ (cgs)
1	2.83	4.90	2.52
11	3.52	6.10	2.71
28	3.75	6.50	2.78
[infinite]	4.62	8.00	3.35

Table 3			
Sample Size Required For Percent Error In The Standard Deviation For A Normal Distribution			
% Error	Confidence Levels (%)		
	90	95	99
	Sample Size		
50	5	7	13
30	15	21	35
20	30	46	80
10	130	200	300
5	550	700	>1000

Table 4				
Amplification Factor M and V/H Ratios M and D Ranges				
F (Hz)	AEF (yr⁻¹)	M	D (km)	
			Empirical	Model 1c, 2c
0.5	10 ⁻⁴ to 10 ⁻⁵	7.69	57	163, 172
1.0	10 ⁻⁴ to 10 ⁻⁵	7.69	57	163, 172
2.5	10 ⁻⁴ to 10 ⁻⁵	7.69	57	163, 172
5.0	10 ⁻⁴ to 10 ⁻⁵	6.25	57	190, 197
10.0	10 ⁻⁴ to 10 ⁻⁵	6.25	57	190, 197
25.0	10 ⁻⁴ to 10 ⁻⁵	6.25	57	190, 197
PGA (100.0)	10 ⁻⁴ to 10 ⁻⁵	7.69	57	163, 172
0.5	10 ⁻⁶ to 10 ⁻⁷	7.69	57	163, 172
1.0	10 ⁻⁶ to 10 ⁻⁷	7.69	57	163, 172
2.5	10 ⁻⁶ to 10 ⁻⁷	7.69	57	163, 172
5.0	10 ⁻⁶ to 10 ⁻⁷	6.25	8	10, 13
10.0	10 ⁻⁶ to 10 ⁻⁷	6.25	8	10, 13
25.0	10 ⁻⁶ to 10 ⁻⁷	6.25	8	10, 13
PGA (100.0)	10 ⁻⁶ to 10 ⁻⁷	6.25	8	10, 13

Table 5	
Model Weights	
Base Case Profiles	Weight
1	0.25
2	0.25
3	0.25
4	0.25
Modulus Reduction and Damping Curves	Weight
Set 1 (uncorrected)	0.5
Set 2 (corrected)	0.5
V/H Ratio	Weight
Empirical	0.5
Model	0.5
Empirical	Embedment (Soil Removed) Outcrop Weight
Rock	0.2
Soil	0.8
Attenuation Relation	Embedment (Soil Removed) Outcrop Weight
Abrahamson and Silva	0.5
Campbell and Borzorgina	0.5
Earthquake Source	Weight
Single-Corner	0.5
Double-Corner	0.5

FIGURES

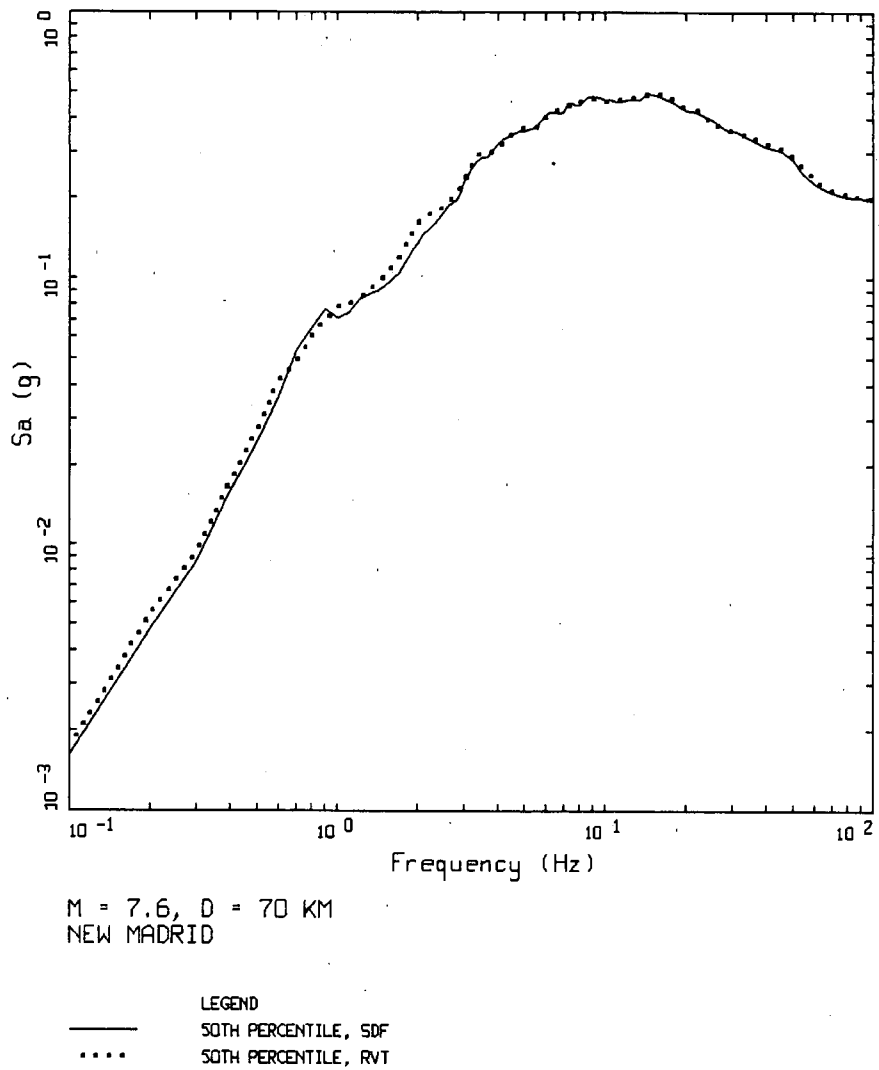
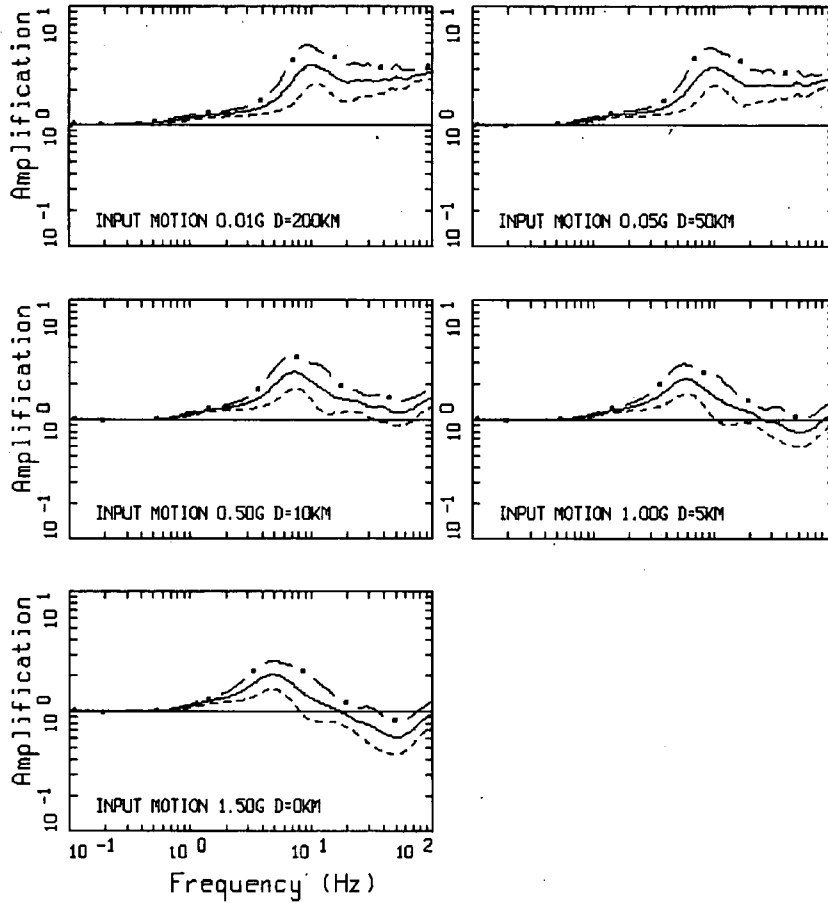
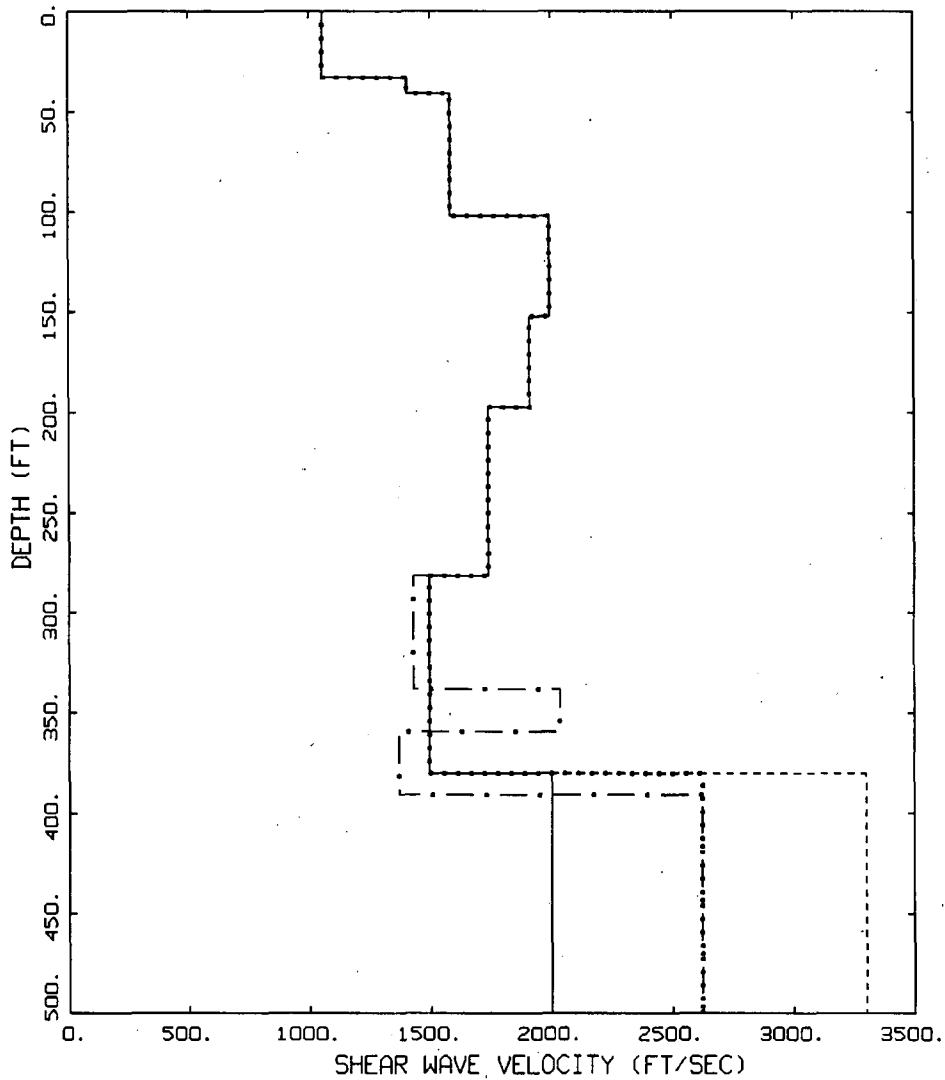


Figure 1 Comparison of median RVT and SDF (computed from acceleration time histories) 5% damped response spectra. RVT computed using Equation 24 in Boore (1983). Medians computed over 30 realizations.



AMPLIFICATION(H), 25 FT OF 1000 FT/SEC OVER HARD ROCK
M 5.0

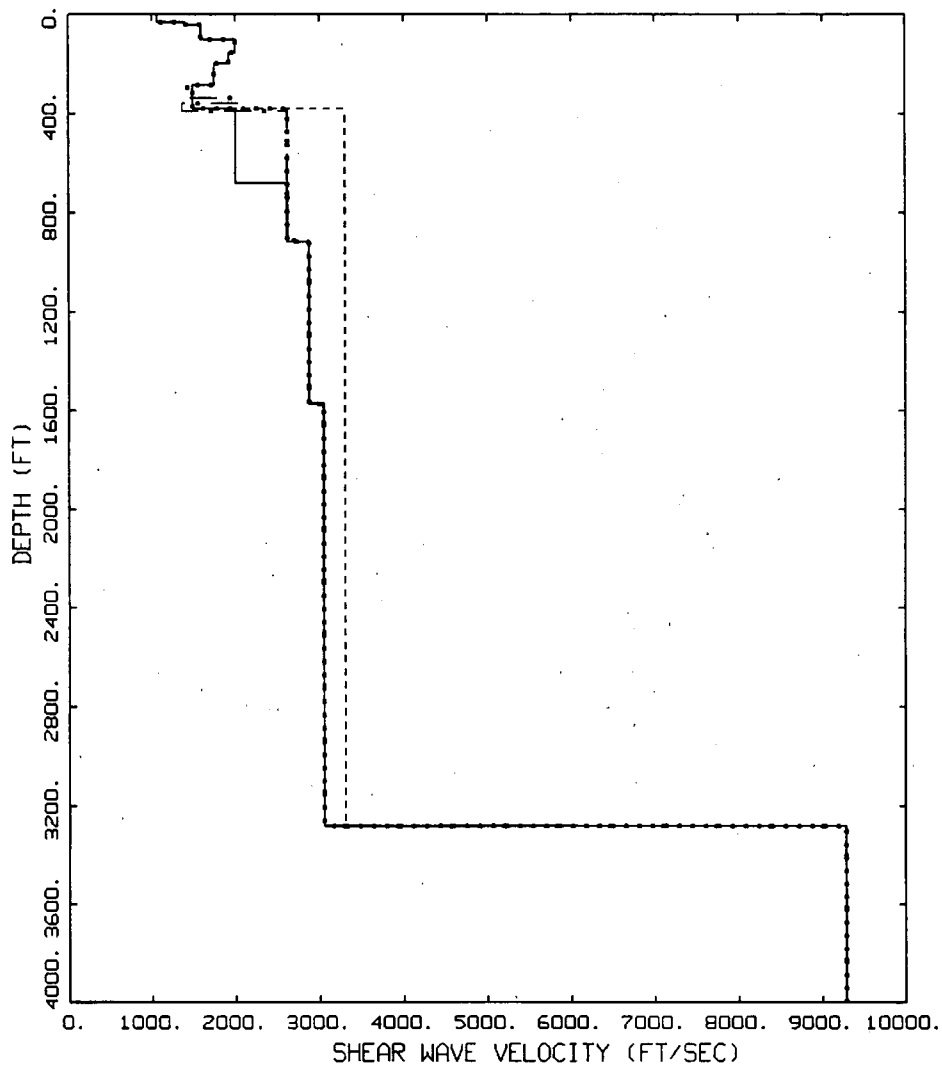
Figure 2 Amplification factors, median and ± 1 sigma estimates, computed for a 25 ft thick (randomized ± 10 ft) layer of 1,000 ft/sec shear-wave velocity over hard rock crustal model (Table 2) at a suite of loading levels. Magnitude is 5.0.



SHEAR-WAVE VELOCITY PROFILE
GRAND GULF REACTOR EMBEDDED

- LEGEND
- Reactor Base Case 1
 - Reactor Base Case 2
 - - - Reactor Base Case 3
 - . - Reactor Base Case 4

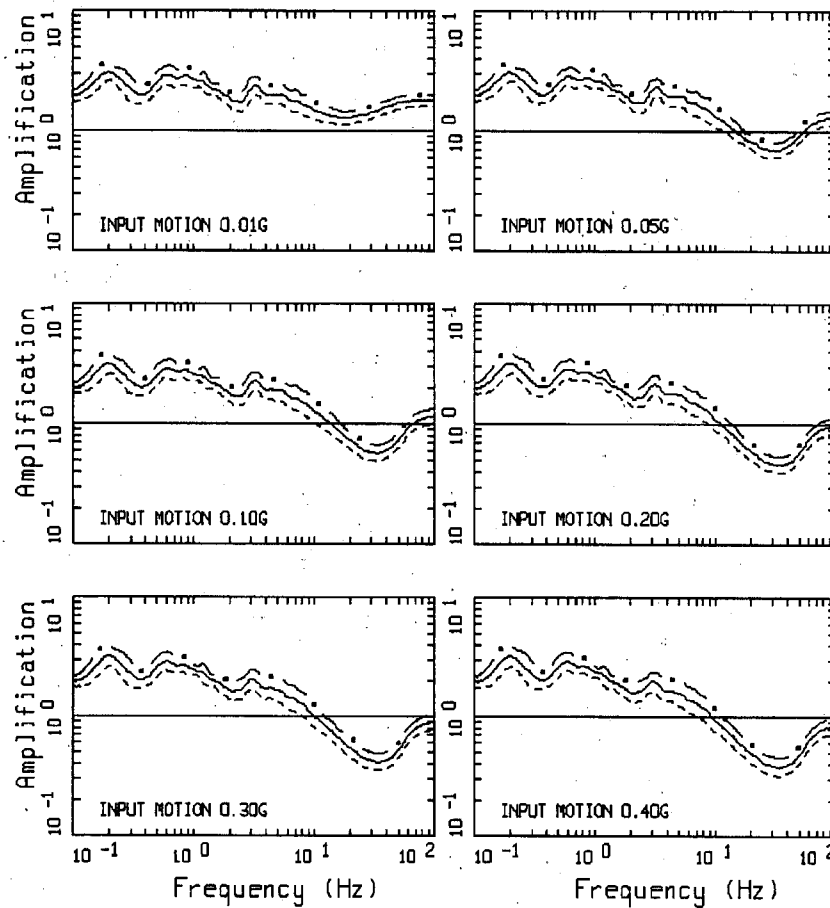
Figure 3a Base-case shear-wave velocity profiles developed for the Grand Gulf Nuclear Station Unit 3 reactor to depths of 500 ft. (Adapted from FSAR Figure 2.5.2-212 (EOI, 2008)).



SHEAR-WAVE VELOCITY PROFILE
GRAND GULF REACTOR EMBEDDED

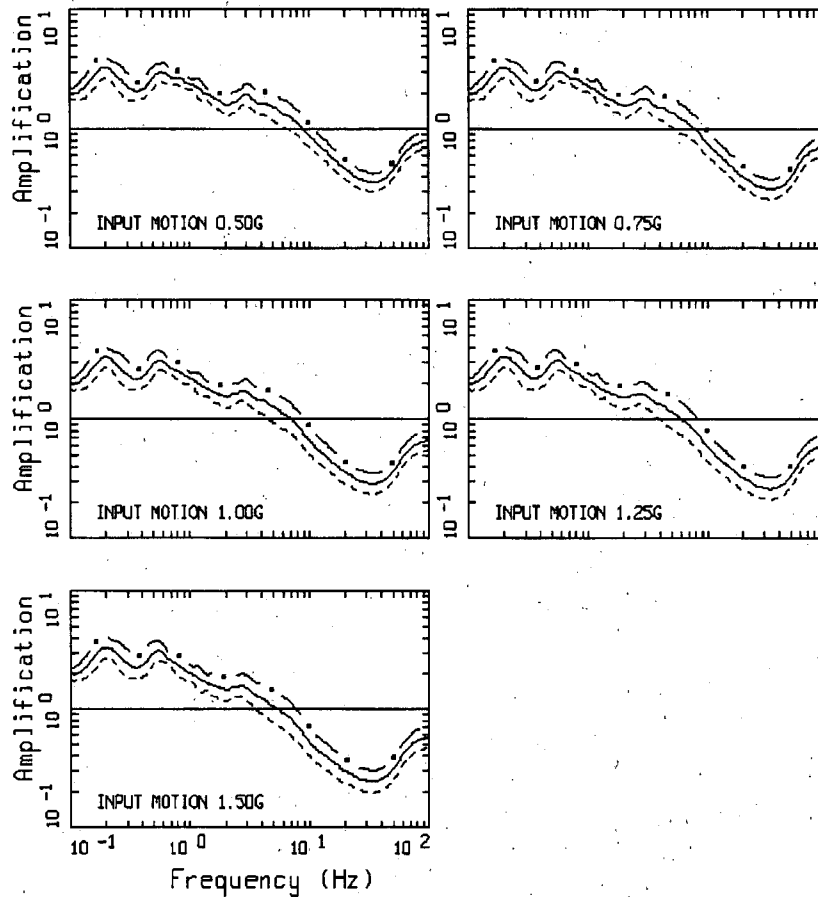
- LEGEND
- Reactor Base Case 1
 - Reactor Base Case 2
 - Reactor Base Case 3
 - . - . Reactor Base Case 4

Figure 3b Base-case shear-wave velocity profiles developed for the Grand Gulf Nuclear Station Unit 3 reactor to depth of 4000 ft. (Adapted from FSAR Figure 2.5.2-213 (EOI, 2008)).



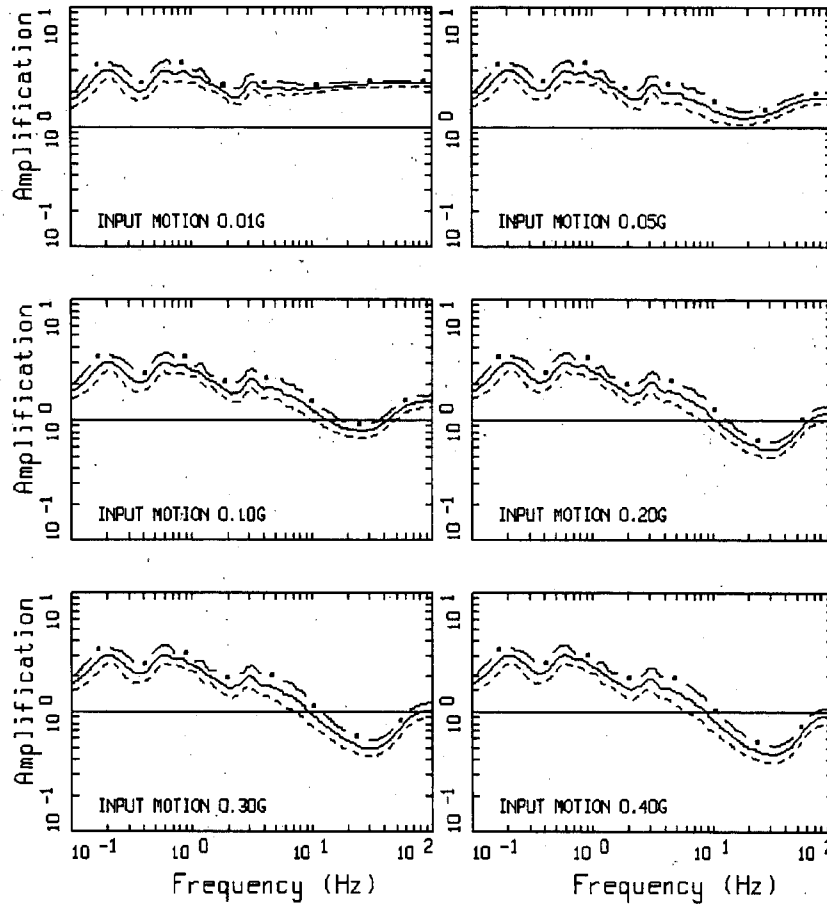
AMPLIFICATION, M = 6.25, 1 CORNER SOURCE SOURCE
RE.1: PROFILE 1, CURVE SET 1: PAGE 1 OF 2

Figure 4a Example of median and ± 1 sigma estimates of amplification factors computed for the Grand Gulf Reactor embedded profile 1 (Figures 3a and 3b) using site-specific G/Gmax and hysteretic damping curves (EOI, 2008). Hard rock reference expected peak acceleration ranges from 0.01g to 1.50g. Distances were adjusted to obtain target (input) median peak acceleration values. Single-corner point-source magnitude is 6.25.



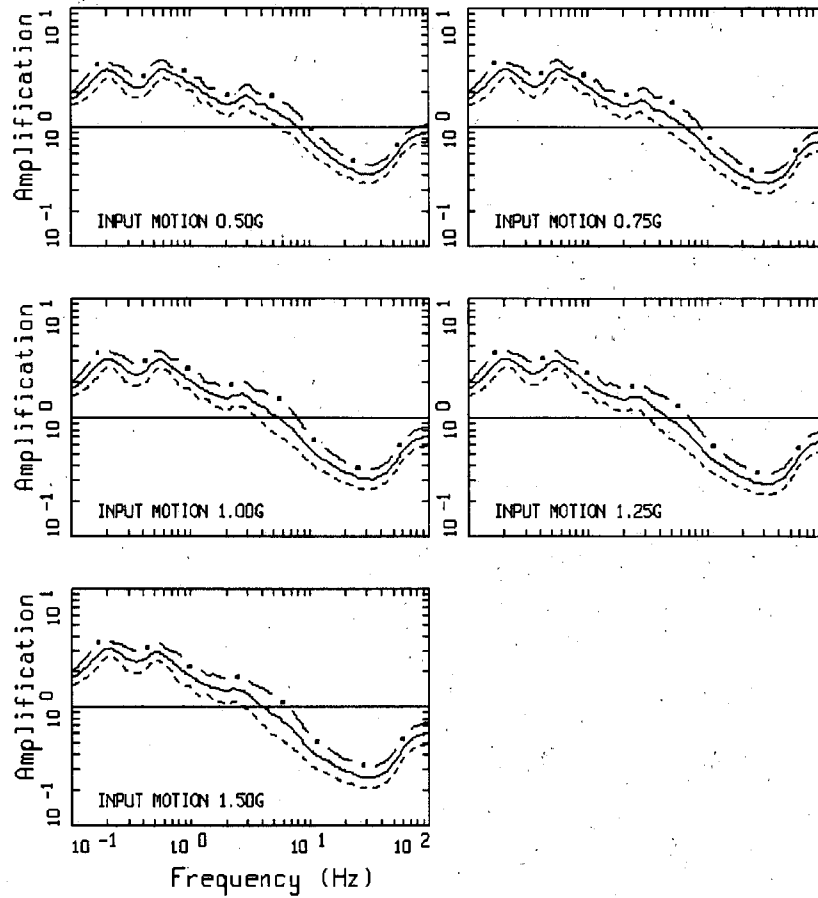
AMPLIFICATION, M = 6.25, 1 CORNER SOURCE SOURCE
RE.1: PROFILE 1, CURVE SET 1: PAGE 2 OF 2

Figure 4a (cont.) Example of median and ± 1 sigma estimates of amplification factors computed for the Grand Gulf Reactor embedded profile 1 (Figures 3a and 3b) using site-specific G/Gmax and hysteretic damping curves (EOI, 2008). Hard rock reference expected peak acceleration ranges from 0.01g to 1.50g. Distances were adjusted to obtain target (input) median peak acceleration values. Single-corner point-source magnitude is 6.25.



AMPLIFICATION, M = 7.69, 1 CORNER SOURCE
RE.1: PROFILE 1, CURVE SET 1: PAGE 1 OF 2

Figure 4b Example of median and ± 1 sigma estimates of amplification factors computed for the Grand Gulf Reactor embedded profile 1 (Figures 3a and 3b) using site-specific G/Gmax and hysteretic damping curves (EOI, 2008). Hard rock reference expected peak acceleration ranges from 0.01g to 1.50g. Distances were adjusted to obtain target (input) median peak acceleration values. Single-corner point-source magnitude is 7.69.



AMPLIFICATION, M = 7.69, 1 CORNER SOURCE
RE.1: PROFILE 1, CURVE SET 1: PAGE 2 OF 2

Figure 4b (cont.) Example of median and ± 1 sigma estimates of amplification factors computed for the Grand Gulf Reactor embedded profile 1 (Figures 3a and 3b) using site-specific G/Gmax and hysteretic damping curves (EOI, 2008). Hard rock reference expected peak acceleration ranges from 0.01g to 1.50g. Distances were adjusted to obtain target (input) median peak acceleration values. Single-corner point-source magnitude is 7.69.

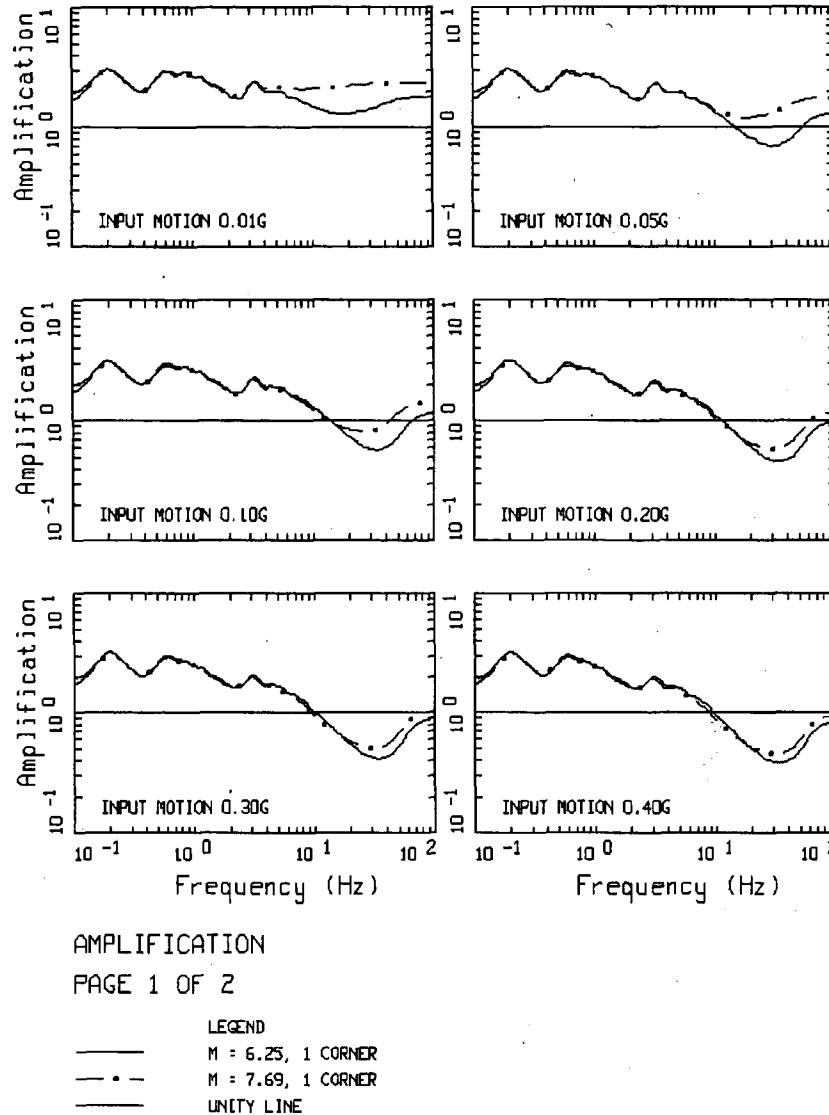


Figure 5a Illustration of the effects of magnitude on median amplification factors computed for the Grand Gulf reactor embedded profile 1 (Figures 3a and 3b) using site-specific G/G_{max} and hysteretic damping curves (EOI, 2008). Hard rock reference expected peak acceleration ranges from 0.01g to 1.50g. Distances were adjusted to obtain target (input) median peak acceleration values. Single-corner point-source magnitudes are 6.25 and 7.69.

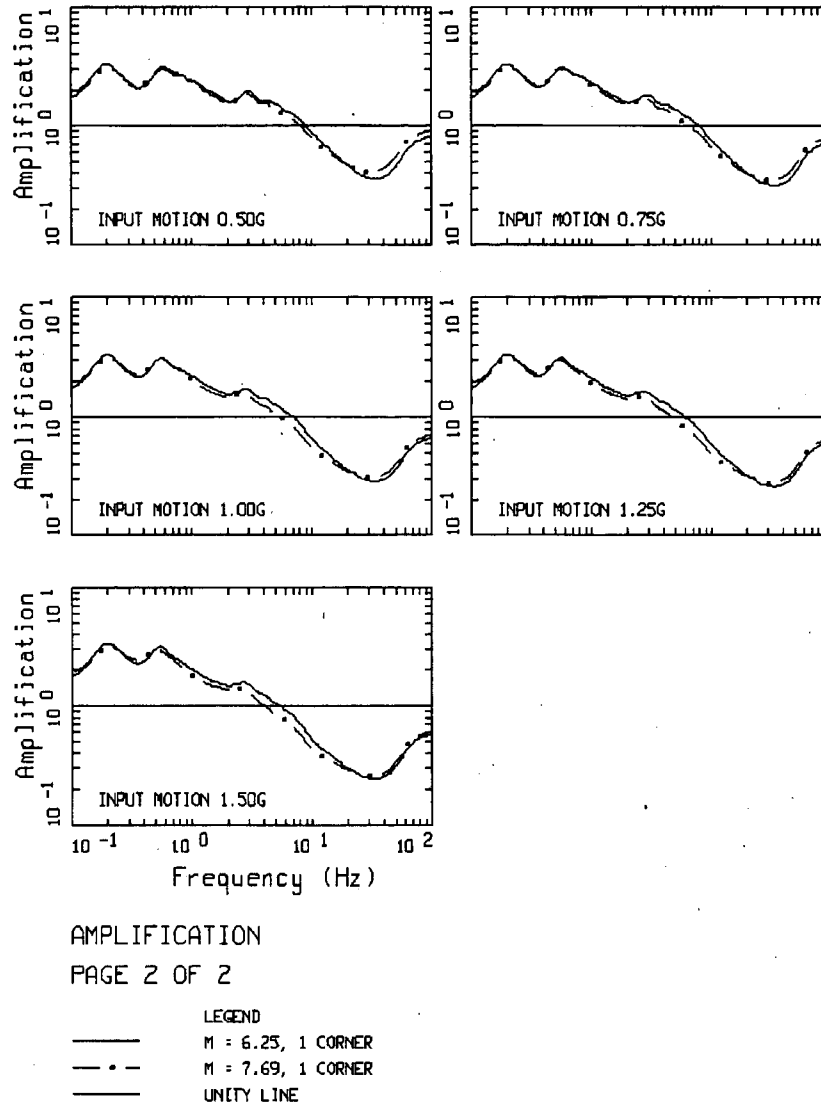
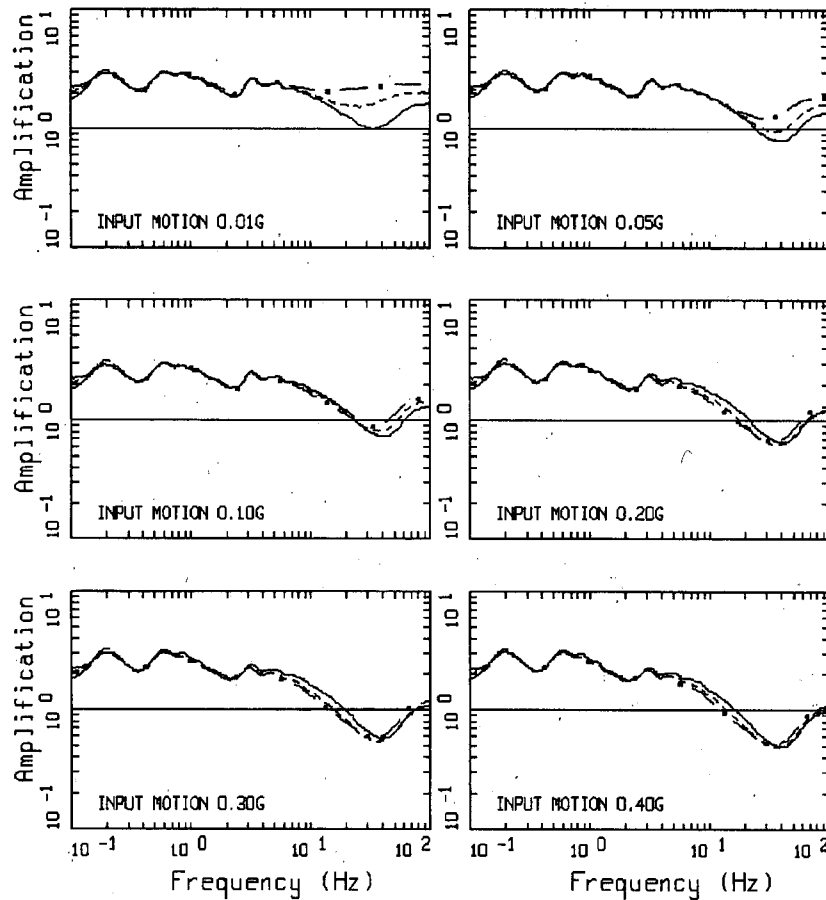


Figure 5a (cont.) Illustration of the effects of magnitude on median amplification factors computed for the Grand Gulf reactor embedded profile 1 (Figures 3a and 3b) using site-specific G/G_{max} and hysteretic damping curves (EOI, 2008). Hard rock reference expected peak acceleration ranges from 0.01g to 1.50g. Distances were adjusted to obtain target (input) median peak acceleration values. Single-corner point-source magnitudes are 6.25 and 7.69.

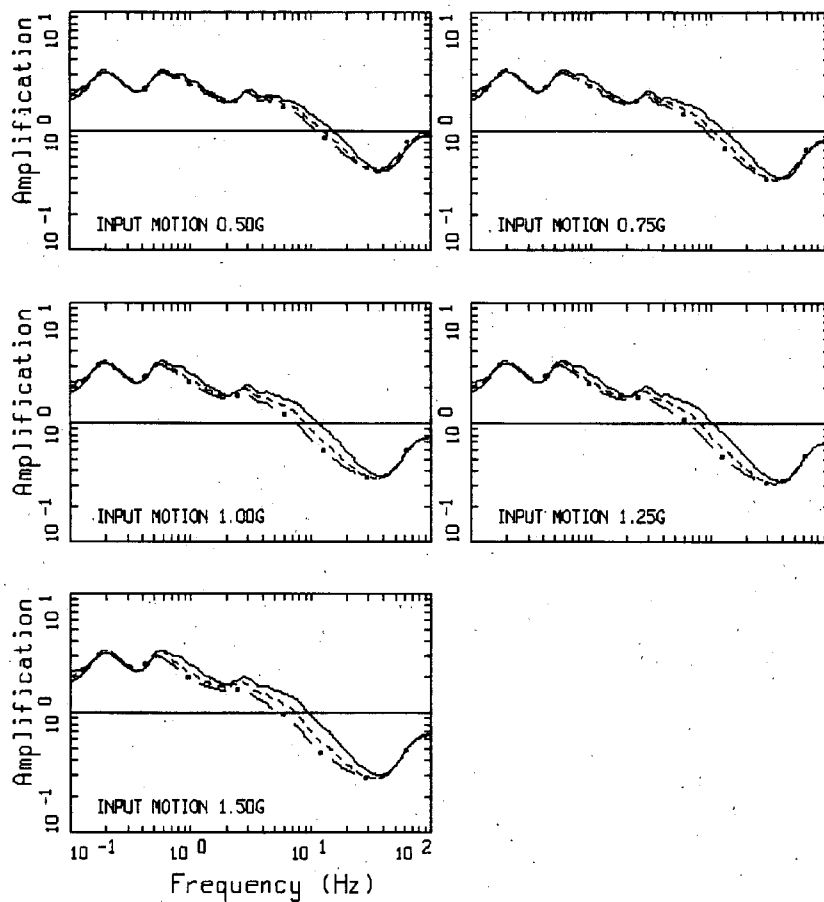


AMPLIFICATION

PAGE 1 OF 2

- LEGEND
- M = 5.0, 1 CORNER
 - - - M = 6.0, 1 CORNER
 - · - M = 7.0, 1 CORNER
 - UNITY LINE

Figure 5b Illustration of the effects of magnitude on median amplification factors computed for the Grand Gulf reactor embedded profile 1 (Figures 3a and 3b) using site-specific G/G_{max} and hysteretic damping curves (EOI, 2008). Hard rock reference expected peak acceleration ranges from 0.01g to 1.50g. Distances were adjusted to obtain target (input) median peak acceleration values. Single-corner point-source magnitudes are 5.0, 6.0, and 7.0.

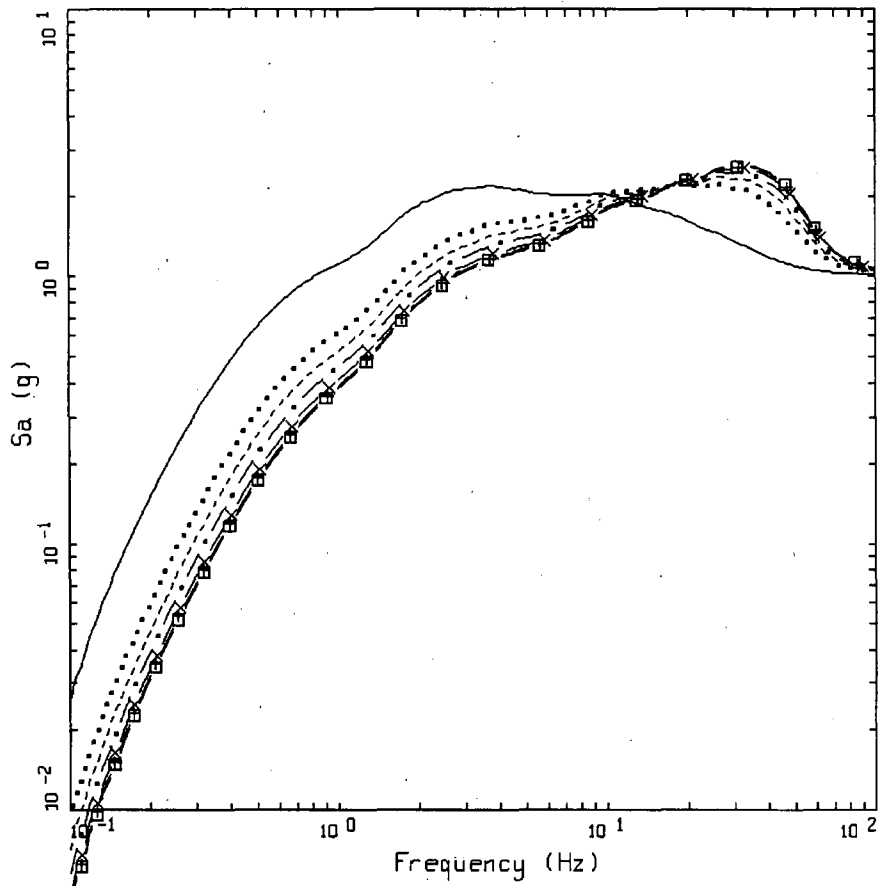


AMPLIFICATION

PAGE 2 OF 2

LEGEND	
————	M = 5.0, 1 CORNER
-----	M = 6.0, 1 CORNER
- · - · -	M = 7.0, 1 CORNER
————	UNITY LINE

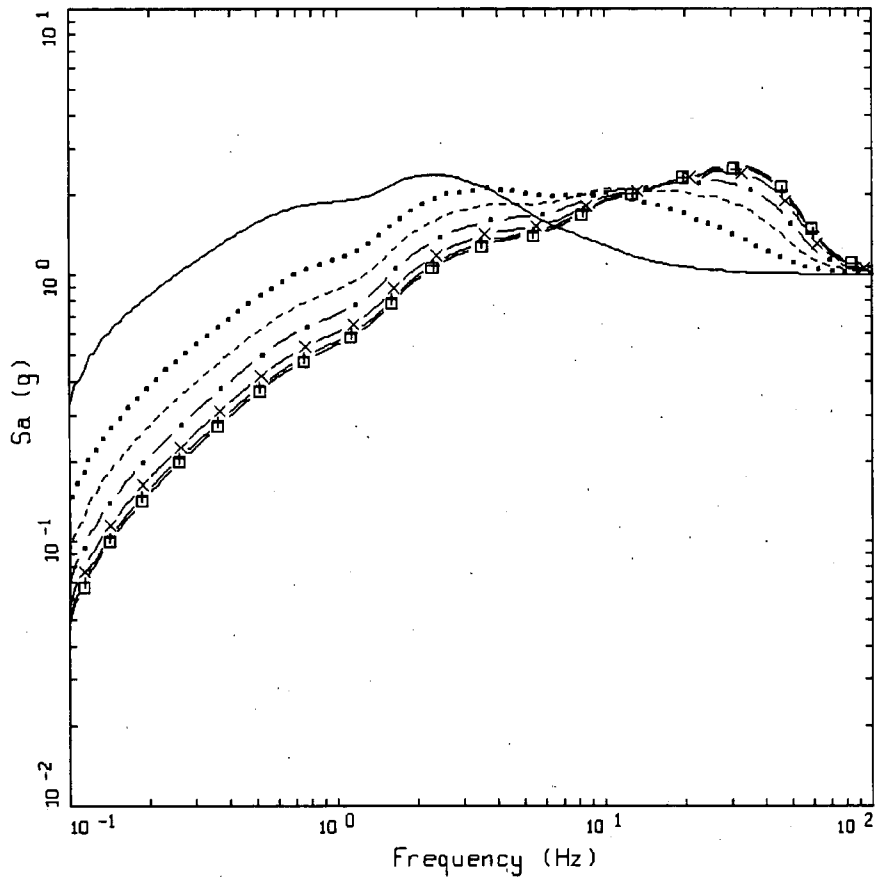
Figure 5b (cont.) Illustration of the effects of magnitude on median amplification factors computed for the Grand Gulf reactor embedded profile 1 (Figures 3a and 3b) using site-specific G/G_{max} and hysteretic damping curves (EOI, 2008). Hard rock reference expected peak acceleration ranges from 0.01g to 1.50g. Distances were adjusted to obtain target (input) median peak acceleration values. Single-corner point-source magnitudes are 5.0, 6.0, and 7.0.



GRAND GULF: M 6.25, 1 CORNER
REFERENCE MOTION

LEGEND	
—	G001, D = 190 KM, 50TH PERCENTILE, 0.01 G
.....	G005, D = 59 KM, 50TH PERCENTILE, 0.05 G
-----	G010, D = 37 KM, 50TH PERCENTILE, 0.10 G
- . - .	G020, D = 21 KM, 50TH PERCENTILE, 0.20 G
- x -	G050, D = 7 KM, 50TH PERCENTILE, 0.50 G
- + -	G100, D = 0 KM, 50TH PERCENTILE, 1.00 G
- □ -	G150, D = 0 KM, 50TH PERCENTILE, 1.50 G

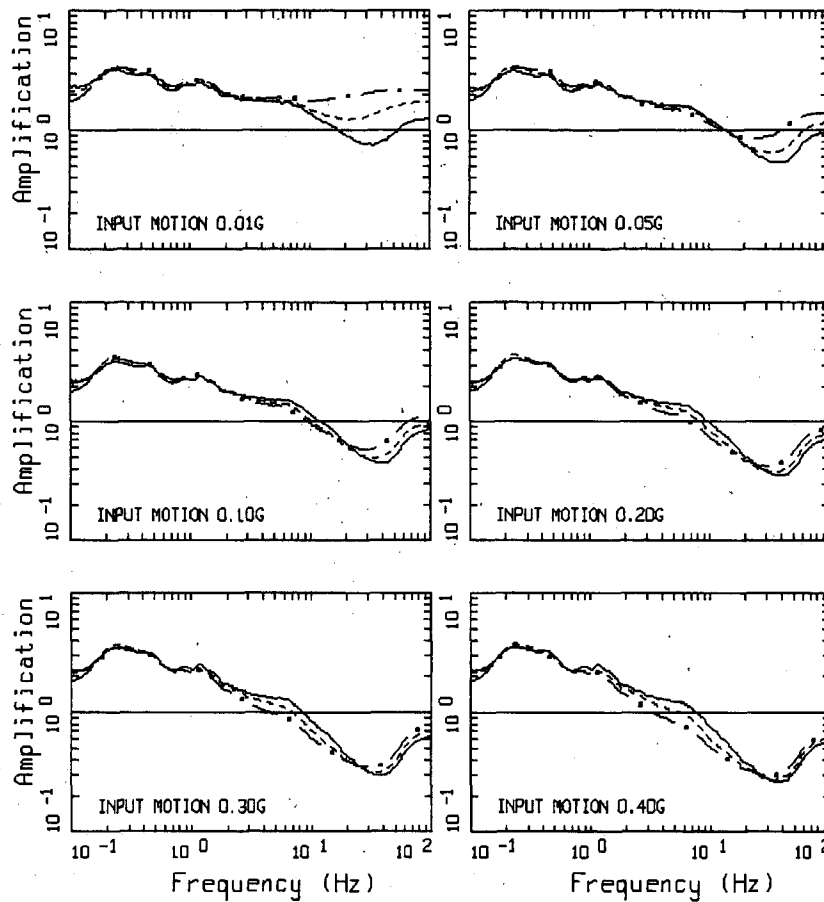
Figure 6a Response spectral shapes (median estimates) computed at the suite of distances to obtain the target peak acceleration values. Single-corner point source magnitude is 6.25.



GRAND GULF: M 7.69, 1 CORNER
REFERENCE MOTION

LEGEND	
————	G001, D = 480 KM, 50TH PERCENTILE, 0.01 G
.....	G005, D = 163 KM, 50TH PERCENTILE, 0.05 G
-----	G010, D = 92 KM, 50TH PERCENTILE, 0.10 G
- . -	G020, D = 50 KM, 50TH PERCENTILE, 0.20 G
- x -	G050, D = 24 KM, 50TH PERCENTILE, 0.50 G
- + -	G100, D = 12 KM, 50TH PERCENTILE, 1.00 G
- □ -	G150, D = 6 KM, 50TH PERCENTILE, 1.50 G

Figure 6b Response spectral shapes (median estimates) computed at the suite of distances to obtain the target peak acceleration values. Single-corner point source magnitude is 7.69.

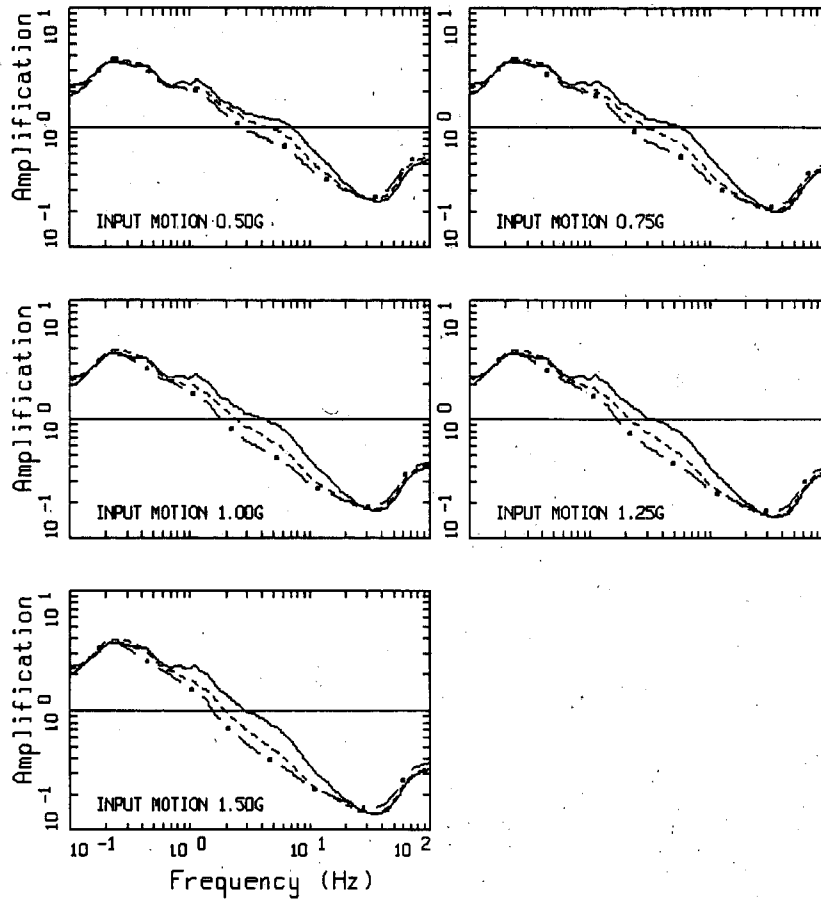


AMPLIFICATION

PAGE 1 OF 2

LEGEND	
————	M = 5.0, 1 CORNER
-----	M = 6.0, 1 CORNER
- . - .	M = 7.0, 1 CORNER
————	UNITY LINE

Figure 7 Test case illustrating the effect of magnitude on median amplification factors computed for a deep stiff soil site in the CENA. Distances were adjusted to obtain the target hard rock (input) median peak acceleration values. Single-corner point-source magnitudes are 5.0, 6.0, and 7.0. Plotted versus structural frequency.

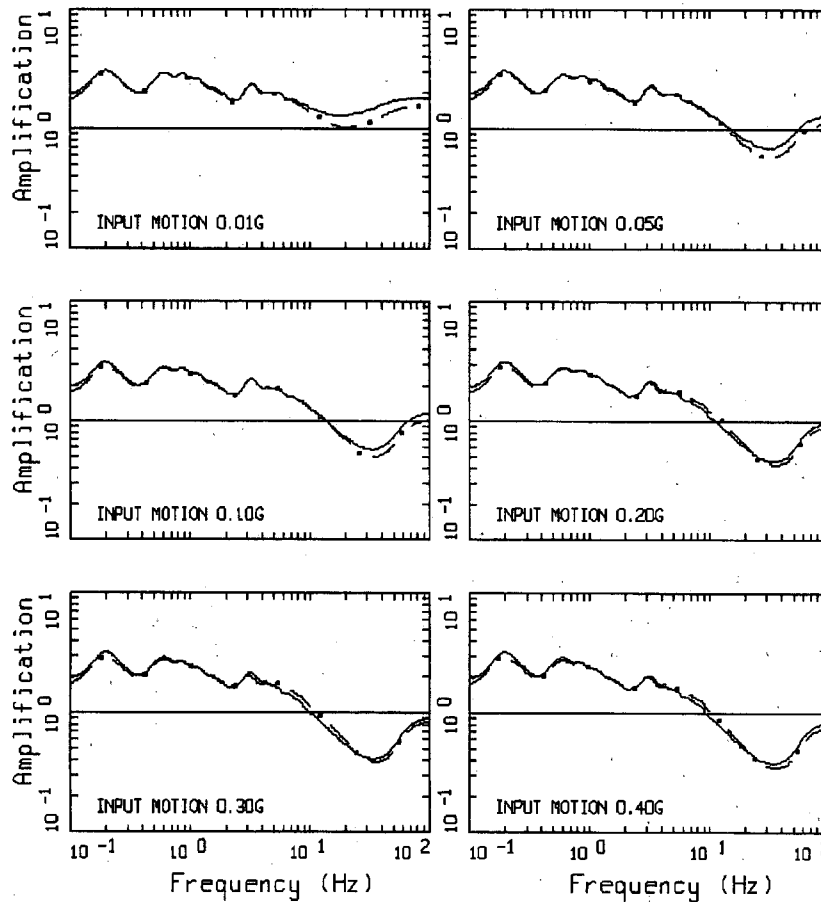


AMPLIFICATION

PAGE 2 OF 2

LEGEND	
—	M = 5.0, 1 CORNER
- - -	M = 6.0, 1 CORNER
- · -	M = 7.0, 1 CORNER
—	UNCY LINE

Figure 7 (cont.) Test case illustrating the effect of magnitude on median amplification factors computed for a deep stiff soil site in the CENA. Distances were adjusted to obtain the target hard rock (input) median peak acceleration values. Single-corner point-source magnitudes are 5.0, 6.0, and 7.0. Plotted versus structural frequency.

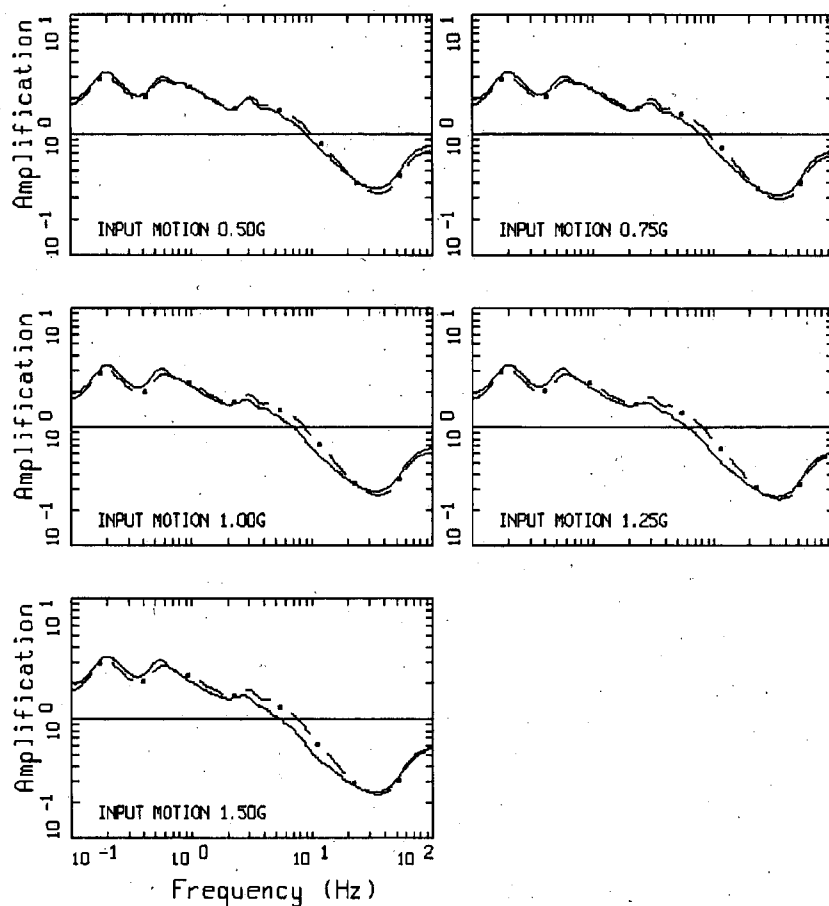


AMPLIFICATION

PAGE 1 OF 2

- LEGEND
- M = 6.25, 1 CORNER
 - · - M = 6.25, 2 CORNER
 - UNITY LINE

Figure 8a Illustration of the effects of single-corner versus double-corner source spectra on median amplification factors computed for the Grand Gulf reactor embedded profile 1 (Figures 3a and 3b) using site-specific G/G_{max} and hysteretic damping curves (EOI, 2008). Hard rock reference expected peak acceleration ranges from 0.01g to 1.50g. Distances were adjusted to obtain target (input) median peak acceleration values. Single-corner and double-corner point-source magnitudes are 6.25.

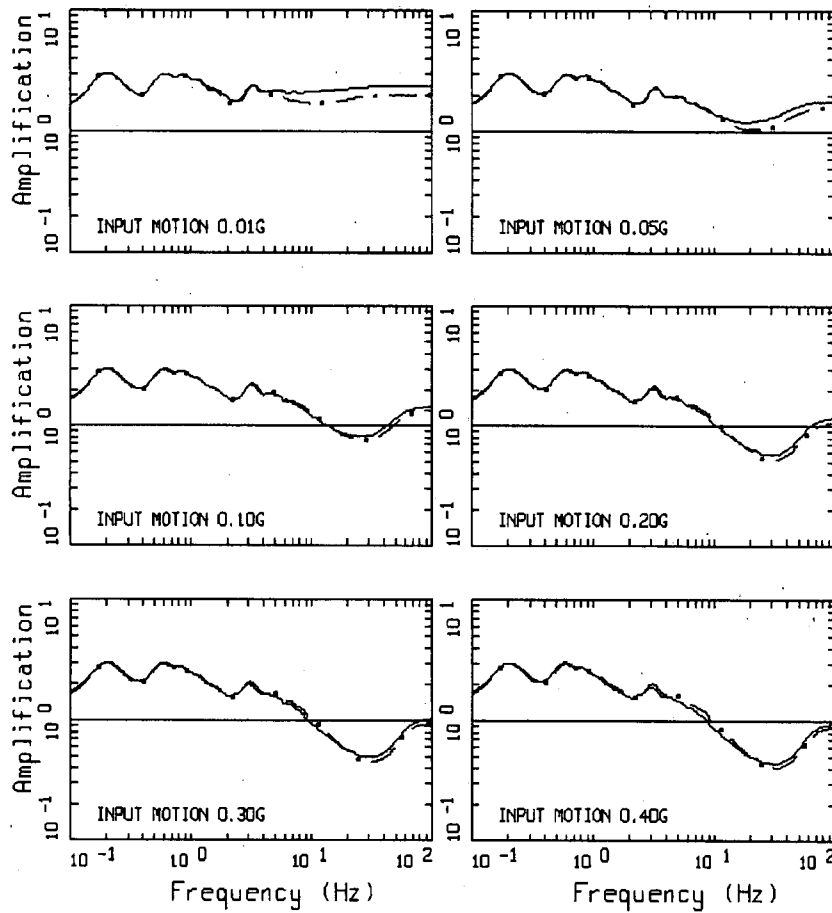


AMPLIFICATION

PAGE 2 OF 2

- LEGEND
- M = 6.25, 1 CORNER
 - - - M = 6.25, 2 CORNER
 - UNITY LINE

Figure 8a (cont.) Illustration of the effects of single-corner versus double-corner source spectra on median amplification factors computed for the Grand Gulf reactor embedded profile 1 (Figures 3a and 3b) using site-specific G/G_{max} and hysteretic damping curves (EOJ, 2008). Hard rock reference expected peak acceleration ranges from 0.01g to 1.50g. Distances were adjusted to obtain target (input) median peak acceleration values. Single-corner and double-corner point-source magnitudes are 6.25.

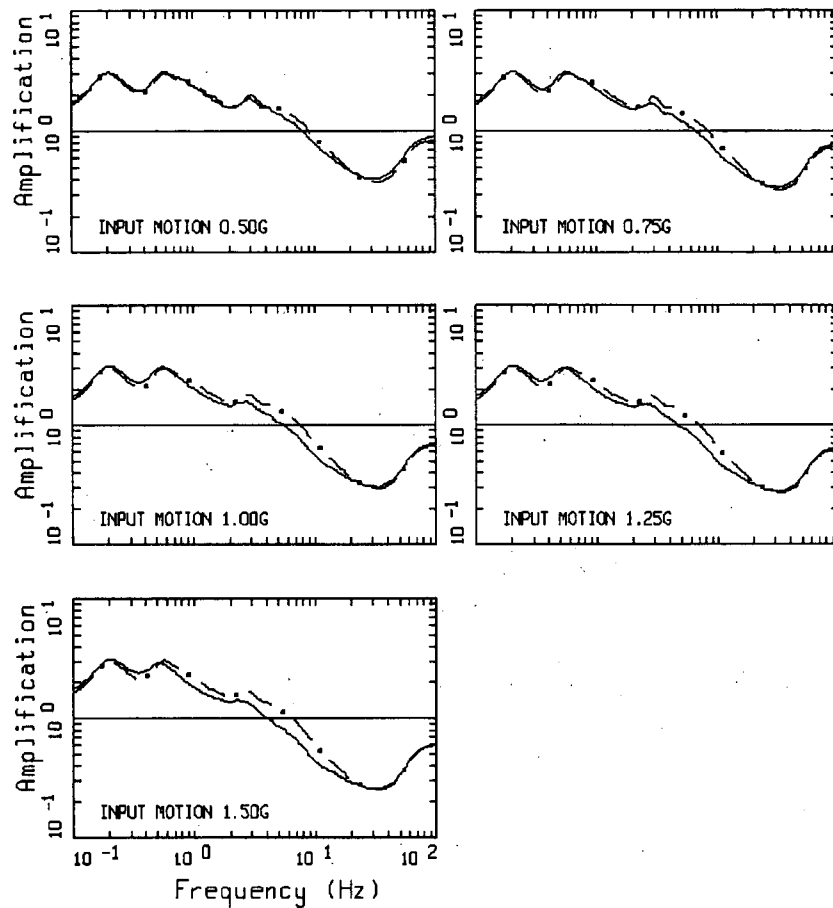


AMPLIFICATION

PAGE 1 OF 2

- LEGEND
- M = 7.69, 1 CORNER
 - - - M = 7.69, 2 CORNER
 - UNITY LINE

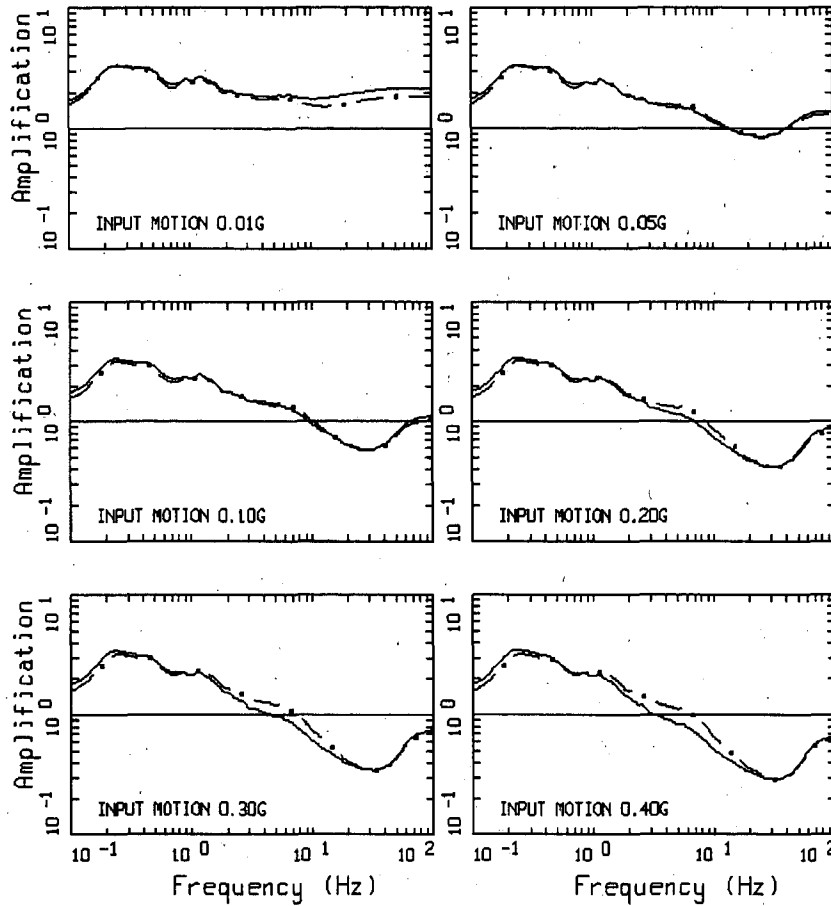
Figure 8b Illustration of the effects of single-corner versus double-corner source spectra on median amplification factors computed for the Grand Gulf reactor embedded profile 1 (Figures 3a and 3b) using site-specific G/G_{max} and hysteretic damping curves (EOI, 2008). Hard rock reference expected peak acceleration ranges from 0.01g to 1.50g. Distances were adjusted to obtain target (input) median peak acceleration values. Single-corner and double-corner point-source magnitudes are 7.69.



AMPLIFICATION
 PAGE 2 OF 2

LEGEND
 — M = 7.69, 1 CORNER
 - · - M = 7.69, 2 CORNER
 — UNITY LINE

Figure 8b (cont.) Illustration of the effects of single-corner versus double-corner source spectra on median amplification factors computed for the Grand Gulf reactor embedded profile 1 (Figures 3a and 3b) using site-specific G/G_{max} and hysteretic damping curves (EOI, 2008). Hard rock reference expected peak acceleration ranges from 0.01g to 1.50g. Distances were adjusted to obtain target (input) median peak acceleration values. Single-corner and double-corner point-source magnitudes are 7.69.

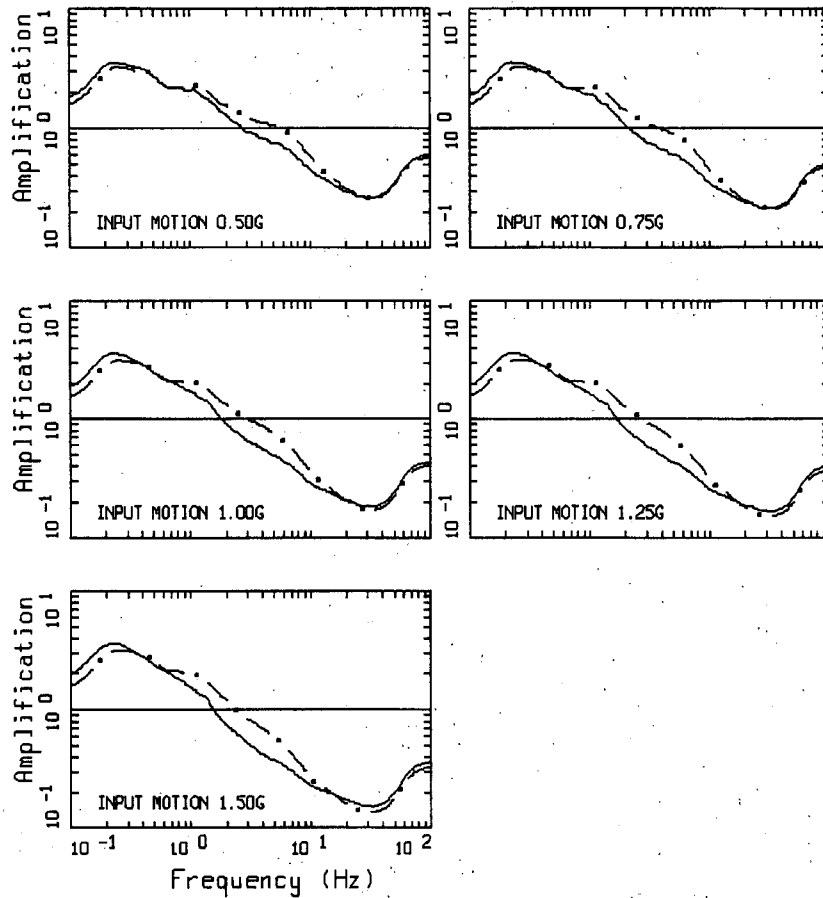


AMPLIFICATION

PAGE 1 OF 2

- LEGEND
- M = 7.0, 1 CORNER
 - - - M = 7.0, 2 CORNER
 - UNITY LINE

Figure 9 Test cases illustrating the effect of single-versus double-corner source spectra on median amplification factors computed for a deep stiff soil site in the CENA. Distances were adjusted to obtain the target hard rock (input) median peak acceleration values. Plotted versus structural frequency. Single-corner and double-corner point-source magnitudes are 7.0.



AMPLIFICATION

PAGE 2 OF 2

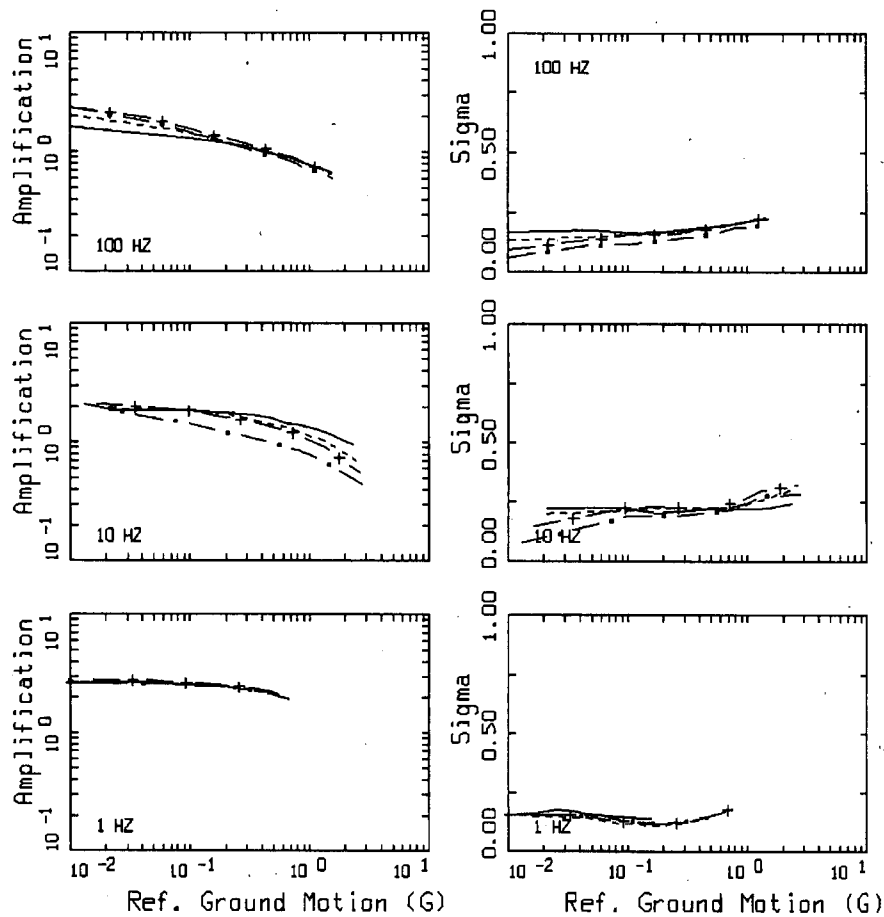
LEGEND

— M = 7.0, 1 CORNER

- · - M = 7.0, 2 CORNER

— UNITY LINE

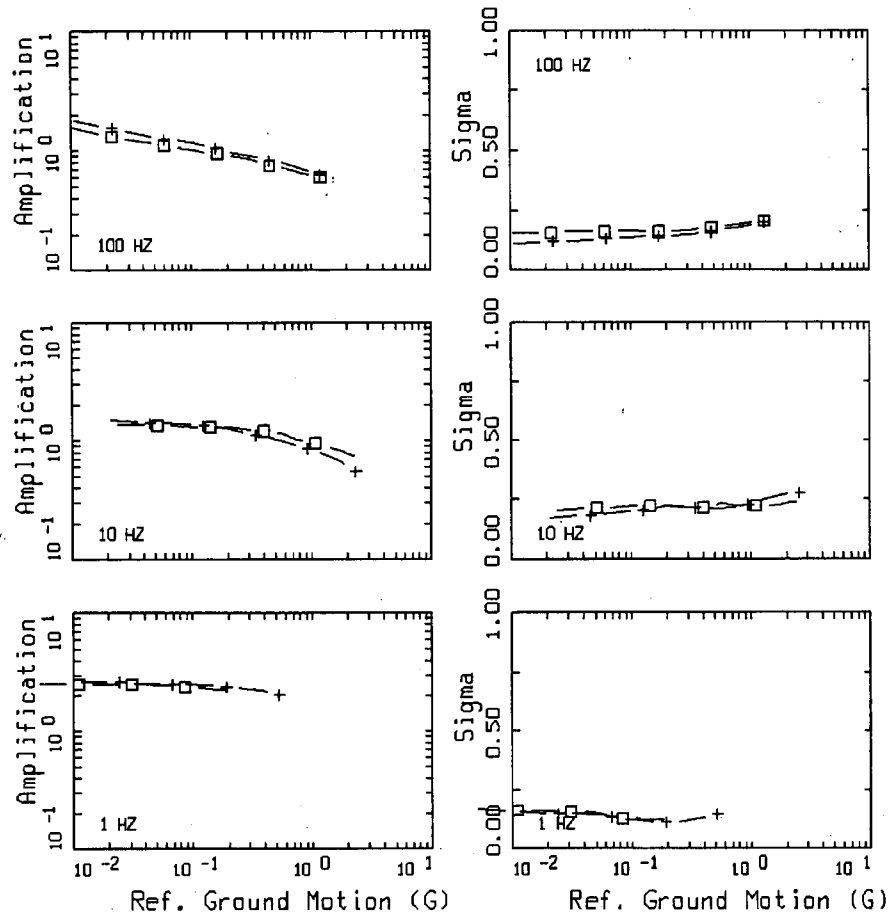
Figure 9 (cont.) Test cases illustrating the effect of single-verses double-corner source spectra on median amplification factors computed for a deep stiff soil site in the CENA. Distances were adjusted to obtain the target hard rock (input) median peak acceleration values. Plotted verses structural frequency. Single-corner and double-corner point-source magnitudes are 7.0.



MEDIAN AMPLIFICATION AND SIGMA

LEGEND	
————	M5.0, 1 CORNER
-----	M6.0, 1 CORNER
— + —	M7.0, 1 CORNER
— x —	M7.69, 1 CORNER

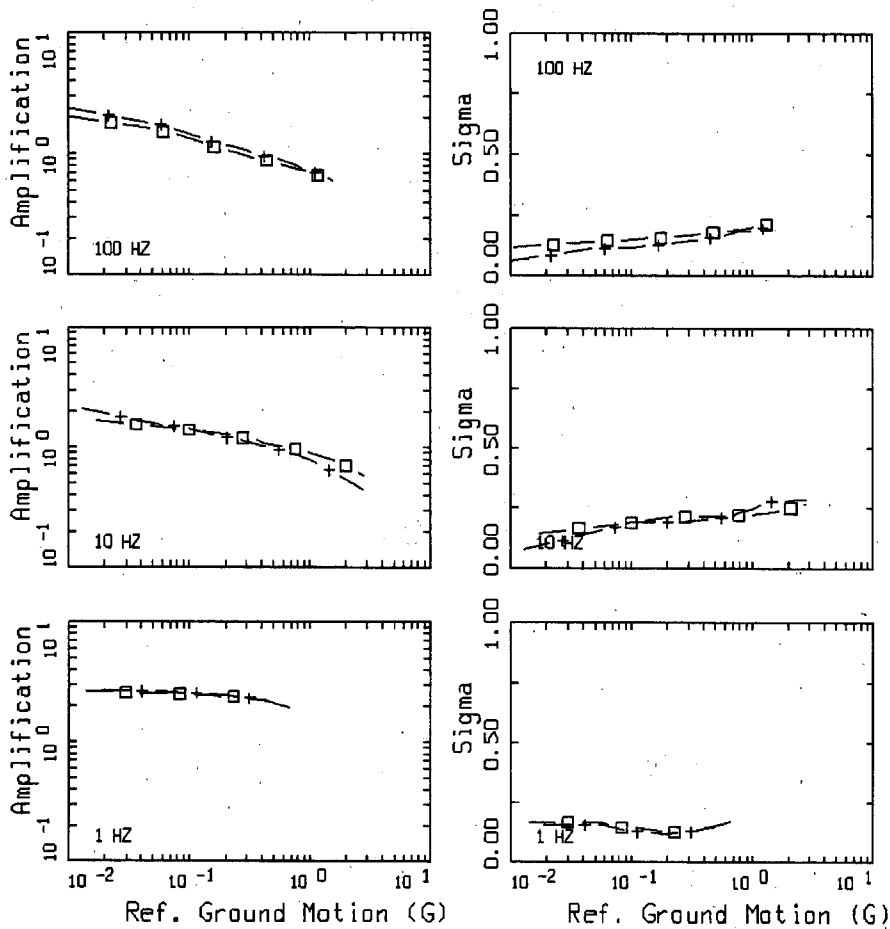
Figure 10 Illustration of the effect of magnitude on median amplification factors and sigma value (σ_m) computed for the Grand Gulf reactor embedded profile 1 (Figures 3a and 3b) using site-specific G/G_{max} and hysteretic damping curves (EOI, 2008). Plotted versus reference site ground motion (5% damped spectral acceleration (S_a)) at three structural frequencies.



MEDIAN AMPLIFICATION AND SIGMA

LEGEND
 — + — M6.25, 1 CORNER
 — □ — M6.25, 2 CORNER

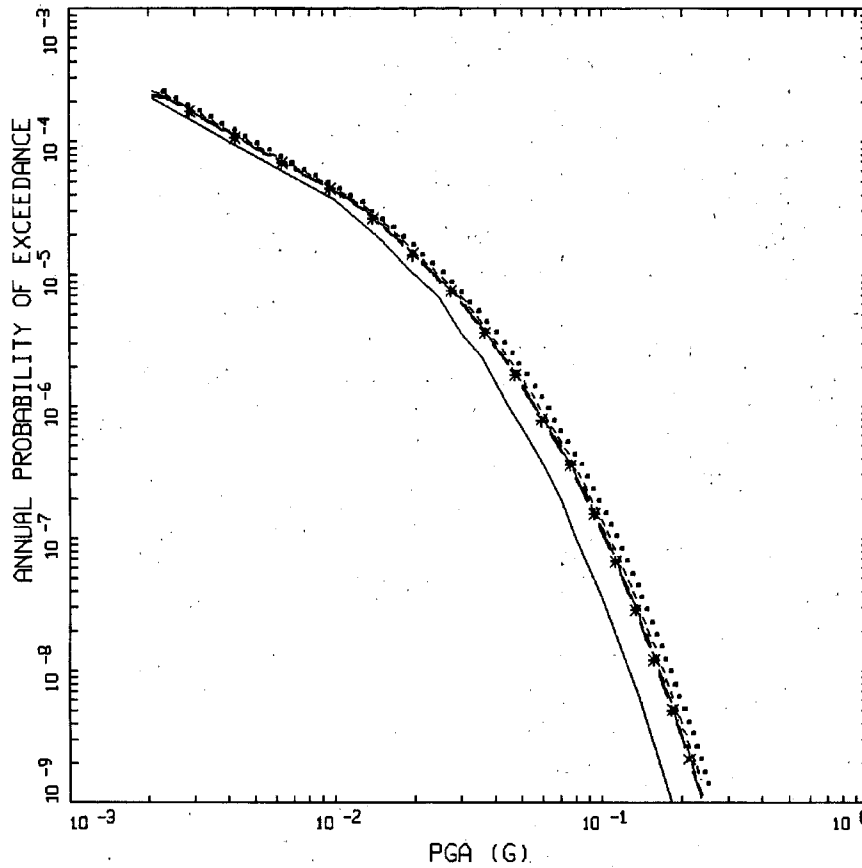
Figure 11a Illustration of the effect of single-verses double-corner source spectra on median amplification factors and sigma value (σ_{in}) computed for the Grand Gulf reactor embedded profile 1 (Figures 3a and 3b) using site-specific G/G_{max} and hysteretic damping curves (EOI, 2008). Single-corner and double-corner point-source magnitude is 6.25. Plotted verses reference site ground motion (5% damped spectral acceleration (Sa) at three structural frequencies.



MEDIAN AMPLIFICATION AND SIGMA

LEGEND	
— + —	M7.69, 1 CORNER
— □ —	M7.69, 2 CORNER

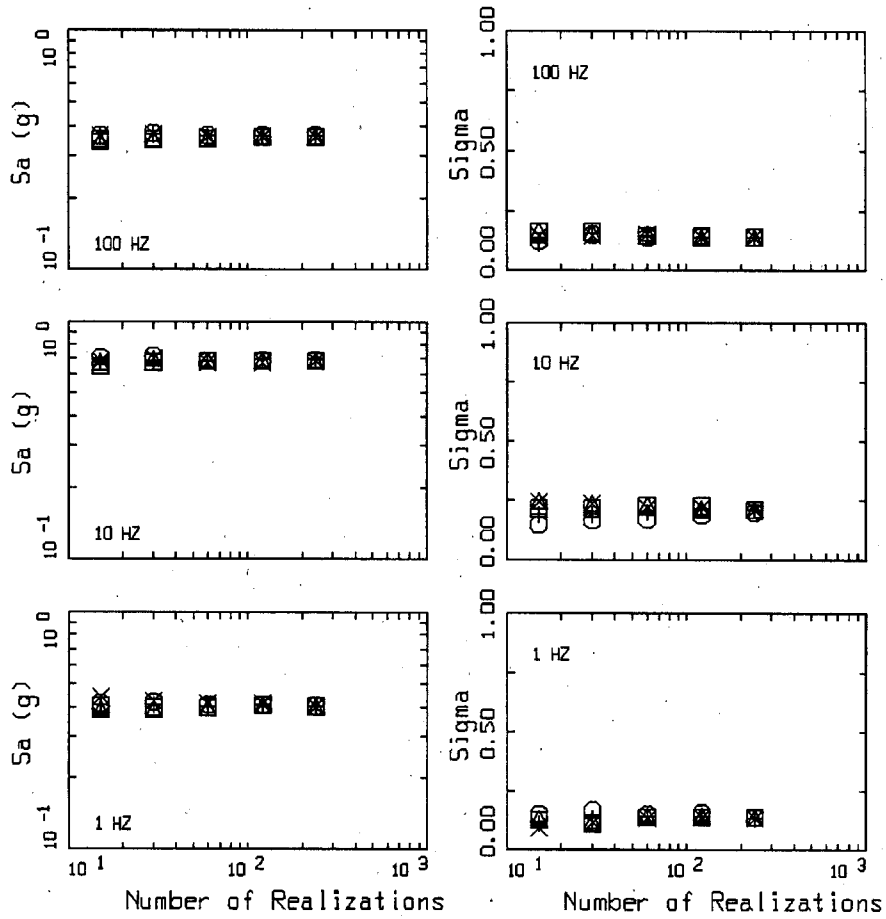
Figure 11b Illustration of the effect of single-verses double-corner source spectra on median amplification factors and sigma value (σ_{in}) computed for the Grand Gulf reactor embedded profile 1 (Figures 3a and 3b) using site-specific G/G_{max} and hysteretic damping curves (EOI, 2008). Single-corner and double-corner point-source magnitude is 7.69. Plotted verses reference site ground motion (5% damped spectral acceleration (S_a) at three structural frequencies.



GENERIC SITE: HAZARD CURVES
MEAN, PGA

- LEGEND
- INPUT HAZARD CURVE, MEAN
 - OUTPUT HAZARD CURVE, MEAN, 25 POINTS INTERPOLATION
 - OUTPUT HAZARD CURVE, MEAN, 50 POINTS INTERPOLATION
 - - - - - OUTPUT HAZARD CURVE, MEAN, 101 POINTS INTERPOLATION
 - . - . - OUTPUT HAZARD CURVE, MEAN, 150 POINTS INTERPOLATION
 - x - - - OUTPUT HAZARD CURVE, MEAN, 200 POINTS INTERPOLATION
 - + - - - OUTPUT HAZARD CURVE, MEAN, 300 POINTS INTERPOLATION

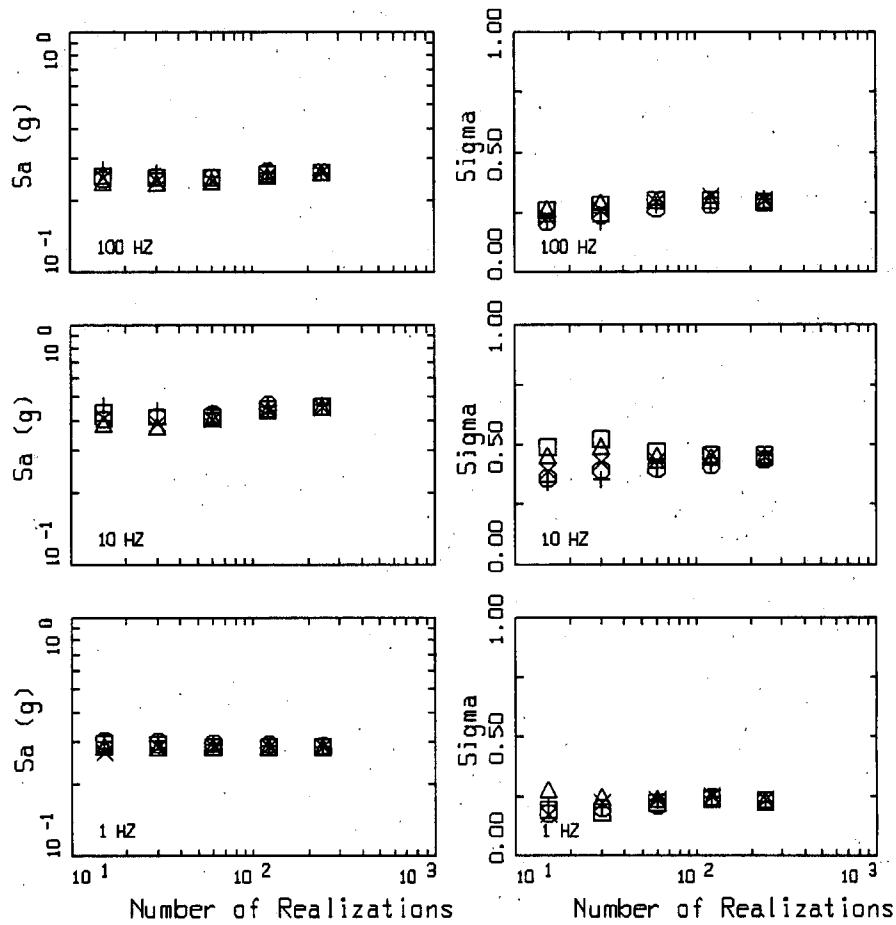
Figure 12 Interpolation test case illustrating the rapid convergence to integration stability. Note the small change in hazard for a large increase in the number of interpolation points.



SPECTRAL ACCELERATION AND SIGMA

LEGEND	
□····□	S1
×····×	S2
△····△	S3
○····○	S4
+····+	S5
□····□	
×····×	

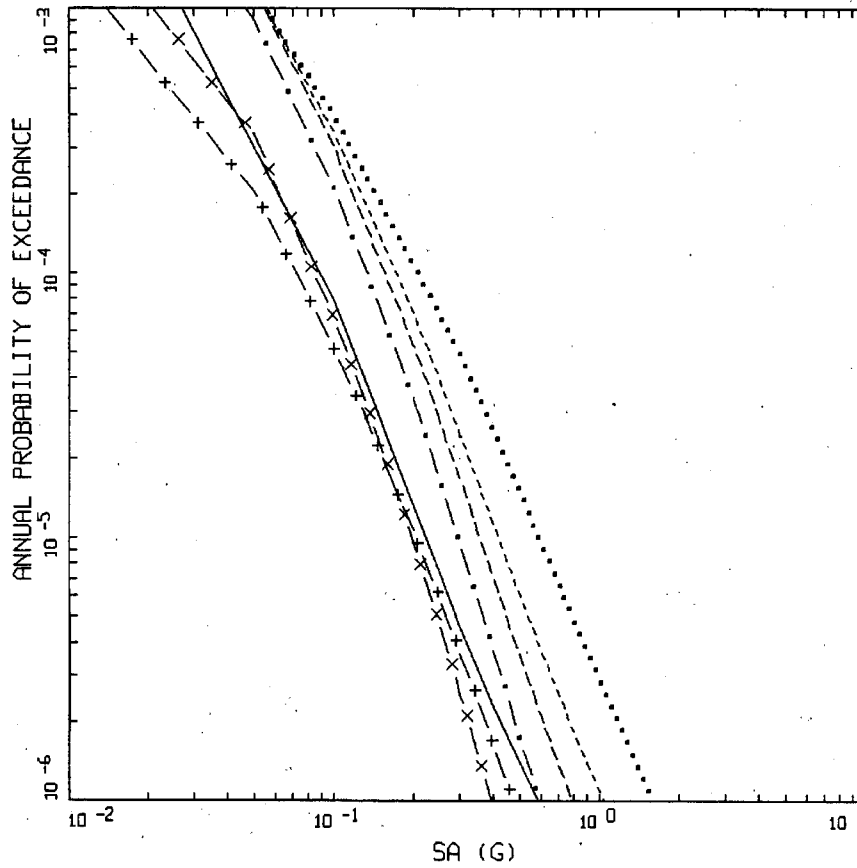
Figure 13a Median and sigma estimates computed for numbers of realizations from 15 to 240 using five different random seeds for the Grand Gulf reactor embedded profile 1 (Figures 3a and 3b) using site-specific G/G_{max} and hysteretic damping curves (EOI, 2008).



SPECTRAL ACCELERATION AND SIGMA

LEGEND	
□····□	S1
X····X	S2
△····△	S3
○····○	S4
+····+	S5
□····□	
X····X	

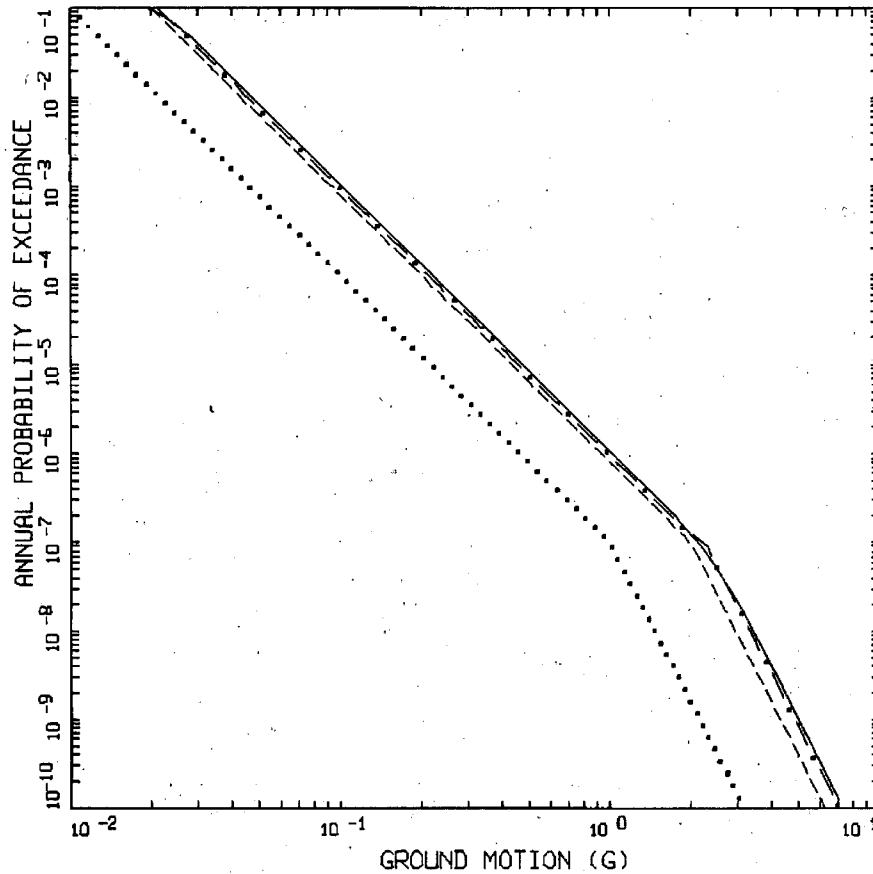
Figure 13b Median and sigma estimates computed for numbers of realizations from 15 to 240 using five different random seeds for a deep stiff soil site in the CENA.



GRAND GULF: HAZARD CURVES
HARD ROCK, MEAN

- LEGEND
- MEAN, PGA
 - MEAN, 25 HZ
 - MEAN, 10 HZ
 - MEAN, 5 HZ
 - . - MEAN, 2.5 HZ
 - x - MEAN, 1 HZ
 - + - MEAN, 0.5 HZ

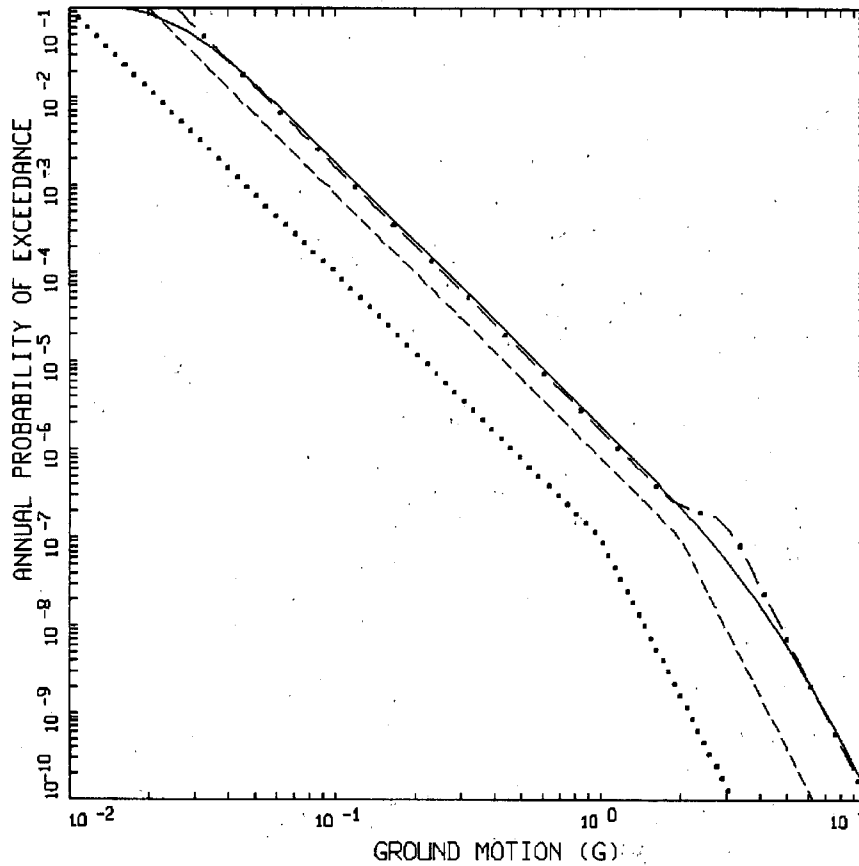
Figure 14 Grand Gulf Nuclear Site Unit 3 hard rock horizontal hazard curves (EOI, 2008).



TEST EXAMPLE
 AMP=2.0, SIGMA AMP=0.20

- LEGEND
- INPUT ROCK HAZARD CURVE, SLOPES=3,6
 - INPUT ROCK HAZARD CURVE MULTIPLIED BY AMP=2.0
 - . - . - . OUTPUT SOIL HAZARD CURVE: APPROACH 3 APPROXIMATE
 - OUTPUT SOIL HAZARD CURVE: APPROACH 3 FULL INTEGRATION

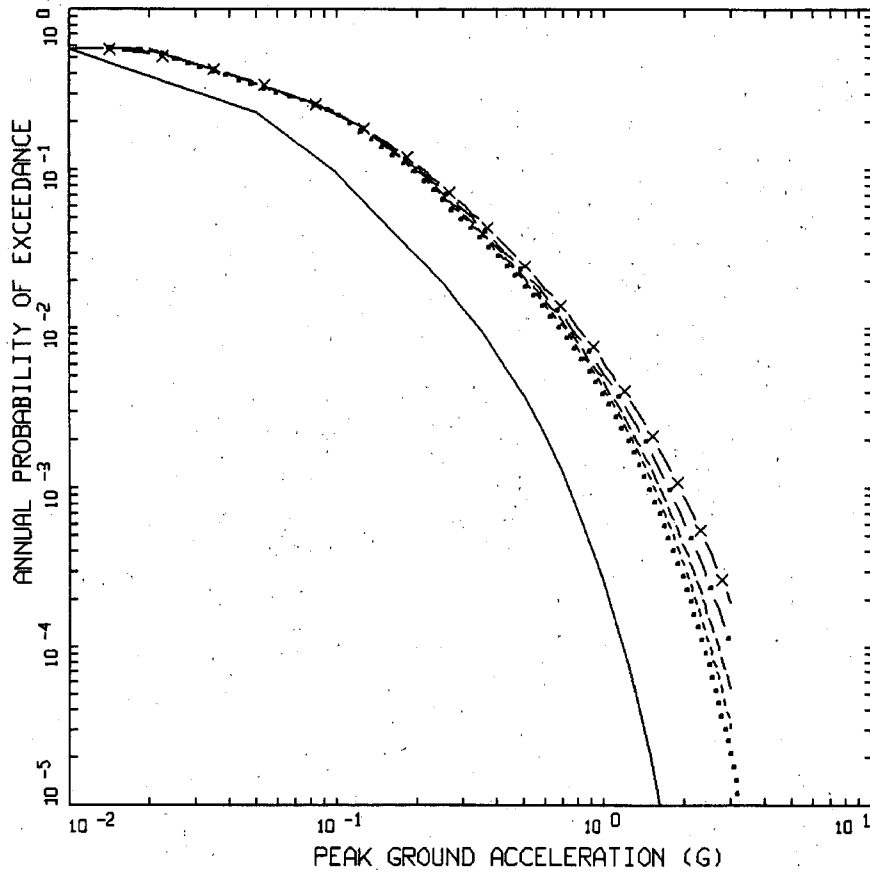
Figure 15 Test case illustrating Approach 3 using a simple bilinear reference site hazard curve (dotted line, slope = 3, 6). Median amplification factor is 2.0, $\sigma_{in} = 0.2$. Dashed line, reference hazard times median amplification, very close to Approach 2 which uses mean amplification (mean = median $e^{\frac{\sigma^2}{2}}$). Dashed-dot line represents approximate Approach 3 (Equation 7), solid line is full integration Approach 3 (Equation 5). Note the impact of the reference hazard curve slope on the difference between Approaches 2 and 3.



TEST EXAMPLE
 AMP=2.0, SIGMA AMP=0.40

- LEGEND
- INPUT ROCK HAZARD CURVE, SLOPES=3,6
 - INPUT ROCK HAZARD CURVE MULTIPLIED BY AMP=2.0
 - .-.-.- OUTPUT SOIL HAZARD CURVE: APPROACH 3 APPROXIMATE
 - OUTPUT SOIL HAZARD CURVE: APPROACH 3 FULL INTEGRATION

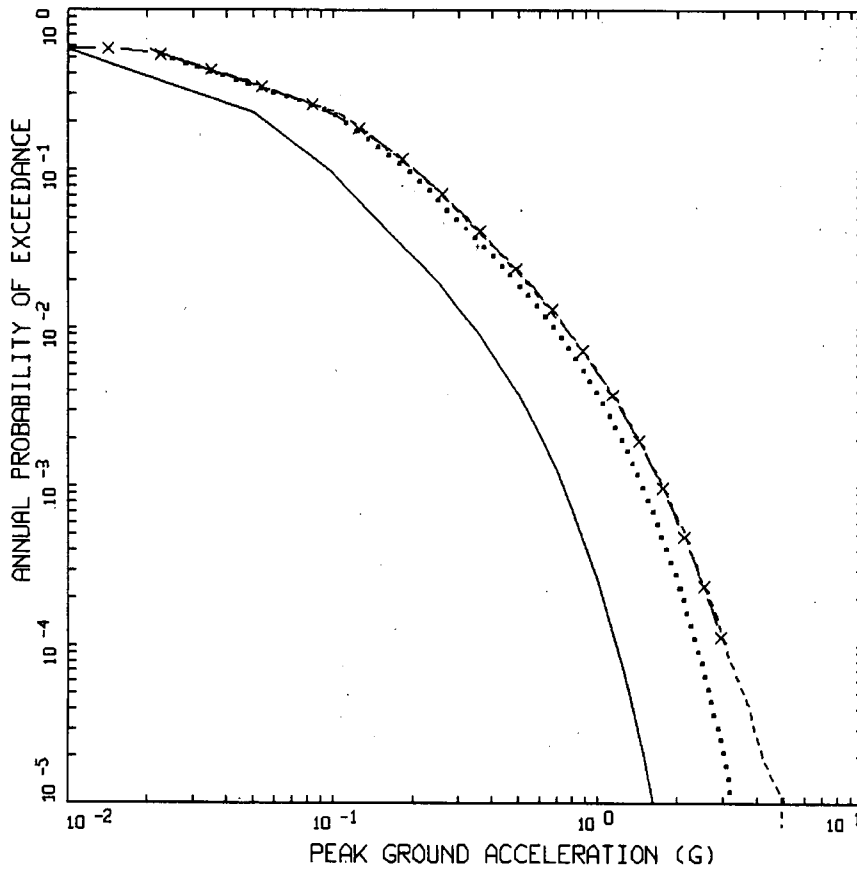
Figure 16 Test case illustrating Approach 3 using a simple bilinear reference site hazard curve (dotted line, slope = 3, 6). Median amplification factor is 2.0, $\sigma_{in} = 0.4$. Dashed line, reference hazard times median amplification, very close to Approach 2 which uses mean amplification (mean = median $e^{\frac{\sigma^2}{2}}$). Dashed-dot line represents approximate Approach 3 (Equation 7), solid line is full integration Approach 3 (Equation 5). Note the impact of the reference hazard curve slope on the difference between Approaches 2 and 3.



TEST EXAMPLE: PGA HAZARD CURVE
 AMP FACTOR = 2.0

- LEGEND
- INPUT HAZARD CURVE
 - INPUT HAZARD CURVE SCALED BY AMP=2.0
 - APPROACH 3 FULL INTEGRATION: SIGMA = 0.10
 - APPROACH 3 FULL INTEGRATION: SIGMA = 0.20
 - · - - APPROACH 3 FULL INTEGRATION: SIGMA = 0.30
 - x - - APPROACH 3 FULL INTEGRATION: SIGMA = 0.40

Figure 17 Test case illustrating Approach 3 using a realistic (WNA) reference site hazard curve (solid line). Median amplification factor is 2.0, $\sigma_m = 0.1, 0.2, 0.3, 0.4$. Dotted line, reference hazard times median amplification, very close to Approach 2 which uses mean amplification (mean = median $e^{\frac{\sigma^2}{2}}$). Note the impact of the reference hazard curve change in slope on the differences between Approaches 2 and 3 (full integration).



TEST EXAMPLE: PGA HAZARD CURVE
 AMP FACTOR = 2.0, SIGMA=0.30

- LEGEND
- INPUT HAZARD CURVE
 - INPUT HAZARD CURVE SCALED BY AMP=2.0
 - APPROACH 3 APPROXIMATE: SIGMA = 0.30
 - x — APPROACH 3 FULL INTEGRATION: SIGMA = 0.30

Figure 18 Test case illustrating Approach 3 using a realistic (WNA) reference site hazard curve (solid line). Median amplification factor is 2.0, $\sigma_{in} = 0.3$. Dotted line, reference hazard times median amplification, very close to Approach 2 which uses mean amplification (mean = median $e^{\frac{\sigma^2}{2}}$). Dashed line represents approximate Approach 3 (Equation 7), solid crosses line reflects full integration Approach 3 (Equation 5). Note the impact of the reference hazard curve change in slope on the differences between Approaches 2 and 3 and the breakdown for approximate Approach 3 below AEF of 2×10^{-4} , in this case.

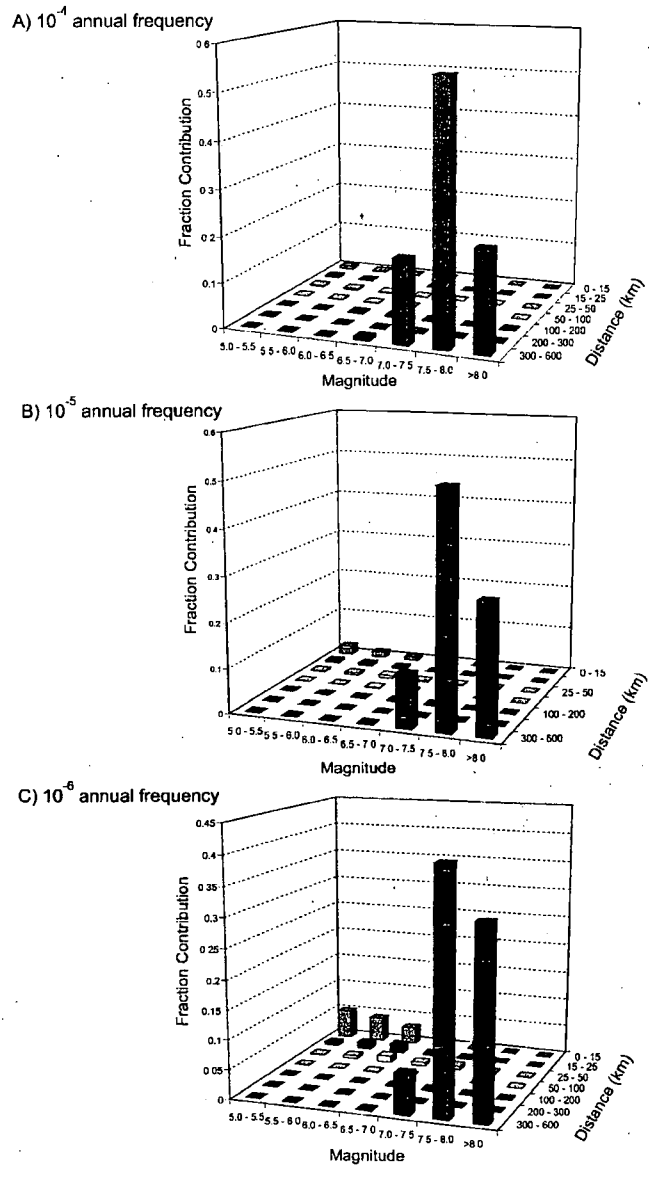


Figure 19a Deaggregation for the Grand Gulf Nuclear Station Unit 3: low-frequency, 1 Hz to 2.5 Hz (FSAR Figure 2.5.2-210, EOI, 2008).

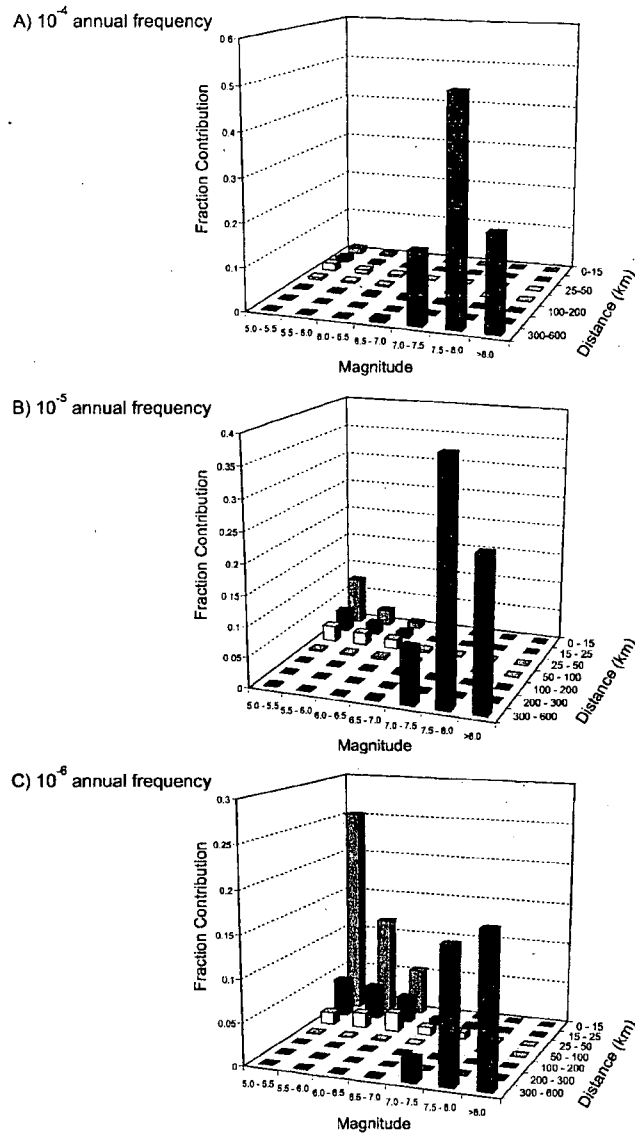
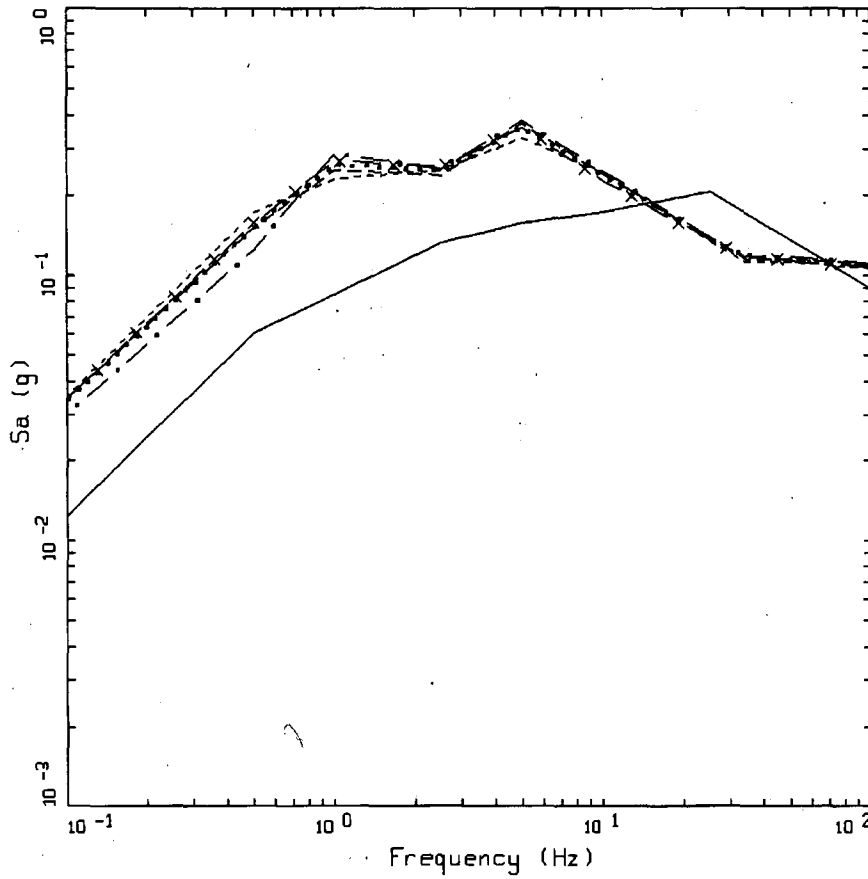


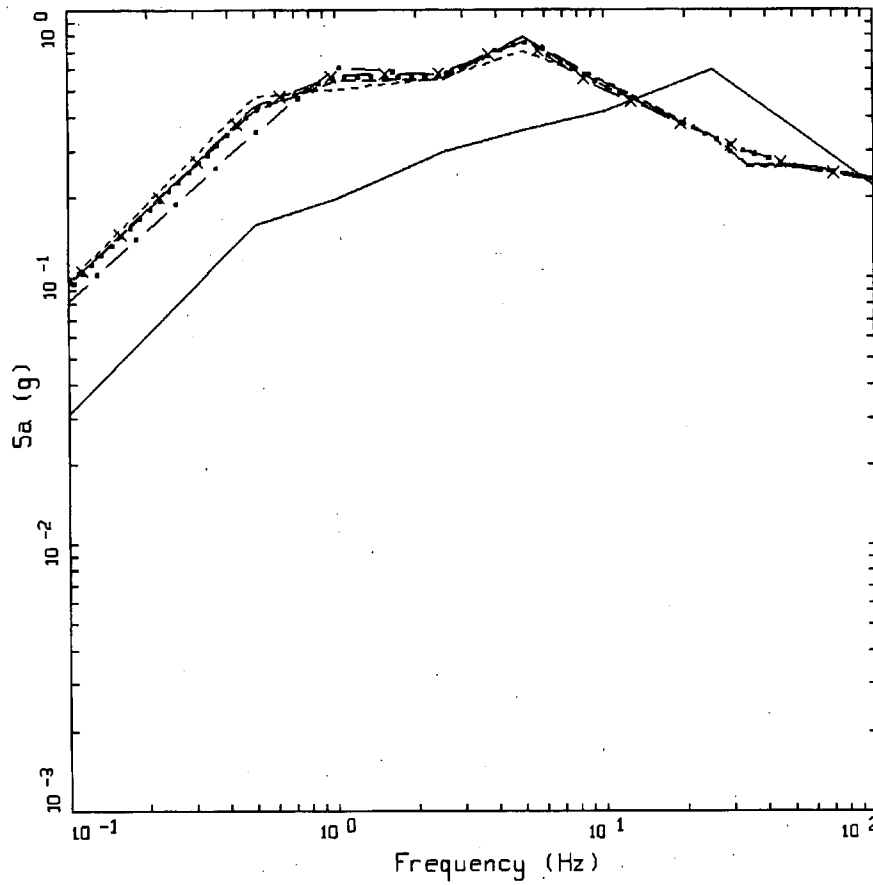
Figure 19b Deaggregation for the Grand Gulf Nuclear Station Unit 3: high-frequency, 5 Hz to 10 Hz (FSAR Figure 2.5.2-211, EOI, 2008).



GRAND GULF UHS, SITE RE
APE 1x10⁻⁴ YR⁻¹

- LEGEND
- 5 %, HARD ROCK: UHRS, MEAN
 - 5 %, HORIZONTAL UHRS, MEAN
 - 5 %, PROFILE 1 HORIZONTAL UHRS, MEAN
 - - - - 5 %, PROFILE 2 HORIZONTAL UHRS, MEAN
 - . - . 5 %, PROFILE 3 HORIZONTAL UHRS, MEAN
 - x - 5 %, PROFILE 4 HORIZONTAL UHRS, MEAN

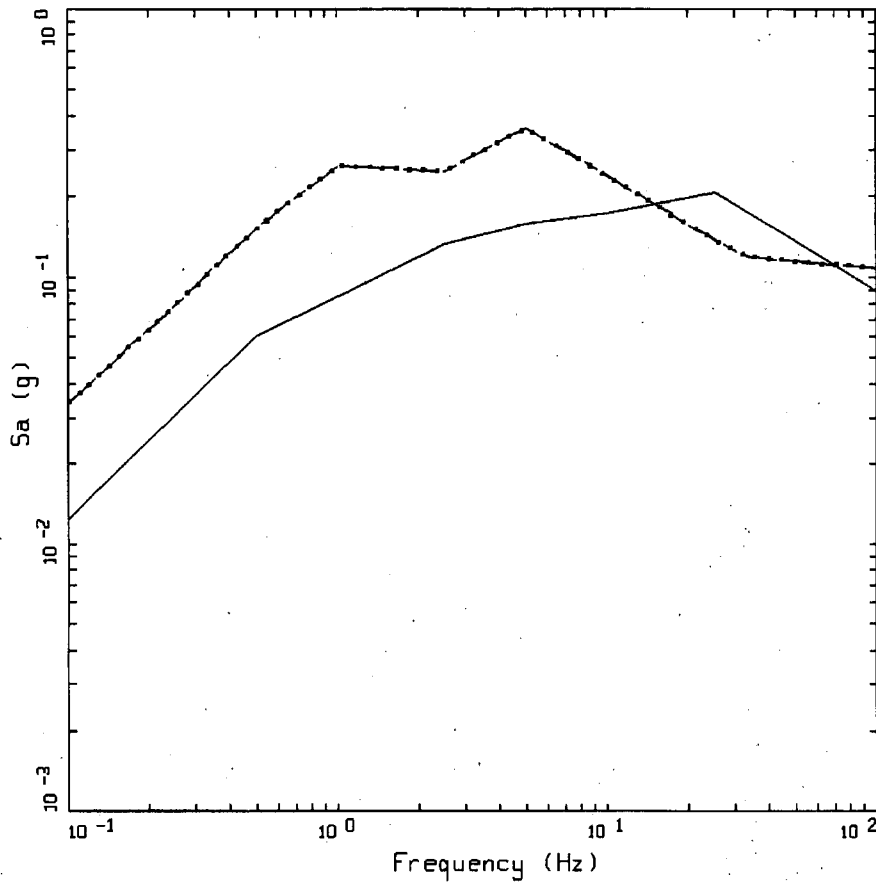
Figure 20a Comparison of UHRS computed for the Grand Gulf Nuclear Station Unit 3 profiles 1 to 4 (Figures 3a and 3b). Each profile UHRS reflects a weighted mean over the two sets of G/Gmax and hysteretic damping curves (Table 5). AEF 10⁻⁴.



GRAND GULF UHS, SITE RE
 APE 1×10^{-5} YR-1

- LEGEND
- 5 %, HARD ROCK: UHS, MEAN
 - 5 %, HORIZONTAL UHS, MEAN
 - 5 %, PROFILE 1 HORIZONTAL UHS, MEAN
 - - - - 5 %, PROFILE 2 HORIZONTAL UHS, MEAN
 - . - . 5 %, PROFILE 3 HORIZONTAL UHS, MEAN
 - x - 5 %, PROFILE 4 HORIZONTAL UHS, MEAN

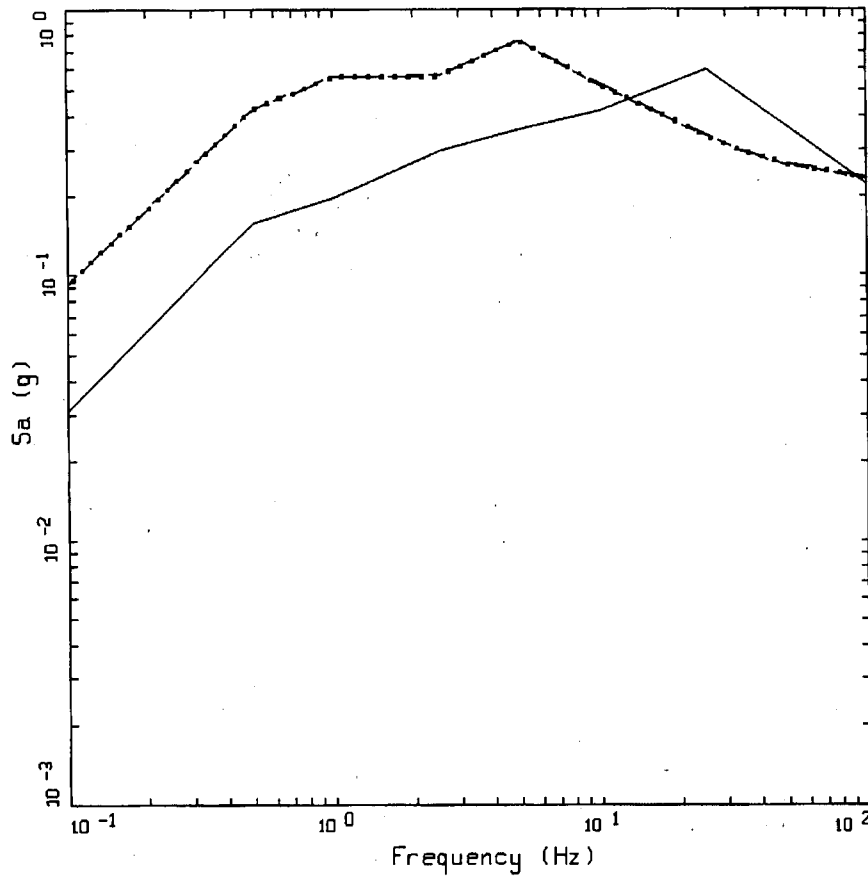
Figure 20b Comparison of UHS computed for the Grand Gulf Nuclear Station Unit 3 profiles 1 to 4 (Figures 3a and 3b). Each profile UHS reflects a weighted mean over the two sets of G/Gmax and hysteretic damping curves (Table 5). AEF 10^{-5} .



GRAND GULF UHS, SITE RE
 APE 1×10^{-4} YR-1

- LEGEND
- 5 %, HARD ROCK: UHRS, MEAN
 - 5 %, HORIZONTAL UHRS, MEAN
 - - - - 5 %, MATERIAL MODEL 1 HORIZONTAL UHRS, MEAN
 - . - . 5 %, MATERIAL MODEL 2 HORIZONTAL UHRS, MEAN

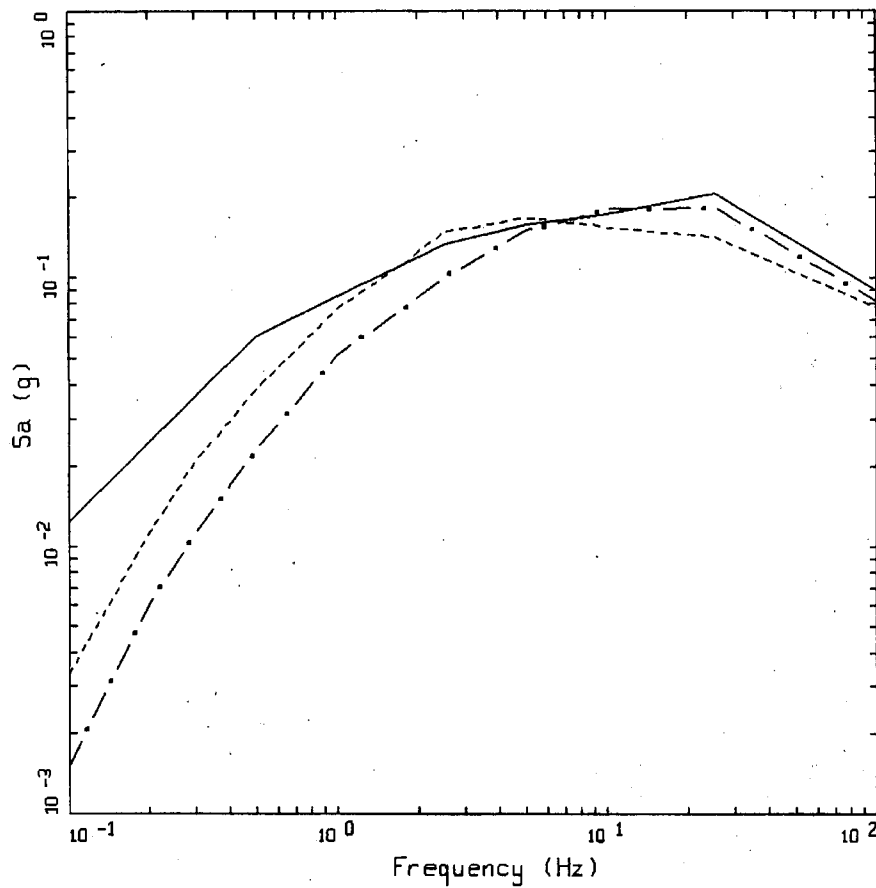
Figure 21a Comparison of UHRS computed for the Grand Gulf Nuclear Station Unit 3 uncorrected and corrected G/G_{max} and hysteretic damping curves (Table 5). Each profile UHRS reflects a weighted mean over the four profiles in Figures 3a and 3b (Table 5). AEF 10^{-4} .



GRAND GULF UHS, SITE RE
APE 1×10^{-5} YR-1

- LEGEND
- 5 %, HARD ROCK: UHS, MEAN
 - 5 %, HORIZONTAL UHS, MEAN
 - - - 5 %, MATERIAL MODEL 1 HORIZONTAL UHS, MEAN
 - . - 5 %, MATERIAL MODEL 2 HORIZONTAL UHS, MEAN

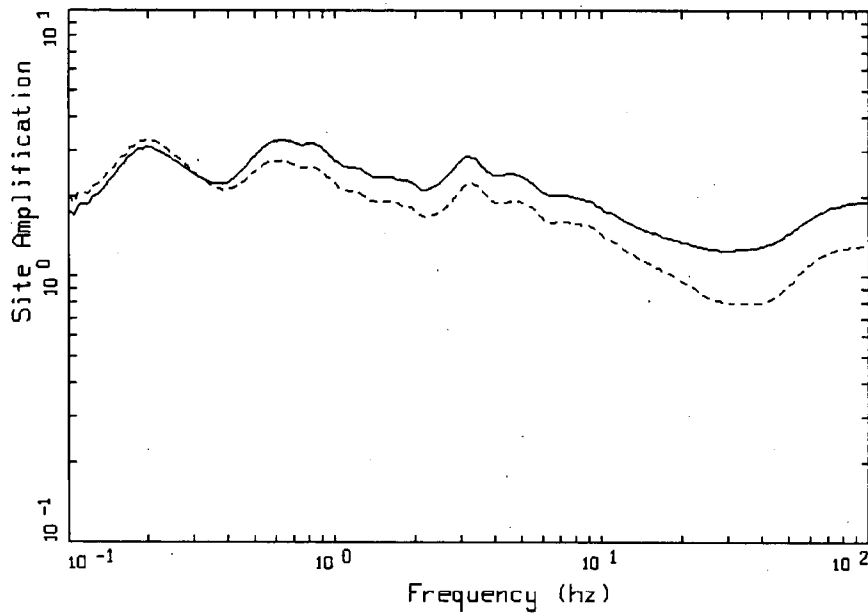
Figure 21b Comparison of UHS computed for the Grand Gulf Nuclear Station Unit 3 uncorrected and corrected G/G_{max} and hysteretic damping curves (Table 5). Each profile UHS reflects a weighted mean over the four profiles in Figures 3a and 3b (Table 5). AEF 10^{-5} .



GRAND GULF UHS: $10E-4$
HARD ROCK, HORIZONTAL

LEGEND
—— UHS: PGA = 0.089 G
- - - 1-2 HZ: REFERENCE; PGA = 0.077 G, M 7.64, 466 KM
- · - 5-10 HZ: REFERENCE; PGA = 0.082 G, M 6.33, 82 KM

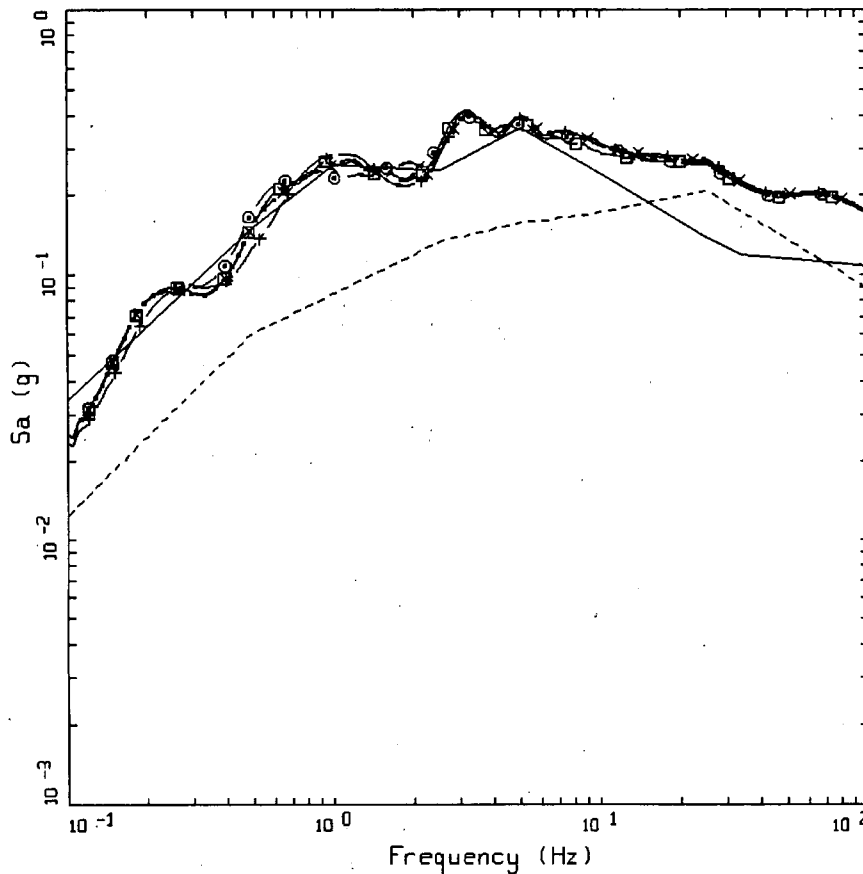
Figure 22 Approach 2A scaled reference earthquake spectra computed for 1 Hz to 2.5 Hz (**M** 7.64, *D* 466 km) and 5 Hz to 10 Hz (**M** 6.33, *D* 82 km) using a weighted average of the EPRI (2004) attenuation relations. $AEF 10^{-4}$.



GRAND GULF: RE.1
MEAN AMPLIFICATION 10E-04

LEGEND
—— MEAN 1-2.5 HZ
- - - MEAN 5-10 HZ

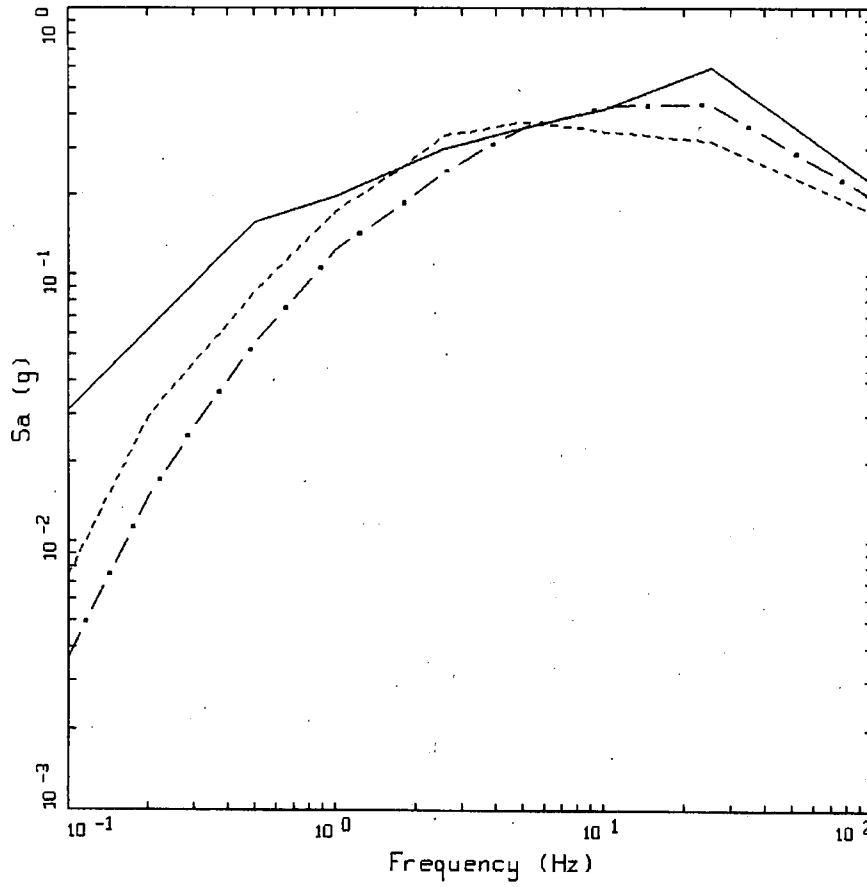
Figure 23 Approach 2A, example of low- and high-frequency mean amplification factors computed for profile 1 (Figures 3a and 3b) using uncorrected G/G_{max} and hysteretic damping curves. AEF 10^{-4} .



GRAND GULF: REACTOR EMBEDDED
 HORIZONTAL: APPROACHS 2A & 3

- LEGEND
- 5 %, APPROACH 3: HORIZONTAL UHS, MEAN FOR APE 10⁻⁴ YR⁻¹ AT LOCATION RE
 - 5 %, APPROACH 2A FOR RE.1: ENVELOPE TRANSFER FUNCTION*UHS
 - 5 %, APPROACH 2A FOR RE.2: ENVELOPE TRANSFER FUNCTION*UHS
 - 5 %, APPROACH 2A FOR RE.3: ENVELOPE TRANSFER FUNCTION*UHS
 - 5 %, APPROACH 2A FOR RE.4: ENVELOPE TRANSFER FUNCTION*UHS
 - 5 %, APPROACH 2A FOR RE.5: ENVELOPE TRANSFER FUNCTION*UHS
 - x— 5 %, APPROACH 2A FOR RE.6: ENVELOPE TRANSFER FUNCTION*UHS
 - +— 5 %, APPROACH 2A FOR RE.7: ENVELOPE TRANSFER FUNCTION*UHS
 - 5 %, APPROACH 2A FOR RE.8: ENVELOPE TRANSFER FUNCTION*UHS
 - 5 %, HARD ROCK UHS: MEAN FOR APE 10⁻⁴ YR⁻¹

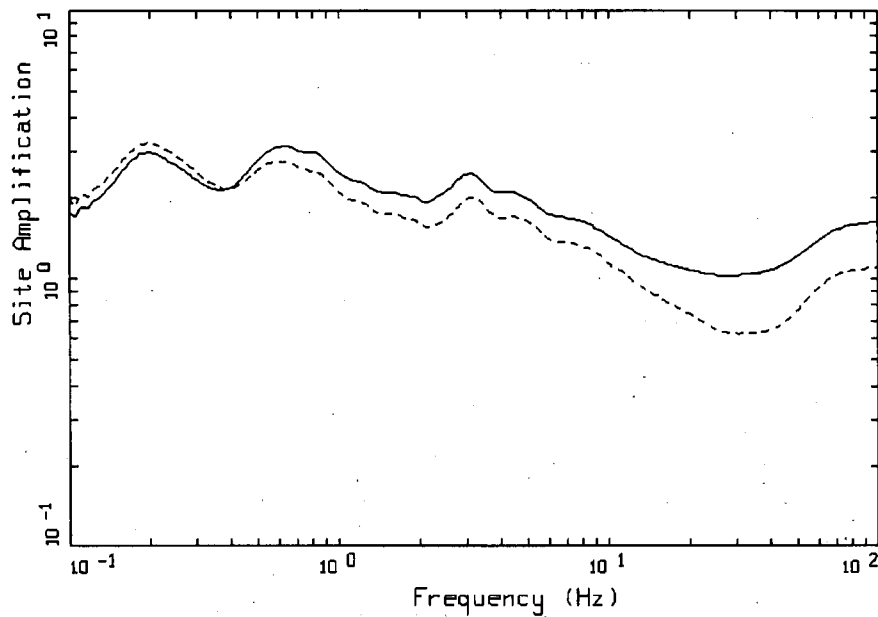
Figure 24 Approach 2A deterministic spectra compared to UHS computed using Approach 3. Approach 2A results shown for each combination of profile (1 to 4, Figures 3a and 3b) and sets of G/Gmax and hysteretic damping curves (labeled as RE.1 – RE.8, P1 to P4 correspond to RE.1 to RE.4 and P5 to P8 correspond to RE.5 to RE.8, respectively; refer to Section 3.4.2.3). AEF 10⁻⁴.



GRAND GULF UHRS: $10E-5$
HARD ROCK, HORIZONTAL

- LEGEND
- UHRS: PGA = 0.222 G
 - - - 1-2 HZ: REFERENCE; PGA = 0.172 G, M 7.64, 466 KM
 - . - 5-10 HZ: REFERENCE; PGA = 0.195 G, M 6.33, 82 KM

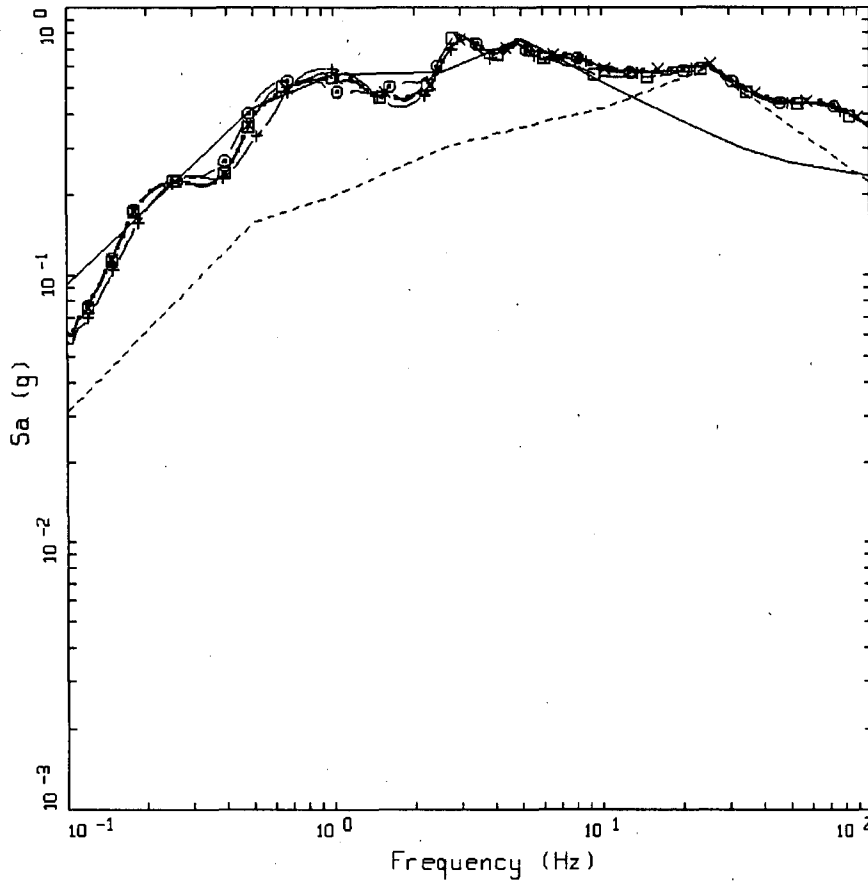
Figure 25 Approach 2A scaled reference earthquake spectra computed for 1 Hz to 2.5 Hz (M 7.64, D 466 km) and 5 Hz to 10 Hz (M 6.33, D 82 km) using a weighted average of the EPRI (2004) attenuation relations. AEF 10^{-5} .



GRAND GULF: RE.1
MEAN AMPLIFICATION 10E-05

LEGEND
—— MEAN 1-2.5 HZ
----- MEAN 5-10 HZ

Figure 26 Approach 2A, example of low- and high-frequency mean amplification factors computed for profile 1 (Figures 3a and 3b) using uncorrected G/G_{max} and hysteretic damping curves. AEF 10^{-5} .

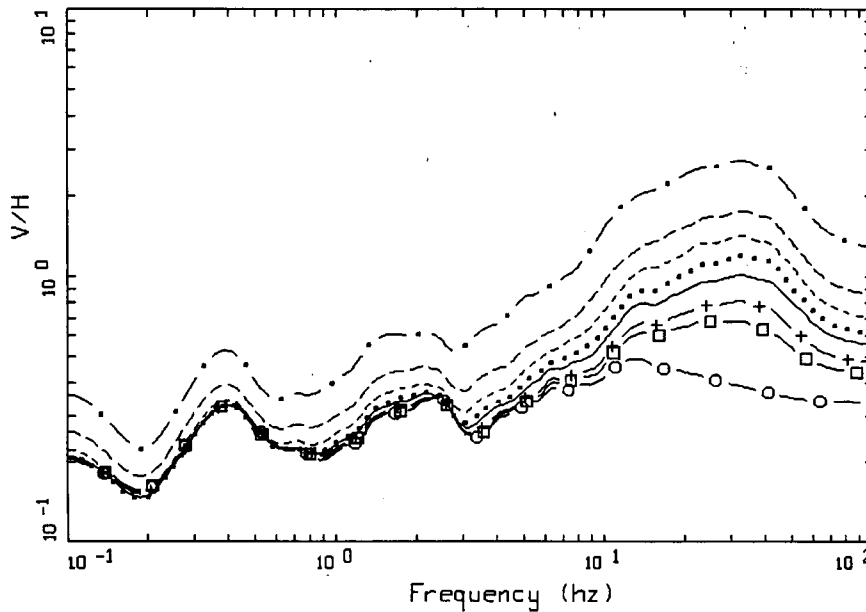


GRAND GULF: REACTOR EMBEDDED
HORIZONTAL: APPROACHS 2A & 3

LEGEND

- 5 %, APPROACH 3: HORIZONTAL UHRS, MEAN FOR APE 10⁻⁵ YR⁻¹ AT LOCATION RE
- 5 %, APPROACH 2A FOR RE.1: ENVELOPE TRANSFER FUNCTION*UHS
- 5 %, APPROACH 2A FOR RE.2: ENVELOPE TRANSFER FUNCTION*UHS
- 5 %, APPROACH 2A FOR RE.3: ENVELOPE TRANSFER FUNCTION*UHS
- 5 %, APPROACH 2A FOR RE.4: ENVELOPE TRANSFER FUNCTION*UHS
- 5 %, APPROACH 2A FOR RE.5: ENVELOPE TRANSFER FUNCTION*UHS
- x- 5 %, APPROACH 2A FOR RE.6: ENVELOPE TRANSFER FUNCTION*UHS
- +- 5 %, APPROACH 2A FOR RE.7: ENVELOPE TRANSFER FUNCTION*UHS
- 5 %, APPROACH 2A FOR RE.8: ENVELOPE TRANSFER FUNCTION*UHS
- 5 %, HARD ROCK UHRS: MEAN FOR APE 10⁻⁵ YR⁻¹

Figure 27 Approach 2A deterministic spectra compared to UHRS computed using Approach 3. Approach 2A results shown for each combination of profile (1 to 4, Figures 3a and 3b) and sets of G/Gmax and hysteretic damping curves (labeled as RE.1 – RE.8, P1 to P4 correspond to RE.1 to RE.4 and P5 to P8 correspond to RE.5 to RE.8, respectively; refer to Section 3.4.2.3). AEF 10⁻⁵.

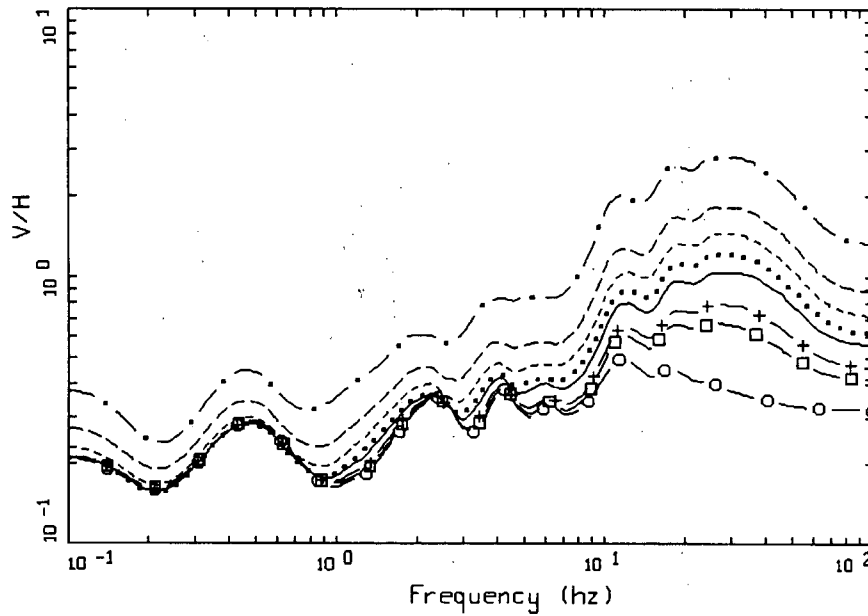


V/H RATIOS
 M6251CF RE.1

LEGEND

—○—	50TH PERCENTILE, D = 190 KM, 0.01 g
—□—	50TH PERCENTILE, D = 59 KM, 0.05 g
—+—	50TH PERCENTILE, D = 37 KM, 0.10 g
—	50TH PERCENTILE, D = 21 KM, 0.20 g
.....	50TH PERCENTILE, D = 15 KM, 0.30 g
-----	50TH PERCENTILE, D = 10 KM, 0.40 g
-----	50TH PERCENTILE, D = 7 KM, 0.50 g
—•—	50TH PERCENTILE, D = 0 KM, 0.75 g

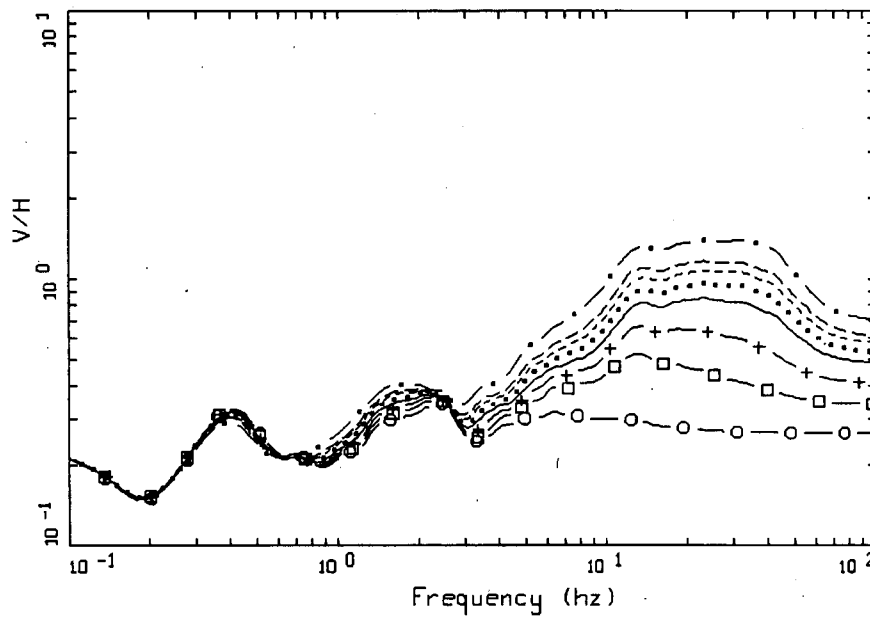
Figure 28a Example of median V/H ratios computed for the Grand Gulf Reactor Unit 3 using site-specific G/G_{max} and hysteretic damping curves (EOI, 2008) with a single-corner source model and **M** 6.25: profile 1. Reference site expected horizontal peak acceleration values and corresponding distances from Table 2.



V/H RATIOS
 M6251CF RE.3

- LEGEND
- 50TH PERCENTILE, D = 190 KM, 0.01 g
 - 50TH PERCENTILE, D = 59 KM, 0.05 g
 - +— 50TH PERCENTILE, D = 37 KM, 0.10 g
 - 50TH PERCENTILE, D = 21 KM, 0.20 g
 - 50TH PERCENTILE, D = 15 KM, 0.30 g
 - 50TH PERCENTILE, D = 10 KM, 0.40 g
 - 50TH PERCENTILE, D = 7 KM, 0.50 g
 - 50TH PERCENTILE, D = 0 KM, 0.75 g

Figure 28b Example of median V/H ratios computed for the Grand Gulf Reactor Unit 3 using site-specific G/G_{max} and hysteretic damping curves (EOI, 2008) with a single-corner source model and **M** 6.25: profile 3. Reference site expected horizontal peak acceleration values and corresponding distances from Table 2.

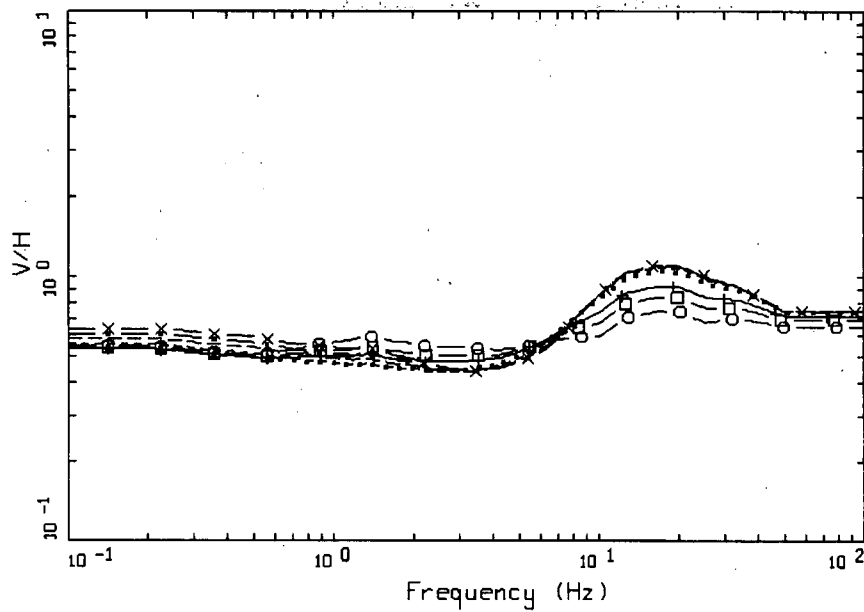


V/H RATIOS
 M7691CF RE.1

LEGEND

—○—	50TH PERCENTILE, D = 480 KM, 0.01 g
—□—	50TH PERCENTILE, D = 163 KM, 0.05 g
—+—	50TH PERCENTILE, D = 92 KM, 0.10 g
—	50TH PERCENTILE, D = 50 KM, 0.20 g
.....	50TH PERCENTILE, D = 37 KM, 0.30 g
-----	50TH PERCENTILE, D = 29 KM, 0.40 g
-----	50TH PERCENTILE, D = 24 KM, 0.50 g
-----	50TH PERCENTILE, D = 16 KM, 0.75 g

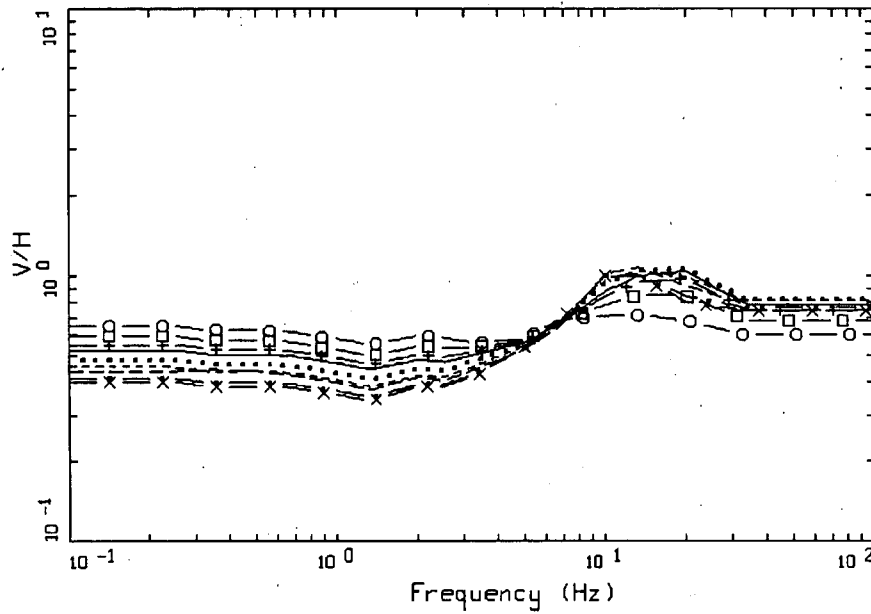
Figure 29 Example of median V/H ratios computed for the Grand Gulf Reactor Unit 3 using site-specific G/G_{max} and hysteretic damping curves (EOI, 2008) with a single-corner source model and **M** 7.69: profile 1. Reference site expected horizontal peak acceleration values and corresponding distances from Table 2.



V/H RATIOS, A AND S
ROCK, M = 6.25

LEGEND	
—○—	0.04G: DISTANCE = 57 KM
—□—	0.08G: DISTANCE = 31 KM
—+—	0.14G: DISTANCE = 19 KM
— — —	0.20G: DISTANCE = 14 KM
.....	0.33G: DISTANCE = 8 KM
-----	0.45G: DISTANCE = 5 KM
-----	0.55G: DISTANCE = 3 KM
—•—	0.59G: DISTANCE = 2 KM
—x—	0.62G: DISTANCE = 1 KM

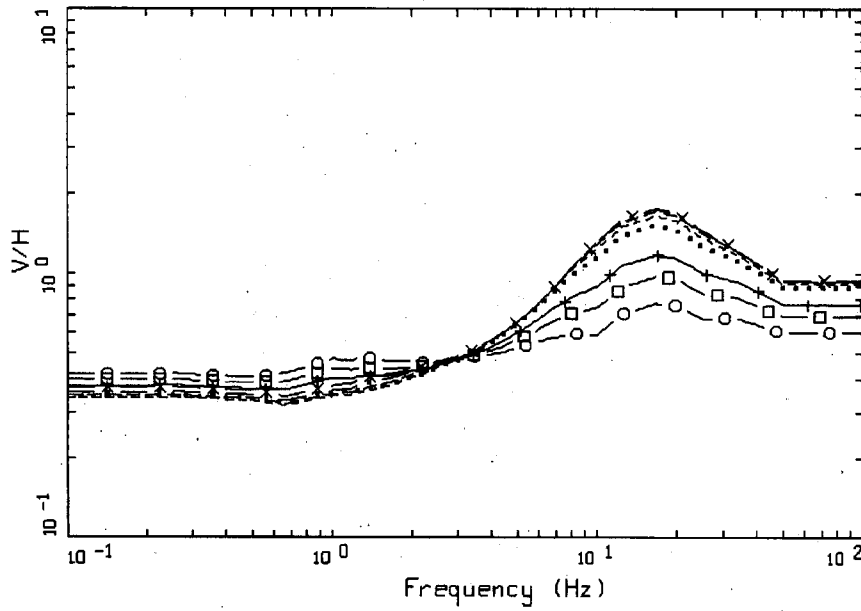
Figure 30a. WNA empirical V/H ratios computed for M 6.25 at a suite of distances for soft rock site conditions: Abrahamson and Silva (1997). Peak acceleration values for horizontal component rock site conditions.



V/H RATIOS, CAMPBELL & BOZORGNIA
ROCK, M = 6.25

LEGEND	
—○—	0.04G: DISTANCE = 57 KM
—□—	0.07G: DISTANCE = 31 KM
—+—	0.12G: DISTANCE = 19 KM
—	0.16G: DISTANCE = 14 KM
.....	0.27G: DISTANCE = 8 KM
-----	0.38G: DISTANCE = 5 KM
-----	0.48G: DISTANCE = 3 KM
—•—	0.54G: DISTANCE = 2 KM
—x—	0.58G: DISTANCE = 1 KM

Figure 30b WNA empirical V/H ratios computed for M 6.25 at a suite of distances for soft rock site conditions: Campbell and Bozorgnia (2003). Peak acceleration values for horizontal component rock site conditions:

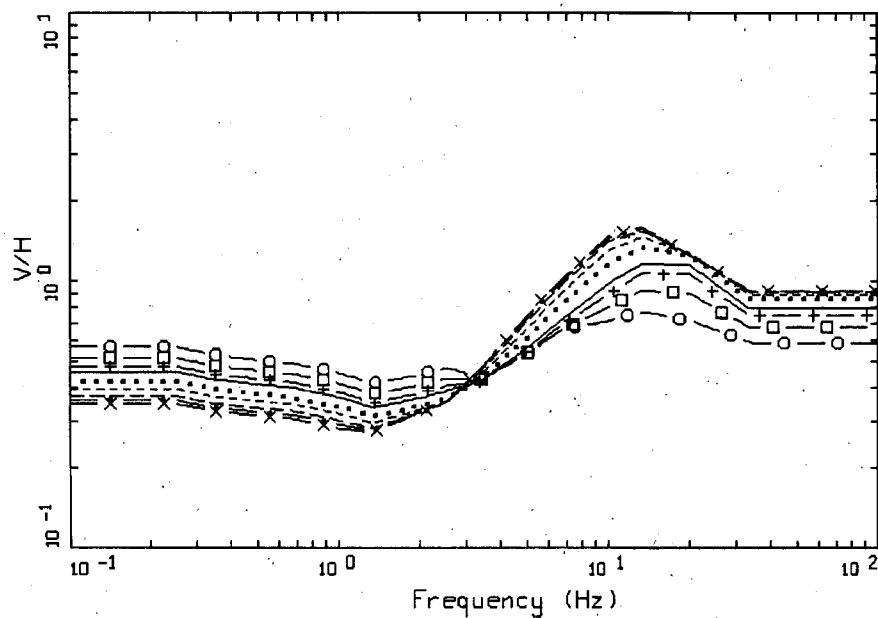


V/H RATIOS, A AND S
SOIL M = 6.25

LEGEND

—○—	0.04G: DISTANCE = 57 KM
—□—	0.08G: DISTANCE = 31 KM
—+—	0.14G: DISTANCE = 19 KM
—	0.20G: DISTANCE = 14 KM
.....	0.33G: DISTANCE = 8 KM
-----	0.45G: DISTANCE = 5 KM
-----	0.55G: DISTANCE = 3 KM
—•—	0.59G: DISTANCE = 2 KM
—x—	0.62G: DISTANCE = 1 KM

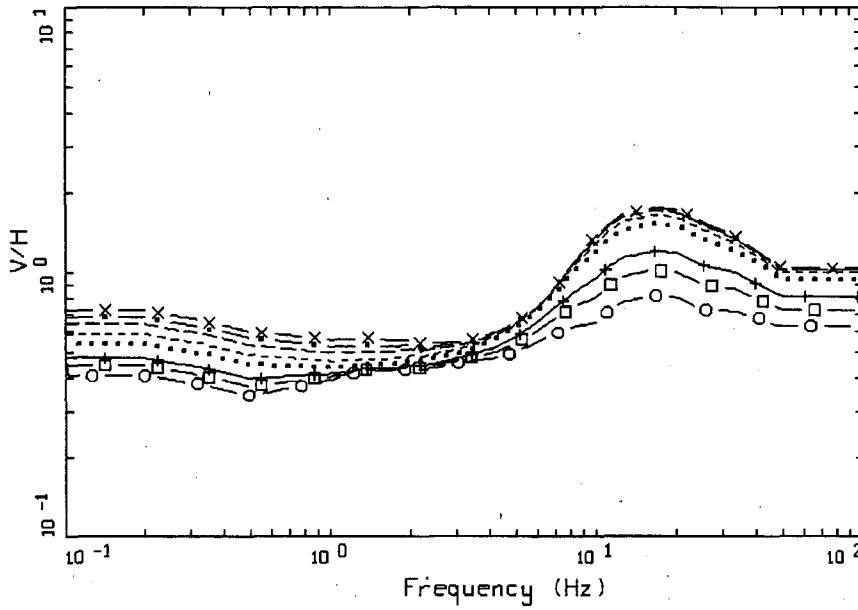
Figure 31a WNA empirical V/H ratios computed for **M** 6.25 at a suite of distances for deep firm soil site conditions: Abrahamson and Silva (1997). Peak acceleration values for horizontal component rock site conditions.



V/H RATIOS, CAMPBELL & BOZORGNIA
SOIL, M = 6.25

- LEGEND
- 0.04G: DISTANCE = 57 KM
 - 0.07G: DISTANCE = 31 KM
 - +— 0.12G: DISTANCE = 19 KM
 - 0.16G: DISTANCE = 14 KM
 - 0.27G: DISTANCE = 8 KM
 - 0.38G: DISTANCE = 5 KM
 - 0.48G: DISTANCE = 3 KM
 - 0.54G: DISTANCE = 2 KM
 - x— 0.58G: DISTANCE = 1 KM

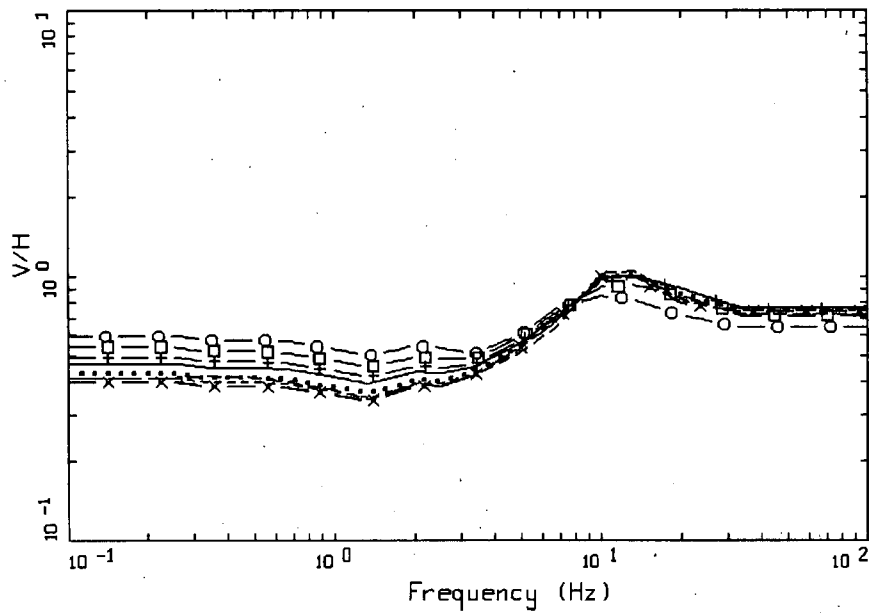
Figure 31b WNA empirical V/H ratios computed for M 6.25 at a suite of distances for deep firm soil site conditions: Campbell and Bozorgnia (2003). Peak acceleration values for horizontal component rock site conditions.



V/H RATIOS, A AND S
ROCK, M = 7.69

LEGEND	
—○—	0.10G: DISTANCE = 57 KM
—□—	0.18G: DISTANCE = 31 KM
—+—	0.27G: DISTANCE = 19 KM
—	0.35G: DISTANCE = 14 KM
.....	0.52G: DISTANCE = 8 KM
-----	0.66G: DISTANCE = 5 KM
-----	0.77G: DISTANCE = 3 KM
—•—	0.82G: DISTANCE = 2 KM
—x—	0.86G: DISTANCE = 1 KM

Figure 32a WNA empirical V/H ratios computed for **M** 7.69 at a suite of distances for soft rock site conditions: Abrahamson and Silva (1997). Peak acceleration values for horizontal component rock site conditions.

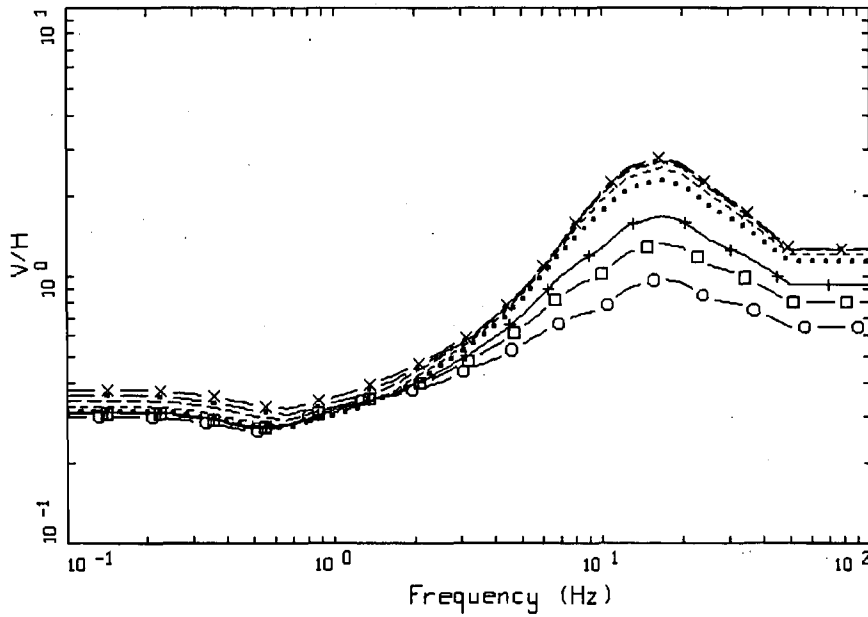


V/H RATIOS, CAMPBELL & BOZORGNIA
ROCK, M = 7.69

LEGEND

—○—	0.10G: DISTANCE = 57 KM
—□—	0.19G: DISTANCE = 31 KM
—+—	0.28G: DISTANCE = 19 KM
— — —	0.36G: DISTANCE = 14 KM
.....	0.48G: DISTANCE = 8 KM
-----	0.54G: DISTANCE = 5 KM
-----	0.59G: DISTANCE = 3 KM
— · —	0.59G: DISTANCE = 2 KM
—x—	0.60G: DISTANCE = 1 KM

Figure 32b WNA empirical V/H ratios computed for M 7.69 at a suite of distances for soft rock site conditions: Abrahamson and Silva (1997). Peak acceleration values for horizontal component rock site conditions.

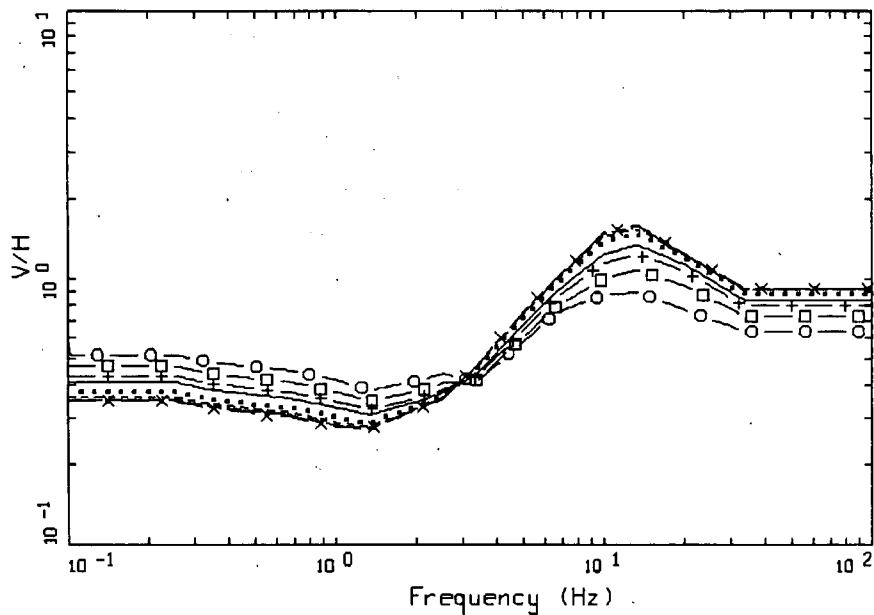


V/H RATIOS, A AND S
SOIL, M = 7.69

LEGEND

—○—	0.10G: DISTANCE = 57 KM
—□—	0.18G: DISTANCE = 31 KM
—+—	0.27G: DISTANCE = 19 KM
—	0.35G: DISTANCE = 14 KM
.....	0.52G: DISTANCE = 8 KM
-----	0.66G: DISTANCE = 5 KM
-----	0.77G: DISTANCE = 3 KM
—•—	0.82G: DISTANCE = 2 KM
—x—	0.86G: DISTANCE = 1 KM

Figure 33a WNA empirical V/H ratios computed for **M** 7.69 at a suite of distances for deep firm soil site conditions: Abrahamson and Silva (1997). Peak acceleration values for horizontal component rock site conditions.

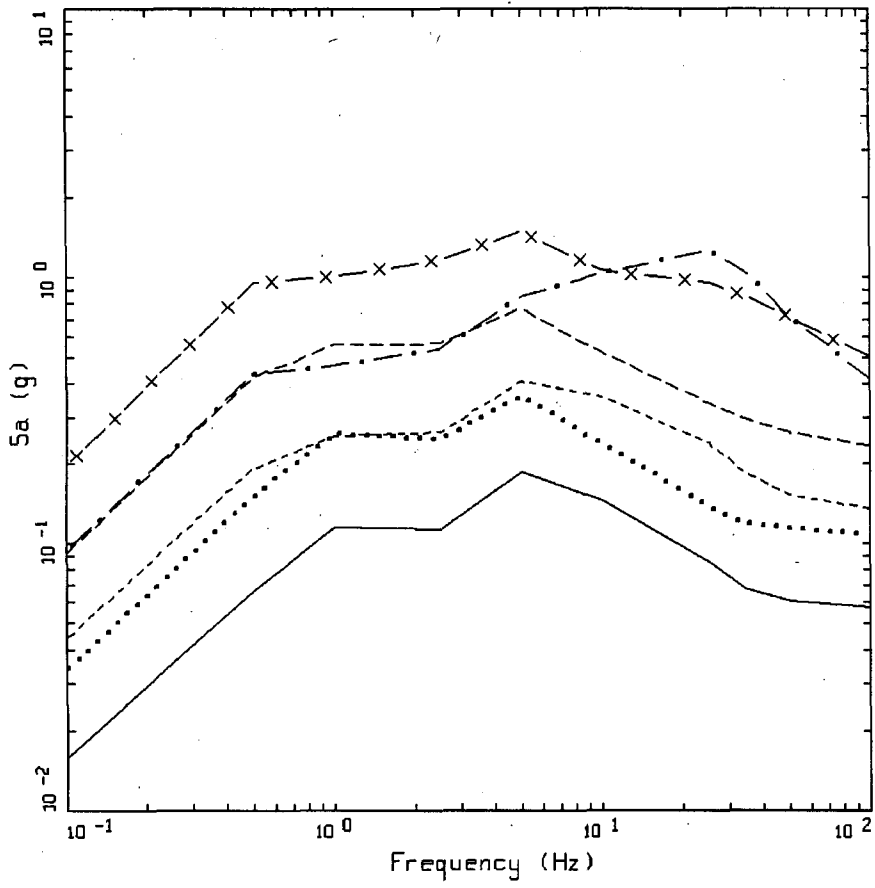


V/H RATIOS, CAMPBELL & BOZORGNIA
SOIL, M = 7.69

LEGEND

—○—	0.10G: DISTANCE = 57 KM
—□—	0.19G: DISTANCE = 31 KM
—+—	0.28G: DISTANCE = 19 KM
— — —	0.36G: DISTANCE = 14 KM
.....	0.48G: DISTANCE = 8 KM
-----	0.54G: DISTANCE = 5 KM
-----	0.59G: DISTANCE = 3 KM
—•—	0.59G: DISTANCE = 2 KM
—x—	0.60G: DISTANCE = 1 KM

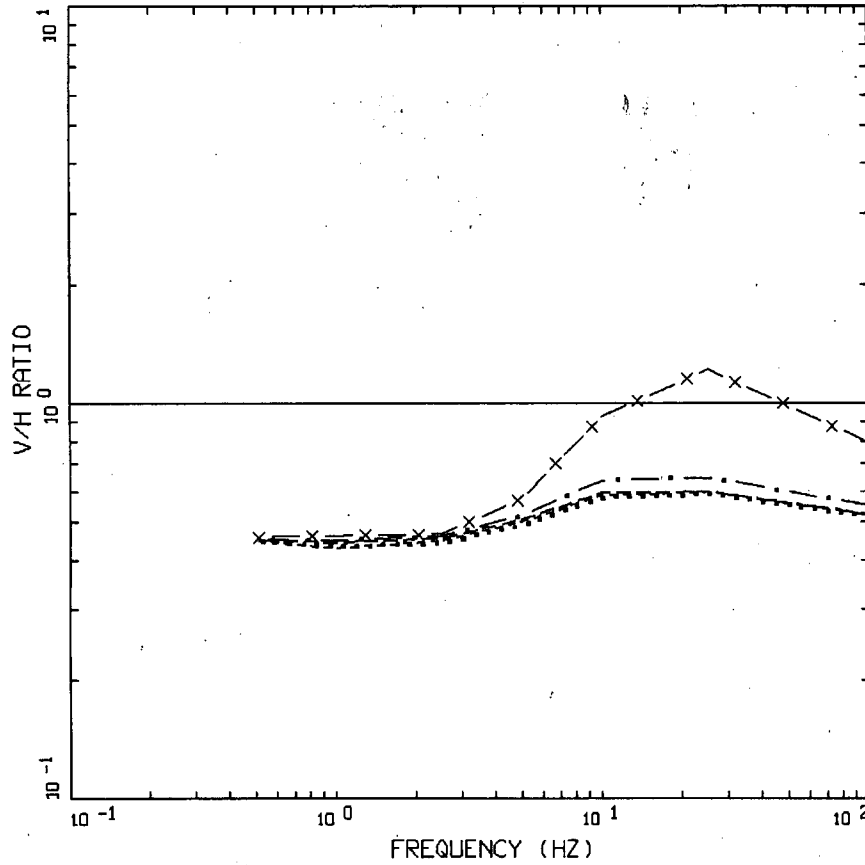
Figure 33b WNA empirical V/H ratios computed for **M** 7.69 at a suite of distances for deep firm soil site conditions: Abrahamson and Silva (1997). Peak acceleration values for horizontal component rock site conditions.



PROFILE RE
 UHRS: HORIZONTAL AND VERTICAL

- LEGEND
- x — 5 %, HORIZONTAL: UHRS, MEAN 1×10^{-6} AEP
 - . - . 5 %, VERTICAL: UHRS, MEAN 1×10^{-6} AEP
 - - - - 5 %, HORIZONTAL: UHRS, MEAN 1×10^{-5} AEP
 - - - - 5 %, VERTICAL: UHRS, MEAN 1×10^{-5} AEP
 - 5 %, HORIZONTAL: UHRS, MEAN 1×10^{-4} AEP
 - 5 %, VERTICAL: UHRS, MEAN 1×10^{-4} AEP

Figure 34 Horizontal and vertical component UHRS at annual exceedance probabilities (AEP) 10^{-4} , 10^{-5} , 10^{-6} , yr^{-1} : Grand Gulf Nuclear Station Unit 3 (EOI, 2008).



GRAND GULF UHS, SITE RE
IMPLIED V/H RATIOS

- LEGEND
- VERTICAL/HORIZONTAL RATIO: 1×10^{-3} APE
 - VERTICAL/HORIZONTAL RATIO: 4×10^{-4} APE
 - . - . VERTICAL/HORIZONTAL RATIO: 1×10^{-4} APE
 - — — VERTICAL/HORIZONTAL RATIO: 1×10^{-5} APE
 - x — VERTICAL/HORIZONTAL RATIO: 1×10^{-6} APE
 - UNITY LINE

Figure 35 V/H Ratio Based on Ratios of UHRS for Reactor Embedment at AEF 10^{-3} to 10^{-6} yr^{-1} (EOI, 2008).